MOLYBDENUM at 565°C						
Ageing time (hours)	No of points	Mean c change (at %)	Mean x_θ μm	Data from best fit $(c - \bar{c})$ v x_θ		
				correlation	gradient	significance
0	29	0.38	0.150	−0.25	−0.055	<0.90
1	26	0.62	0.146	−0.10	−0.018	<0.90
2	27	0.56	0.140	−0.13	−0.020	<0.90
4	32	0.56	0.143	0.13	0.020	<0.90
12	32	0.80	0.150	0.10	0.016	<0.90
24	28	0.97	0.164	0.17	0.045	<0.90
48	28	0.61	0.145	0.45	0.111	0.95
96	31	0.56	0.152	0.22	0.050	<0.90
168	27	1.17	0.152	0.59	0.152	0.98
336	27	1.02	0.135	0.67	0.170	0.99
672	29	0.77	0.150	−0.18	−0.048	<0.90
1344	31	1.28	0.157	0.22	0.090	<0.90
2688	26	1.39	0.152	0.34	0.104	<0.90
5376	31	1.44	0.156	0.61	0.213	0.99

Table 6.4 (c) Fe–Cr–Mo power plant steel, initially with a mixed ferritic and bainitic microstructure, aged at 565°C. EDX analysis data obtained for molybdenum content of cementite.

SILICON at 565°C						
Ageing time (hours)	No of points	Mean c change (at %)	Mean x_θ μm	Data from best fit $(c - \bar{c})$ v x_θ		
				correlation	gradient	significance
0	29	−0.39	0.150	0.20	0.030	<0.90
1	26	−0.29	0.146	0.17	0.018	<0.90
2	27	−0.21	0.140	0.26	0.026	<0.90
4	32	−0.40	0.143	−0.10	−0.011	<0.90
12	32	−0.23	0.150	−0.03	−0.003	<0.90
24	28	−0.36	0.164	0.10	0.012	<0.90
48	28	−0.21	0.145	0.15	0.010	<0.90
96	31	−0.39	0.152	0.23	0.009	<0.90
168	27	−0.10	0.152	0.09	0.012	<0.90
336	27	−0.37	0.135	−0.46	−0.039	0.95
672	29	−0.19	0.150	0.33	0.040	<0.90
1344	31	−0.51	0.157	−0.08	−0.012	0.98
2688	26	−0.28	0.152	−0.15	−0.016	<0.90
5376	31	−0.32	0.156	−0.14	−0.020	<0.90

Table 6.4 (d) Fe–Cr–Mo power plant steel, initially with a mixed ferritic and bainitic microstructure, aged at 565°C. EDX analysis data obtained for silicon content of cementite.

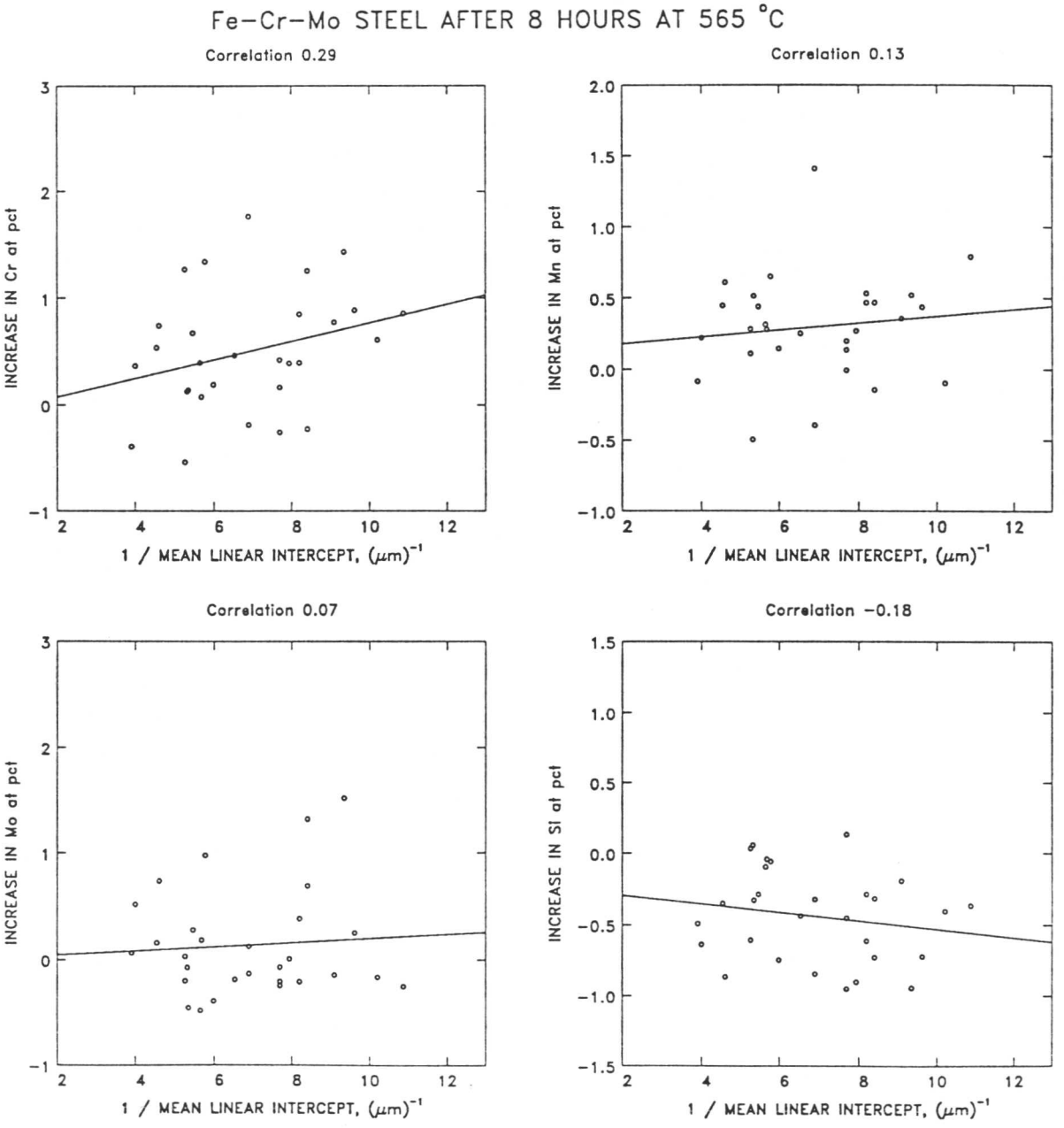

Figure 6.1(b): EDX microanalytical data for steel 1

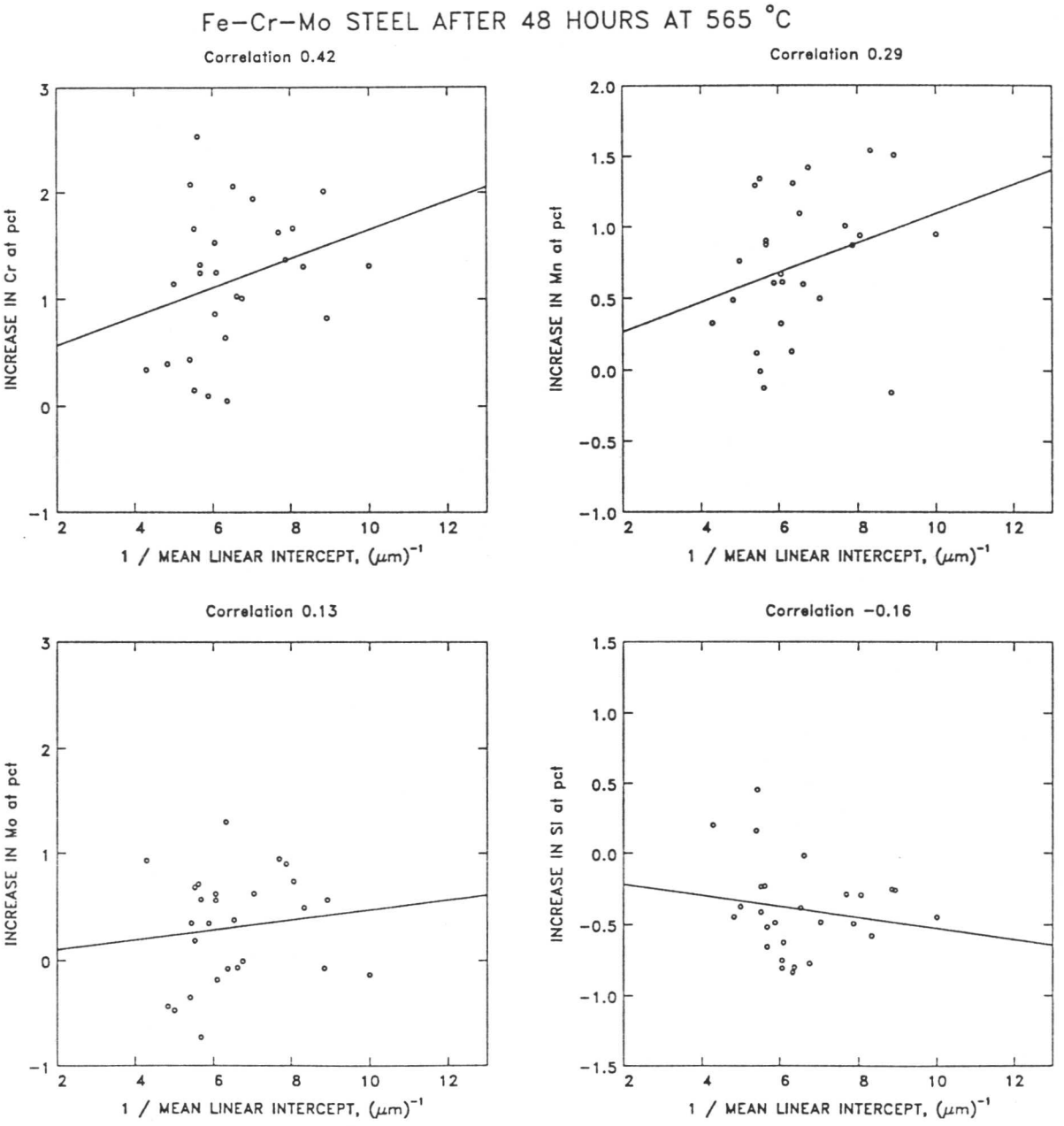

Figure 6.1(c): EDX microanalytical data for steel 1

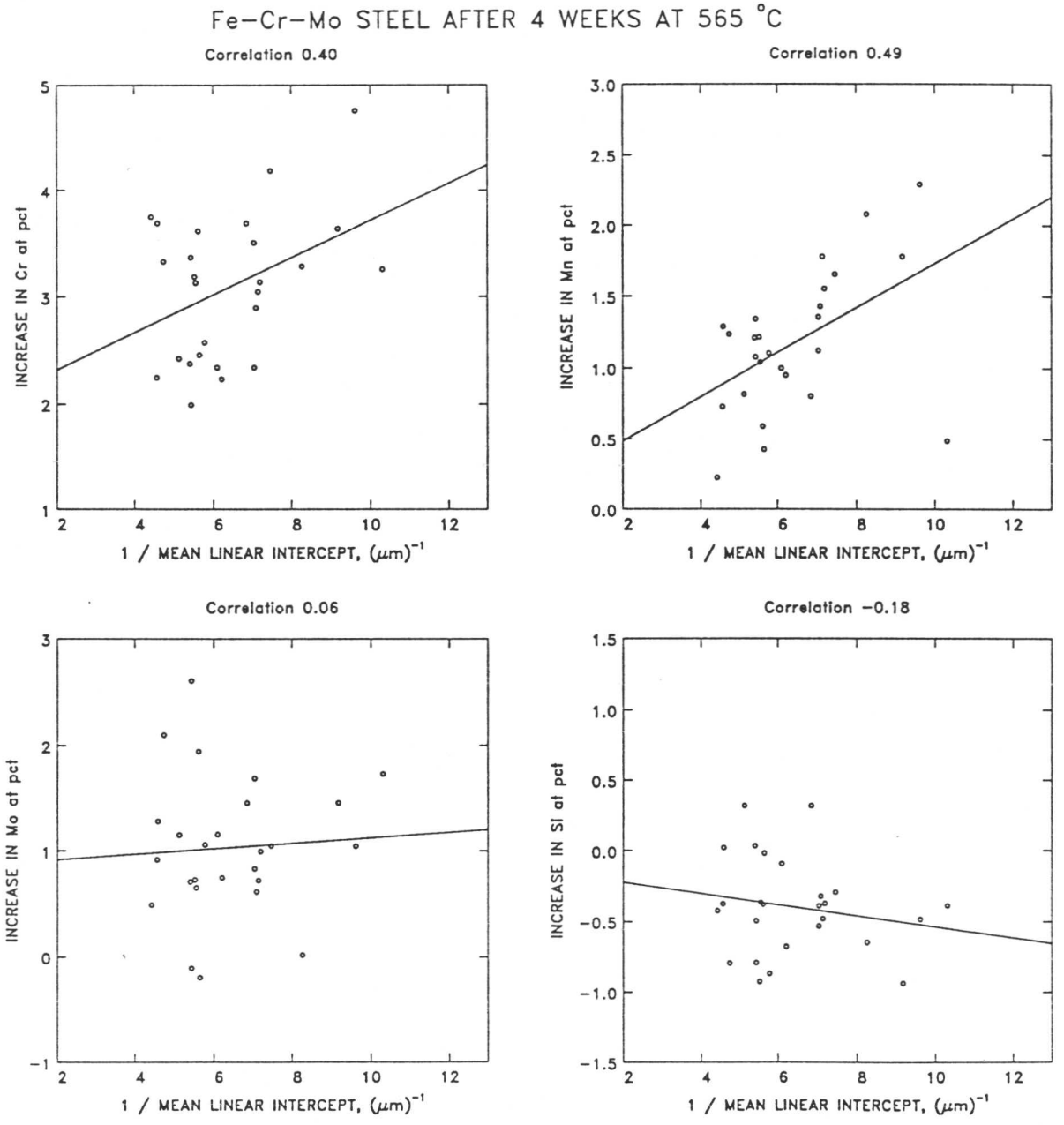

Figure 6.1(d): EDX microanalytical data for steel 1

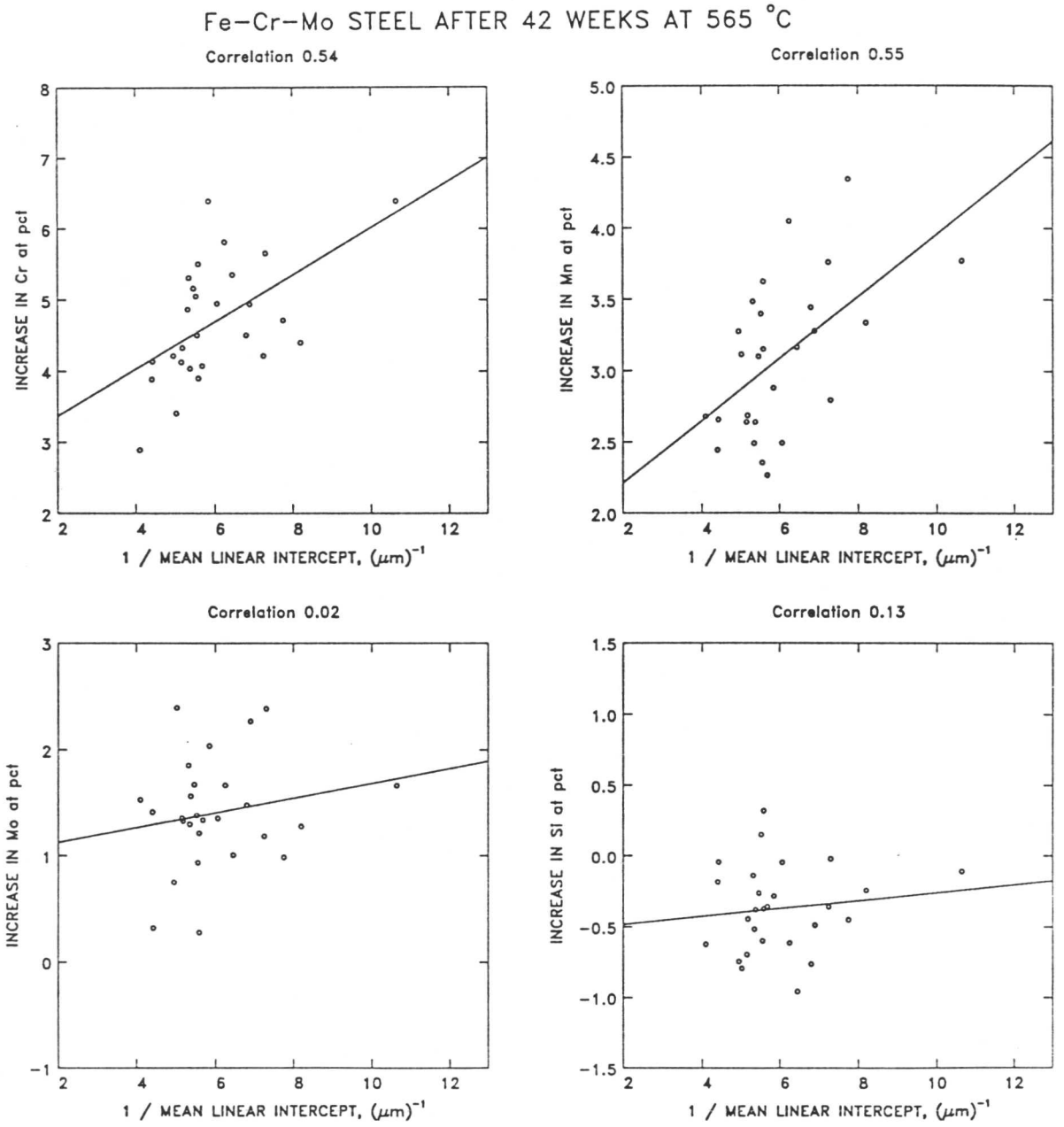

Figure 6.1(e): EDX microanalytical data for steel 1

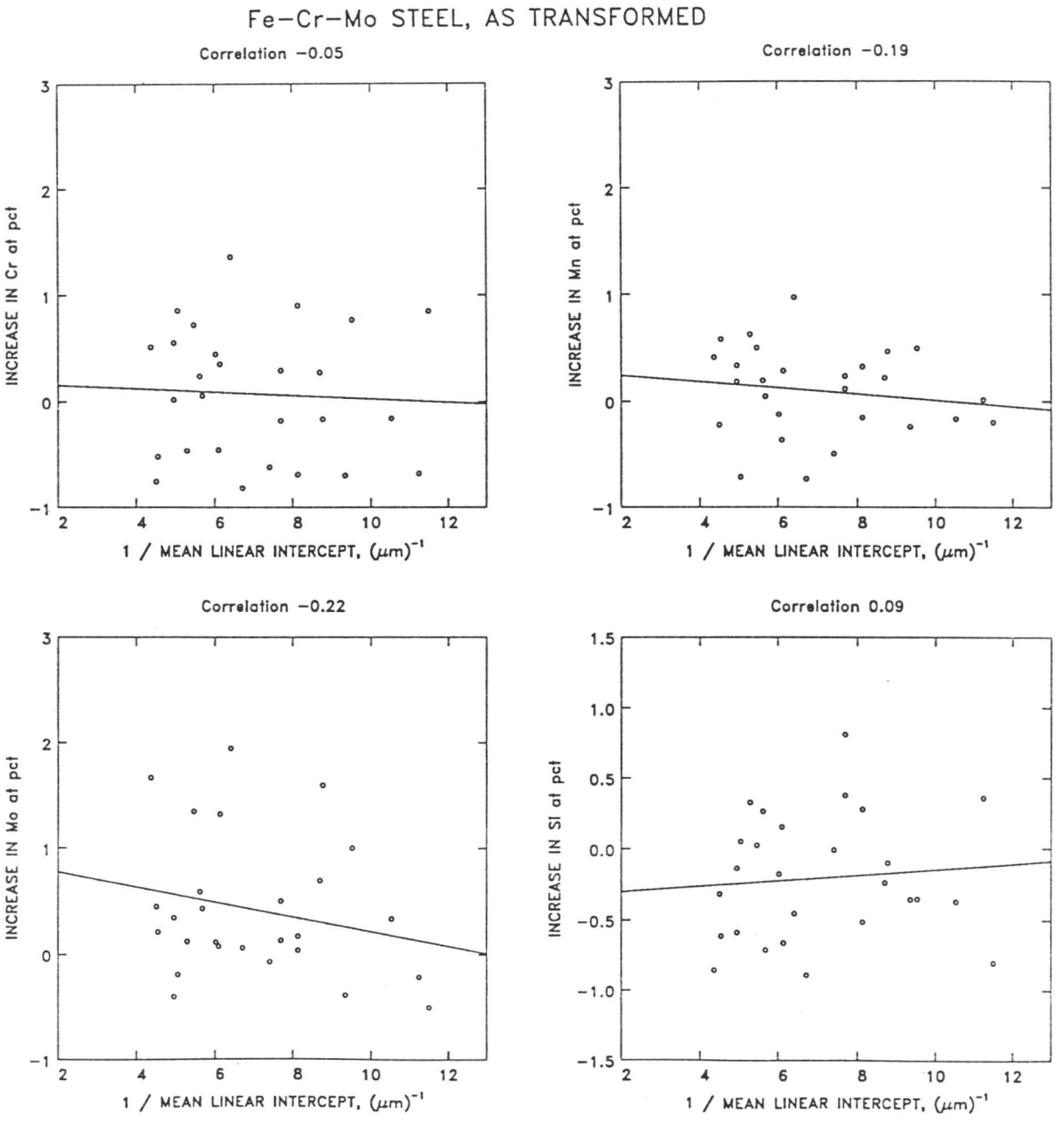

Figure 6.2: EDX microanalytical data for unaged specimens

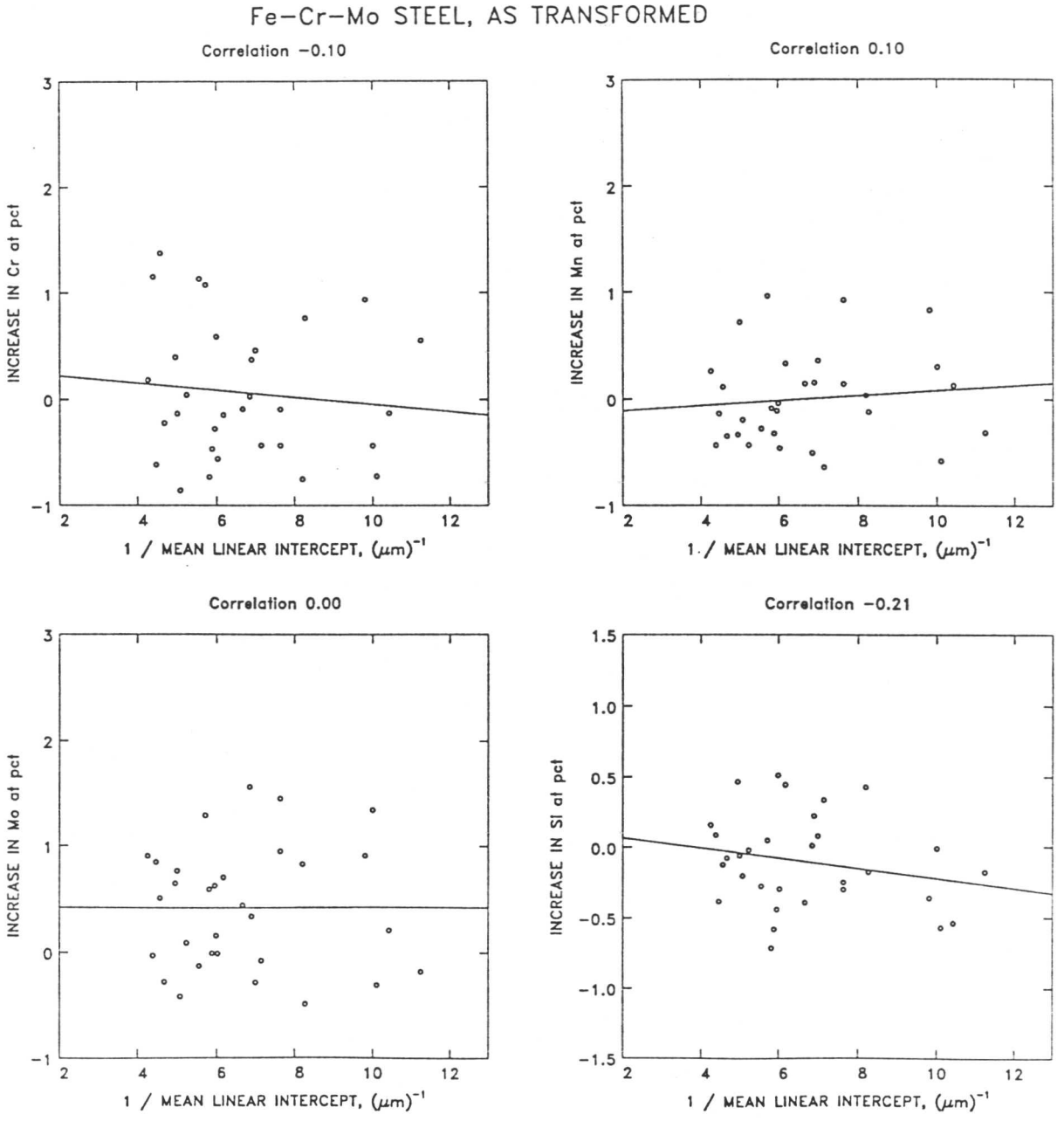

Figure 6.2: EDX microanalytical data for unaged specimens

6.2.4 Effect of particle size on ageing behaviour of cementite

It has been noted that the analytical model (equation (6.1)) predicts that differing x_θ will affect the rate of enrichment of cementite, and that such a size effect was observed experimentally for composition measurements made on particles of varied x_θ at a particular ageing time. The model also predicts that the rate of enrichment at a particular temperature will also be affected by mean particle size, and an attempt was made to illustrate this effect using the collected composition data.

To this end, values representative of the experimental data were obtained for $x_\theta = 0.100\mu$m, 0.180μm, and 0.260μm (which were chosen arbitrarily as being representative of the smaller, mean, and larger sizes of cementite observed), from the best fit lines on each by $(c - \bar{c})$ versus $1/x_\theta$ plot that had been calculated earlier using a regression analysis. This was done by taking these three values for x_θ on a $(c - \bar{c})$ versus $1/x_\theta$ plot, and extrapolating from the best fit line to determine the corresponding value of composition change; these could then be plotted against time to give an approximate indication of the fact that smaller cementite particle size was associated with larger degrees of enrichment. The extrapolation procedure is illustrated in figure 6.3.

It is important to realize that such values were not direct experimental results, but were rather a representation of the experimental data: the analysis relies on a complete absence of coarsening for its assumption that data for the same x_θ at different ageing times are comparable, as the development of individual cementite particles during ageing is impossible to follow. We know that this assumption is not strictly true, so the analysis must be considered with reservations, although the current work has shown coarsening to be of less significance than diffusion on the enrichment process.

Calculations were carried out using enrichment data for all four elements, but only those for chromium and manganese are presented here and used in subsequent analysis. Silicon was ignored because of the lack of statistical significance which could be attached to the small measured composition values as a result of the inherent statistical scatter in the EDX technique, and because

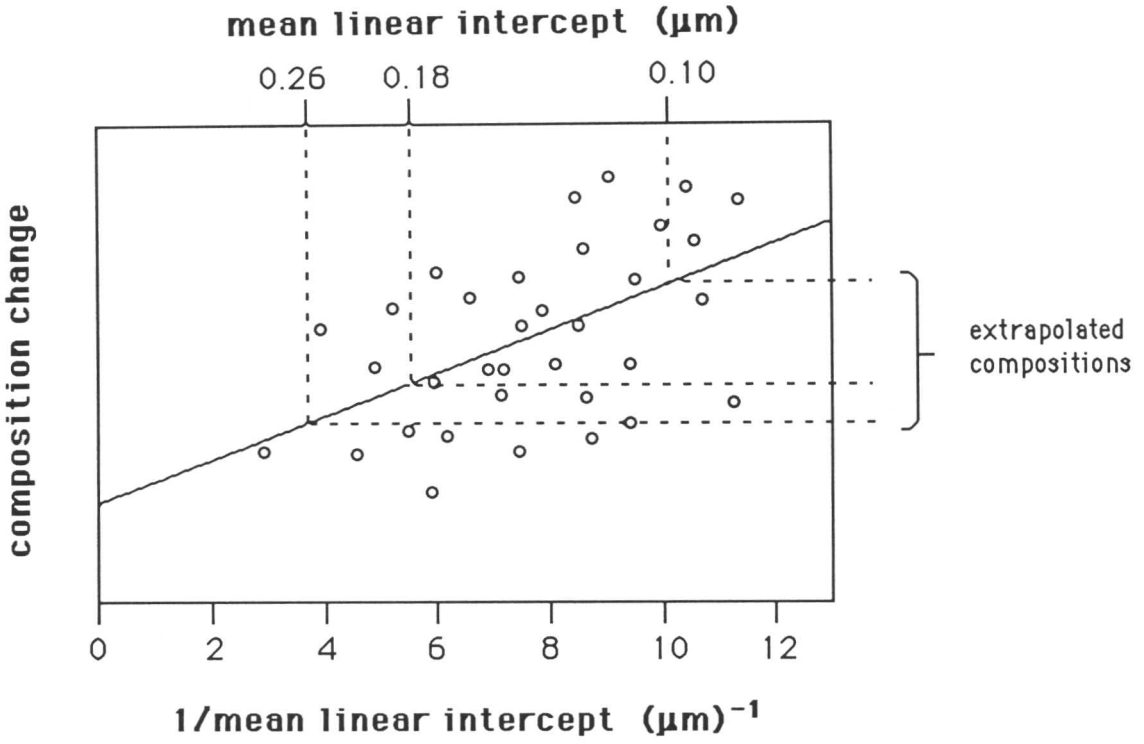

Figure 6.3: Method of extrapolation to produce values representative of experimentally-obtained compositions illustrating the effect of variations in x_θ on rate of enrichment of cementite

it partitions from cementite to ferrite, so that the relationship in equation (6.1) does not apply; and molybdenum because the large scatter and suspicion of overlap with the sulphur K line made the data similarly unreliable, as discussed in Section 6.1. The resulting extrapolated values of cementite composition are presented in tables 6.5–6.7 for the three ageing temperatures for the fully-bainitic microstructure, and in table 6.8 for the partially-bainitic microstructure aged at 565°C.

Graphs were plotted for the data obtained for chromium and manganese (the two alloying elements which showed a statistically-significant size effect) against $(\text{time})^{1/2}$, the relationship predicted by equation (6.1) , and are presented in figure 6.4 and 6.5 for the fully-bainitic case, and figure 6.6 for the partially-bainitic case.

Ageing time (hours)	Experimental data $(c - \bar{c})$ intercepts at: 0.100μm	0.180μm	0.260μm
	CHROMIUM		
0	−0.07	0.08	0.14
2	0.05	−0.05	−0.08
6	0.71	0.37	0.24
12	0.58	0.28	0.16
24	0.17	0.32	0.37
48	0.94	0.50	0.33
96	0.81	0.56	0.46
168	1.46	0.82	0.57
336	2.02	1.40	1.17
672	2.58	1.86	1.58
1008	2.76	2.14	1.90
1344	2.84	2.18	1.92
2016	3.06	2.28	1.97
2688	3.42	2.57	2.24
4032	3.70	2.67	2.27
6240	5.07	3.81	3.32
8064	5.50	4.41	4.00
	MANGANESE		
0	0.09	−0.02	−0.06
2	−0.04	0.07	0.11
6	0.48	0.15	0.03
12	0.57	0.16	0.00
24	0.42	0.33	0.29
48	0.73	0.34	0.19
96	0.41	0.23	0.16
168	0.92	0.61	0.50
336	0.74	0.55	0.48
672	1.01	0.73	0.62
1008	0.94	0.69	0.59
1344	1.15	0.76	0.61
2016	1.28	0.83	0.66
2688	1.42	0.91	0.72
4032	1.48	1.07	0.92
6240	1.76	1.22	1.02
8064	2.27	1.63	1.38

Table 6.5: Representative experimental values for varying x_θ in Fe–Cr–Mo power plant steel aged at 510°C

Ageing time (hours)	Experimental data $(c - \bar{c})$ intercepts at: 0.100μm	0.180μm	0.260μm
	CHROMIUM		
0	0.03	0.12	0.16
1	0.40	0.55	0.60
4	0.60	0.52	0.49
8	0.81	0.43	0.28
12	0.82	0.55	0.44
24	0.94	0.63	0.52
48	1.69	1.09	0.86
96	2.28	1.60	1.35
168	2.54	1.65	1.30
336	2.66	1.84	1.52
672	3.77	2.99	2.69
1344	4.85	3.68	3.22
2688	4.55	3.45	3.03
4032	5.34	4.00	3.48
7002	6.10	4.63	4.06
	MANGANESE		
0	−0.04	0.07	0.11
1	0.19	0.23	0.25
4	0.31	0.34	0.35
8	0.39	0.28	0.24
12	0.47	0.30	0.24
24	1.05	0.38	0.12
48	1.23	0.64	0.42
96	1.38	1.03	0.89
168	1.31	0.79	0.59
336	2.08	1.32	1.03
672	1.77	1.08	0.81
1344	2.73	1.90	1.58
2688	2.82	1.90	1.55
4032	3.07	2.41	2.16
7002	3.83	3.05	2.74

Table 6.6: Representative experimental values for varying x_θ in Fe–Cr–Mo power plant steel aged at 565°C

Ageing time (hours)	Experimental data $(c - \bar{c})$ intercepts at: 0.100μm	0.180μm	0.260μm
	CHROMIUM		
0	0.01	0.09	0.11
1	0.40	0.09	−0.03
2	0.64	0.37	0.27
4	1.18	0.82	0.68
8	1.79	1.24	1.03
12	2.46	1.78	1.52
24	2.52	1.57	1.20
48	3.97	2.83	2.39
96	4.07	2.77	2.27
168	4.63	3.31	2.80
336	6.02	4.60	4.05
672	7.28	5.74	5.14
1344	7.84	6.24	5.63
2688	8.21	6.90	6.39
4032	9.27	7.90	7.37
6048	10.46	8.76	8.11
	MANGANESE		
0	−0.07	0.06	0.11
1	0.28	0.06	−0.02
2	0.29	0.16	0.10
4	0.98	0.68	0.57
8	1.02	0.58	0.41
12	1.19	0.79	0.63
24	1.44	1.05	0.91
48	1.73	1.31	1.15
96	1.14	0.74	0.59
168	2.00	1.70	1.59
336	1.98	1.50	1.32
672	2.53	1.74	1.43
1344	2.67	2.25	2.09
2688	3.51	2.77	2.48
4032	4.24	3.39	3.07
6048	4.04	3.31	3.03

Table 6.7: Representative experimental values for varying x_θ in Fe–Cr–Mo power plant steel aged at 625°C

Ageing time (hours)	Experimental data $(c - \bar{c})$ intercepts at: 0.100μm	0.180μm	0.260μm
	CHROMIUM		
0	0.02	0.19	0.26
1	0.65	0.42	0.33
2	0.37	0.34	0.33
4	0.90	0.78	0.74
12	1.13	0.78	0.65
24	1.62	1.26	1.12
48	2.63	1.68	1.32
96	3.62	2.46	2.02
168	4.55	3.24	2.73
336	5.28	3.72	3.12
672	5.16	4.23	3.87
1344	6.44	4.46	3.69
2688	7.01	5.42	4.81
5376	8.12	6.15	5.39
	MANGANESE		
0	−0.10	0.07	0.14
1	0.43	0.40	0.39
2	0.36	0.30	0.27
4	0.33	0.31	0.31
12	0.55	0.35	0.28
24	1.17	0.92	0.82
48	1.35	0.69	0.44
96	1.35	0.87	0.68
168	1.76	1.03	0.75
336	2.40	2.03	1.88
672	3.00	2.61	2.47
1344	3.27	2.40	2.07
2688	3.28	2.40	2.05
5376	4.29	3.62	3.36

Table 6.8: Representative experimental values for varying x_θ in Fe–Cr–Mo power plant steel with a mixed starting microstructure aged at 565°C

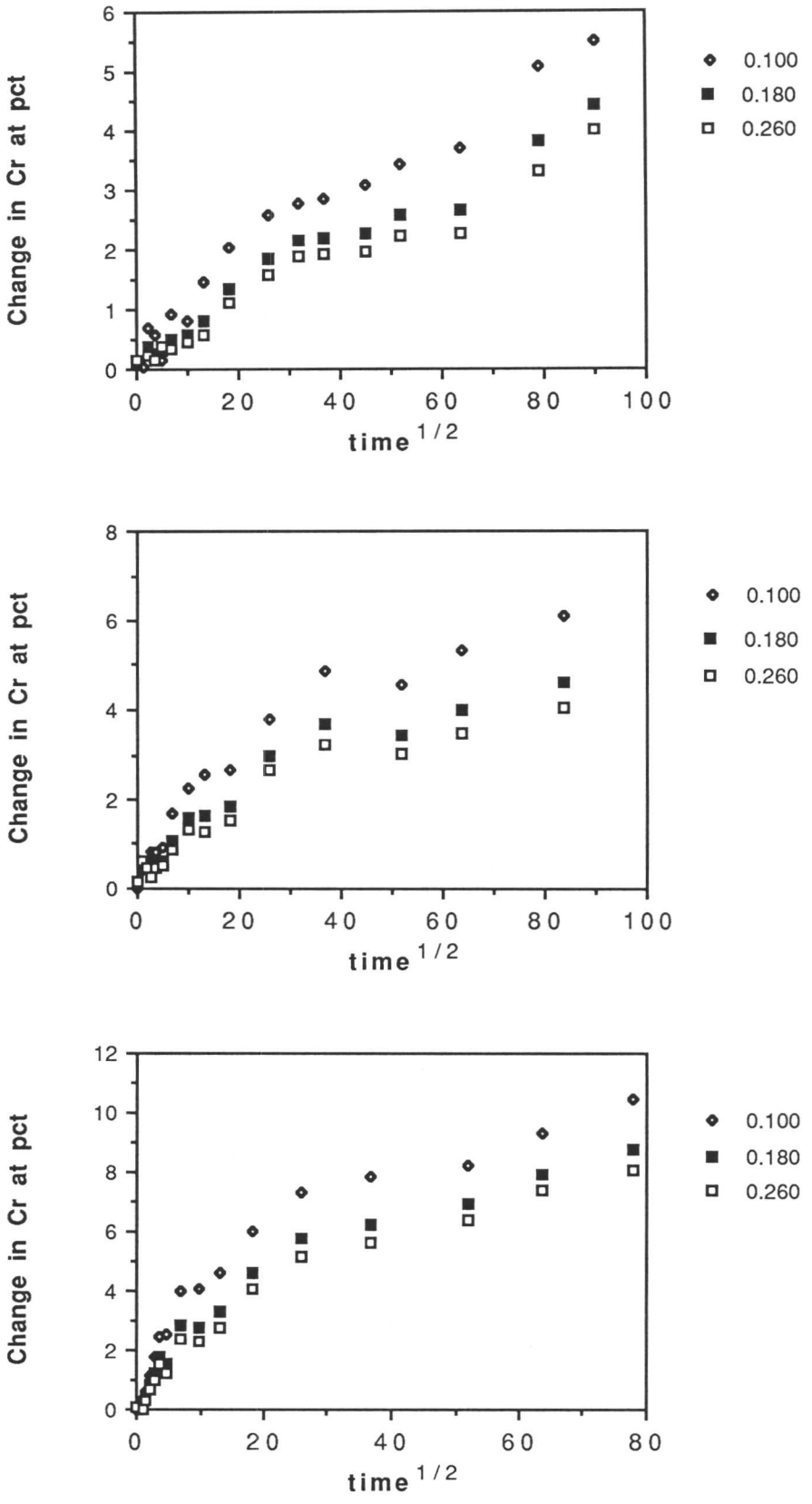

Figure 6.4: A representation of experimental data for chromium enrichment compared for varying x_θ in the fully-bainitic 1Cr–$\frac{1}{2}$Mo type power plant steel

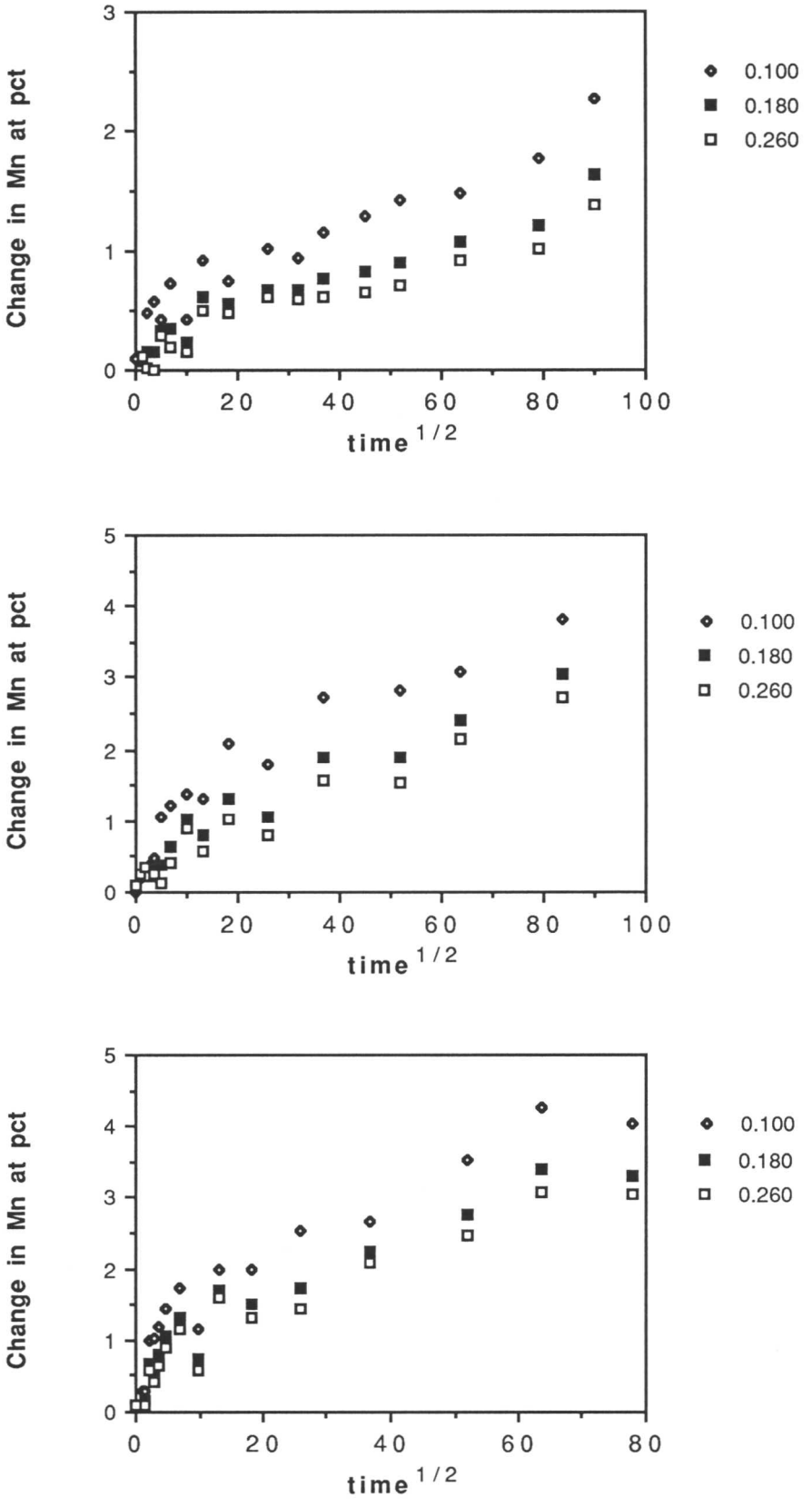

Figure 6.5: A representation of experimental data for manganese enrichment compared for varying x_θ in the fully-bainitic 1Cr–$\frac{1}{2}$Mo type power plant steel

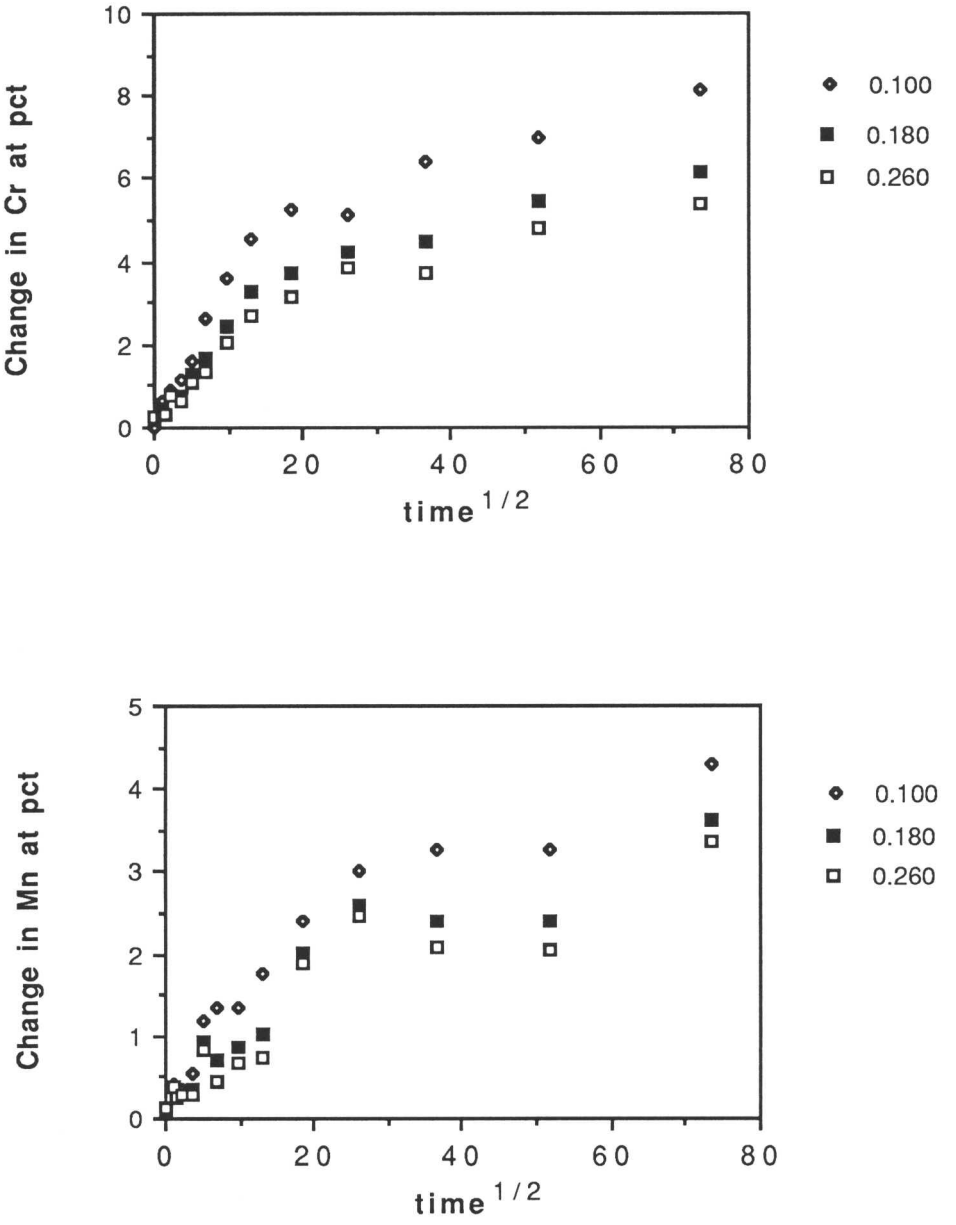

Figure 6.6: A representation of experimental data for the enrichment of cementite with chromium and manganese compared for varying x_θ in the ferritic/bainitic 1Cr–$\frac{1}{2}$Mo type power plant steel

6.2.5 Summary

This analysis provides an illustration that the size effect predicted by equation (6.1) is present in the experimental data for this alloy. The correlation of experimental data to theory generally increases as ageing time is increased. At longer ageing times, especially at the higher temperature, there is a tendency for the correlation to get slightly poorer, which suggests that the approximations in the analytical model are beginning to break down, but in general the fit with equation (6.1) is reasonable, and a statistically-significant $(c - \bar{c}) \propto x_\theta^{-1}$ relationship has been shown for the ageing data in this alloy.

6.3 Variation of c^θ with Time: Analytical Approach

6.3.1 Analysis of results

It is evident from equation (6.1) and equation (6.2) that the analytical model for diffusion-controlled enrichment of cementite predicts a variation of cementite composition with $(\text{time})^{1/2}$ for a constant x_θ, and that this is at variance with industrial practice, in which an empirical $(\text{time})^{1/3}$ relationship is generally applied. The collected data are analysed here for both relationships. A further regression analysis is performed for the more rigorous relationship derived from equation (6.1), which suggests the mean value of the product of composition change and particle size, $\Sigma(c - \bar{c})(x_\theta)/N$, where N is the number of individual particles measured, at a given time, should vary as $(\text{time})^{1/2}$; $\Sigma(c - \bar{c})(x_\theta)/N$ is not analysed against $(\text{time})^{1/3}$ as such a relationship could have no physical significance. The correlation between experimental data and the theoretical model, together with that for the empirical method, is presented in table 6.9 below. Graphical representations of composition change versus $(\text{time})^{1/2}$ for the four temperature/microstructure combinations are presented in figures 6.7–6.10.

It can be seen from the figures and the table that the collected mean composition data generally fits the linearity with $(\text{time})^{1/2}$ predicted by equation (6.2) better at short and medium ageing times. For the longest ageing times at higher

temperatures there is a tendency to deviation from this linearity. This may well be indicative of the onset of significant levels of soft impingement between the diffusion fields of different cementite particles, which would be expected to be of greater importance under conditions of increased ageing temperature and time, but which cannot be predicted by the analytical model. Such effects would reduce the diffusion rate in ferrite, and hence the rate of enrichment, so that a composition versus $(\text{time})^n$ relationship would tend in practice to fit $n > 2$. This may explain why the purely empirical $(\text{time})^{1/3}$ relationship frequently used in industrial practice met with some success.

It has been noted that in the case of the mixed microstructure, the increase in the effective carbon composition, and hence V_θ, which is caused by partition of that element into the retained austenite when the allotriomorphic ferrite forms, and the concomitant reduction in x_α, would be expected to lead to an earlier significant soft impingement effect. It is evident that this deviation from a strict $(\text{time})^{1/2}$ is especially marked in the case of the mixed microstructure (figure 6.10), which supports the supposition that a slowing down of diffusion rates within ferrite due to soft impingement is a factor in the observed non-linearity at longer ageing times.

It can be noted from table 6.9 that correlation to both $(\text{time})^n$ relationships is fairly similar. On the basis of this simple analysis alone no conclusion could rigorously be made within meaningful confidence limits. Nevertheless, when account is taken of the slight variation in x_θ between different samples (*i.e.,* the data are analysed for a $\Sigma(c-\bar{c})(x_\theta)/N$ vs $(\text{time})^{1/2}$ relationship), the agreement is consistently better than it is with $(\text{time})^{1/3}$.

It appears that equation (6.1) describes the experimental situation rather well. Chromium and manganese are found to show better correlation to theory than molybdenum, suggesting that the larger degree of scatter in the molybdenum composition measurement has once more led to a less conclusive result for that element.

Ageing temp. °C	R^2 correlation of experimental data to: $(c-\bar{c})$ v. $t^{1/2}$	$(c-\bar{c})x_\theta$ v. $t^{1/2}$	$(c-\bar{c})$ v. $t^{1/3}$
	(chromium)		
510	0.96	0.97	0.97
565	0.89	0.95	0.94
625	0.88	0.93	0.91
565 30% α_b	0.86	0.91	0.93
	(manganese)		
510	0.93	0.97	0.95
565	0.94	0.96	0.86
625	0.88	0.92	0.88
565 30% α_b	0.87	0.90	0.92
	(molybdenum)		
510	0.64	0.70	0.61
565	0.61	0.73	0.58
625	0.64	0.59	0.57
565 30% α_b	0.58	0.63	0.51

Table 6.9: Correlation coefficients between experimental data for the Fe–Cr–Mo Steel and the three methods to analyse $(c-\bar{c})$ versus a function of (time)

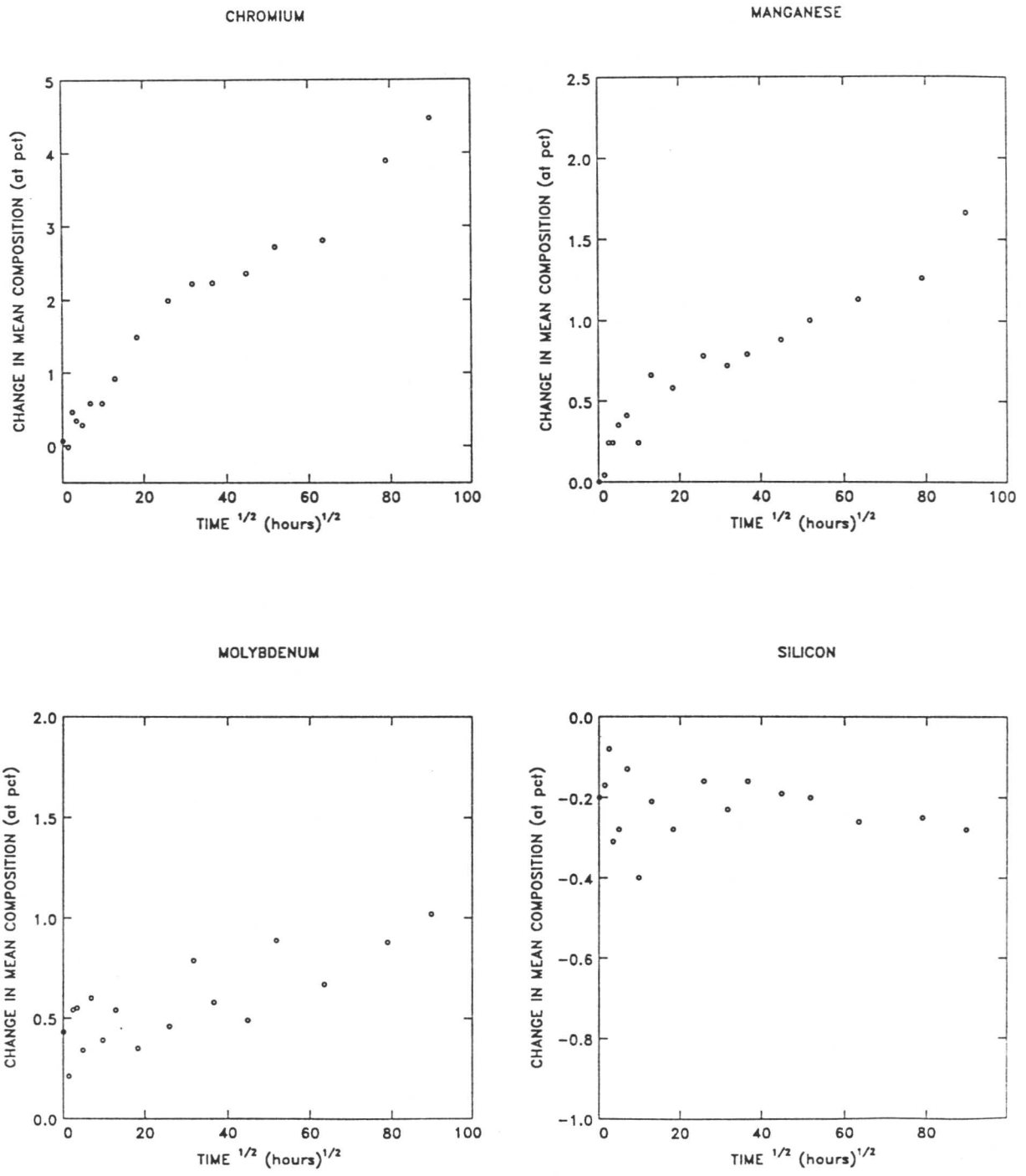

Figure 6.7: Mean $(c - \bar{c})$ versus ageing time for the Fe–Cr–Mo power plant steel, initially having a fully-bainitic starting microstructure, aged at 510°C.

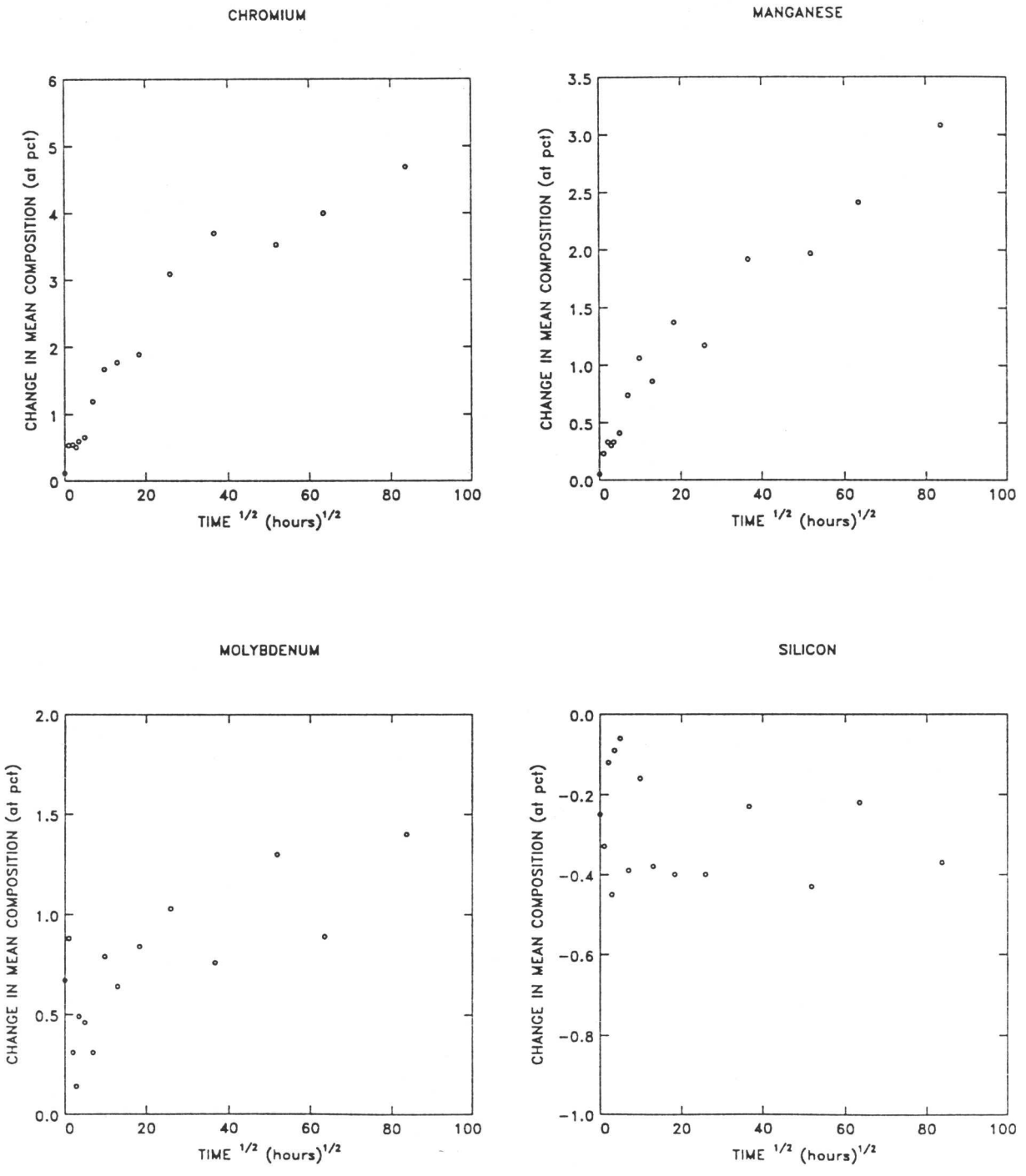

Figure 6.8: Mean $(c - \bar{c})$ versus ageing time for the Fe–Cr–Mo power plant steel, having a fully-bainitic starting microstructure, aged at 565°C.

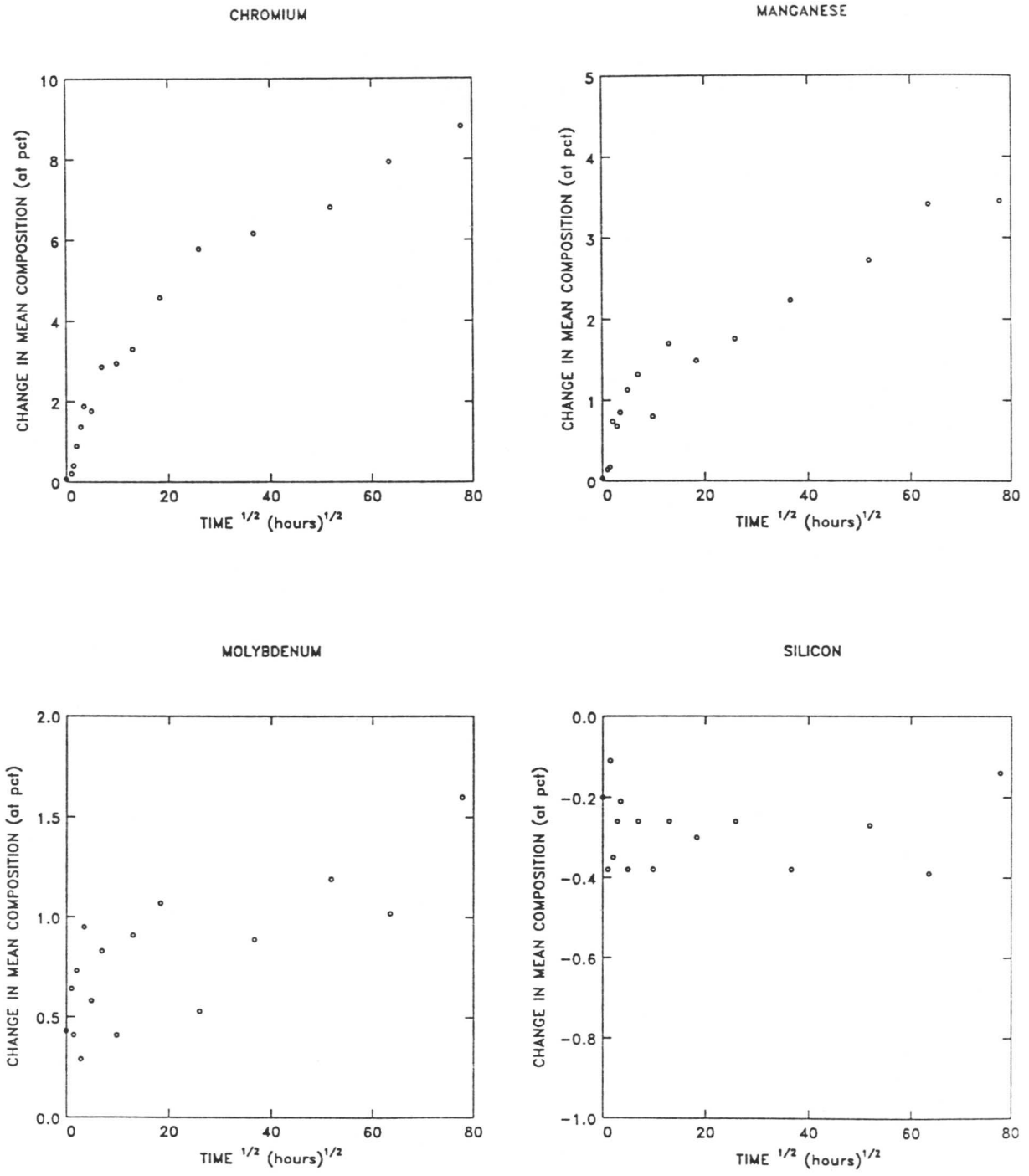

Figure 6.9: Mean $(c - \bar{c})$ versus ageing time for the Fe–Cr–Mo power plant steel, having a fully-bainitic starting microstructure, aged at 625°C.

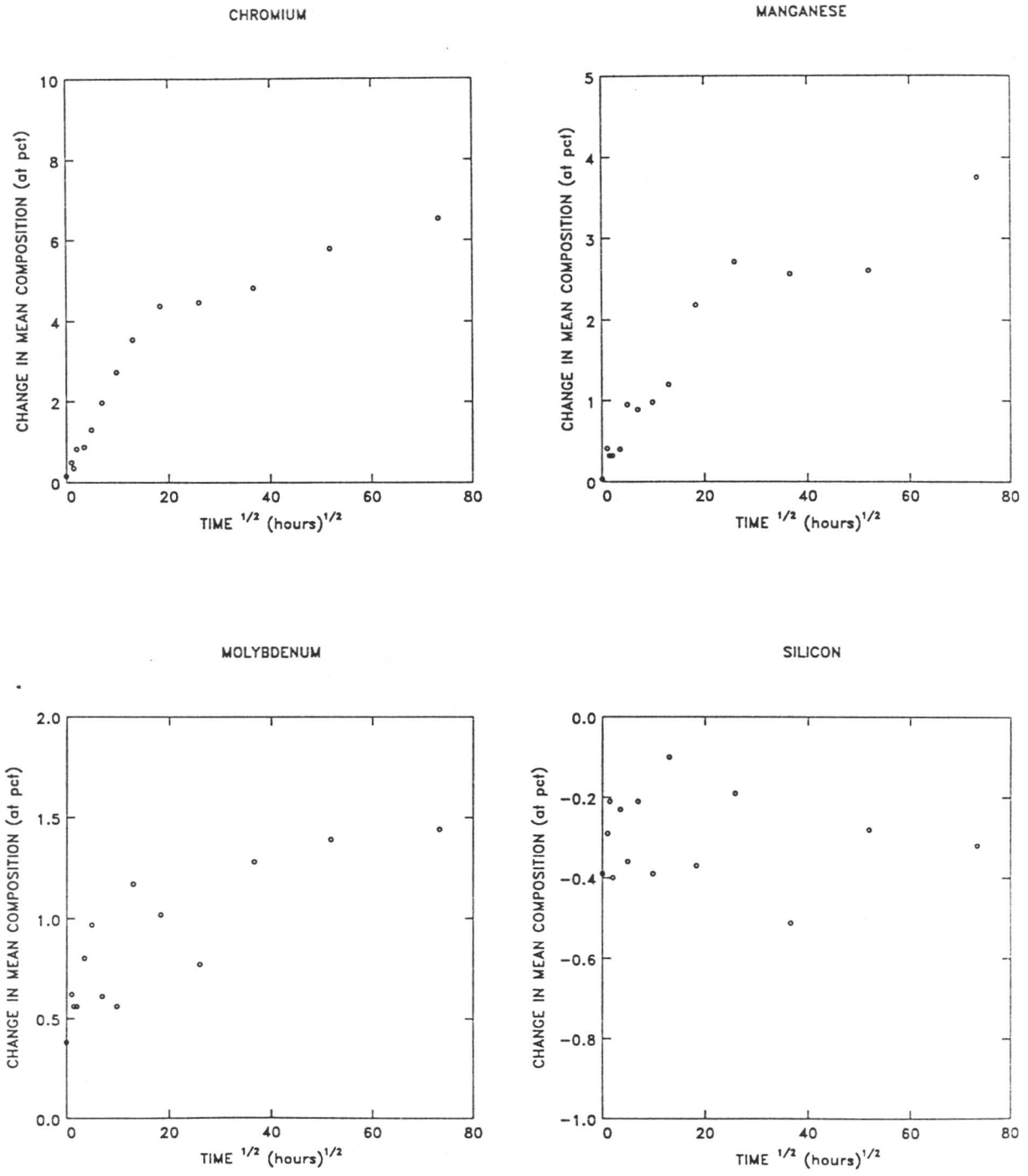

Figure 6.10: Mean $(c - \bar{c})$ versus ageing time for the Fe–Cr–Mo power plant steel, initially having a mixture of allotriomorphic ferrite and bainite as a starting microstructure, aged at 565°C.

6.3.2 Diffusion coefficients

Rearranging equation (6.1) enables the gradient of the $(c-\bar{c})(x_\theta)$ versus $(\text{time})^{1/2}$ graph to be used to produce values for the diffusion coefficient of the alloying elements under consideration:

$$x_\theta(\bar{c} - c^\theta) = \frac{4D^{1/2}(c^{\alpha\theta} - \bar{c})t^{1/2}}{\pi^{1/2}} \tag{6.3}$$

$\Rightarrow$ gradient of $(c - \bar{c})(x_\theta)$ v. $t^{1/2}$ line:

$$\frac{4D^{1/2}(c^{\alpha\theta} - \bar{c})}{\pi^{1/2}} \tag{6.4}$$

In a general case, if the partition coefficient for a given element Z between cementite and ferrite (k_z) is known, a value for $c^{\alpha\theta}$ can be calculated from equation (6.5) and equation (6.6) with V_θ, the volume fraction of cementite, being calculated from the lever rule assuming a stoichiometric carbon concentration in cementite.

$$\bar{c} = c^{\theta\alpha}V_\theta + (c^{\theta\alpha}/k_z) - (c^{\theta\alpha}V_\theta/k_z) \tag{6.5}$$

$$k_z = \frac{c^{\theta\alpha}}{c^{\alpha\theta}} \tag{6.6}$$

However, in the case of the power plant material, equilibrium cementite and ferrite compositions and volume fractions were calculated using the MTDATA computer package which was developed by the National Physical Laboratory (NPL). The method used by the MTDATA package involves a large database of accurate composition measurements from simple, extensively-studied systems, from which data for more complex systems are extrapolated. The results obtained by applying this method to the four temperature/microstructure combinations under test are presented in table 6.10. Two values of $c^{\theta\alpha}$ (in atomic percent) are presented: $c^{\theta\alpha}_{sub}$ is the equilibrium concentration of an element in cementite as a percentage of the total substitutional content only, and $c^{\theta\alpha}_{all}$ is the

concentration including carbon; hence, it is the former value which corresponds to the method used for presenting the experimental data.

It should be noted that the values for the bainitic region of the mixed microstructure were generated by assuming that all of the carbon had partitioned to that region when allotriomorphic ferrite formed, but that the relative proportions of substitutional elements had remained the same.

Temp (K)	Element	V_θ (pct)	equilibrium compositions				
			weight pct		atomic pct		
			$c^{\alpha\theta}$	$c^{\theta\alpha}$	$c^{\alpha\theta}$	$c^{\theta\alpha}_{all}$	$c^{\theta\alpha}_{sub}$
783	chromium	1.67	0.34	30.2	0.36	25.9	34.5
	manganese		0.30	11.9	0.31	9.7	12.9
	molybdenum		0.43	4.3	0.25	2.1	2.8
838	chromium	1.66	0.43	25.3	0.46	21.7	29.0
	manganese		0.35	9.3	0.36	7.6	10.1
	molybdenum		0.43	4.2	0.25	2.0	2.6
898	chromium	1.63	0.52	20.7	0.55	17.8	23.8
	manganese		0.40	6.9	0.40	5.6	7.5
	molybdenum		0.44	3.8	0.26	1.8	2.4
838	chromium	5.63	0.19	11.3	0.20	9.9	13.2
30% α_b	manganese		0.18	4.4	0.19	4.6	6.1
	molybdenum		0.24	4.4	0.14	2.1	2.8

Table 6.10: Calculated equilibrium compositions for a cementite/ferrite mixture in the Fe–Cr–Mo power plant steel at the temperatures used for ageing

Substituting values for these parameters into equation (6.3) generates experimental measurements for D_{Cr} and D_{Mn}, which are presented in table 6.11 and table 6.12. The scatter in the EDX data for molybdenum and silicon is such that meaningful diffusion coefficients cannot be obtained from this approach. These are compared with the reported values for tracer diffusion coefficients (obtained from the 57th edition of the CRC handbook) (see the tables). Fair agreement is found between the experimentally-determined and published values for both chromium and manganese at all three temperatures.

The simple analytical method used to generate these values is only valid before soft impingement occurs in the ferrite. In calculating diffusion coefficients, only those values of $(c-\bar{c})(x_\theta)$ prior to soft impingement should be used, but the analytical model makes no prediction of the time when soft impingement starts to be of substantive influence on the ageing process. It was decided that, in the $(c-\bar{c})(x_\theta)$ versus $(\text{time})^{1/2}$ plot at 625°C, where appreciable deviation from linearity at the longest ageing time suggested the possibility of soft impingement, diffusion coefficients should be calculated using data from the linear region only (which in all cases is the major part of the data), disregarding those points at longer ageing times where a slowing down of the enrichment rate suggests a soft impingement regime to which the model does not apply.

A more representative interdiffusion coefficient is also calculated using a procedure described by Fridberg *et al.* (1969). They propose that for practical purposes the diffusion coefficient of an alloying element can be described by the self diffusion coefficient of iron modified by a scale factor independent of temperature, but varying regularly with atomic number. This method produces values for the interdiffusion coefficient which are given in table 6.11 and table 6.12.

These calculated values are in good agreement with that derived from the experimental data and equation (6.1), indicating that the experimental regime so far is one for which equation equation (6.1) holds.

A similar analysis can be performed on the measured x_θ data using equation (6.7), which provides a value for the diffusion coefficient based on coarsening theory:

$$D = \frac{(r^3 - r_0^3)9RT}{8\sigma^{\theta\alpha}c^{\alpha\theta}V_\theta t} \tag{6.7}$$

where r is the particle size, r_0 is the initial particle size, and $\sigma^{\theta\alpha}$ is the surface energy, taken from Puls and Kirkaldy (1972) to be $0.7\,\text{Jm}^{-2}$. These calculated values are also presented in the tables.

When the experimental data are used in this equation, the calculated diffusion coefficients differ from the reported values by at least an order of magni-

Method of calculation	Diffusion coefficients (m^2s^{-1}) at 510°C	at 565°C	at 625°C
Experimental (equation (6.3))			
all α_b:	1.19×10^{-20}	7.07×10^{-20}	3.11×10^{-19}
30% α_b:	-	9.36×10^{-20}	-
Interdiffusion (from Fridberg)	1.22×10^{-20}	1.37×10^{-19}	1.37×10^{-18}
Tracer (from CRC)	2.26×10^{-20}	2.56×10^{-19}	2.57×10^{-18}
coarsening theory	3.83×10^{-21}	6.22×10^{-21}	9.79×10^{-21}

Table 6.11: Analysis of $(c - \bar{c})(x_\theta)$ versus $(\text{time})^{1/2}$ plot for chromium in the Fe–Cr–Mo power plant steel

Method of calculation	Diffusion coefficients (m^2s^{-1}) at 510°C	at 565°C	at 625°C
Experimental (equation (6.3))			
all α_b:	1.58×10^{-20}	9.97×10^{-20}	3.77×10^{-19}
30% α_b:	-	8.76×10^{-20}	-
Interdiffusion (from Fridberg)	9.50×10^{-21}	1.07×10^{-19}	1.06×10^{-18}
Tracer (from CRC)	7.77×10^{-20}	7.11×10^{-19}	5.85×10^{-18}
coarsening theory	3.92×10^{-21}	6.45×10^{-21}	1.21×10^{-20}

Table 6.12: Analysis of $(c - \bar{c})(x_\theta)$ versus $(\text{time})^{1/2}$ plot for manganese in the Fe–Cr–Mo power plant steel

tude; indeed, with the mixed-microstructure data, no coarsening was observed, so that this calculation is meaningless. As expected, this suggests that diffusion of substitutional alloying elements from the supersaturated ferrite phase is the dominant process, with cementite coarsening theory inapplicable in this case.

The process being studied here is really one where the cementite and ferrite are approaching their equilibrium compositions.

6.4 Theoretical Modelling of the Ageing Process

6.4.1 Correlation of experimental data to the $(c - \bar{c}) \propto 1/x_\theta$ *relationship*

As noted above, a consistent increase in the expected composition change versus particle size correlation is observed, but with the correlation coefficient only rising to around 0.5 after many weeks of ageing treatment. Based on intuition, the correlation coefficient was expected to rise rapidly once the mean solute content of the particles rose to levels above which the variations noted in c_θ at time = 0 for different particles became negligible. This expectation that the correlation coefficients should rapidly approach unity was tested by the development of a simple computer model for the ageing process.

The computer model of the ageing problem utilized a large (400 point) starting dataset of a distribution of cementite sizes and compositions in keeping with the initial size and composition distributions measured from as-transformed and unaged specimens. The data points are then 'aged' by the computer program in accordance with equation (6.3). The program then selects random selection of a point from the set of 'aged particles' 30 times in order to simulate experimental procedure, and derives the mean composition ($\Sigma(c_\theta - \bar{c})/n$) and the correlation coefficient of the data to the $(c - \bar{c}) \propto 1/x_\theta$ relationship. When this procedure is carried out for a whole series of time periods, and the data analysed along the same lines as the real experimental data, the model predicts a correlation coefficient for the $(c - \bar{c}) \propto 1/x_\theta$ relationship which rises rapidly to unity as soon as $(c - \bar{c})$ becomes large relative to the observed random variation in c_θ at zero time. The approach of the correlation coefficient to unity when the model is applied is found to be much more rapid in the model than in the experimental case, suggesting that another contributory factor exists in practice.

6.4.2 Statistical scatter in EDX readings

The nature of energy dispersive X-ray analysis is that the signal is produced when electrons within the atoms of the material under test, which have been energized into an excited state, return to their ground state in a process which is stochastic. The result therefore suffers from an unavoidable statistical error, though this can be minimized by detecting a large number of events. It is, however, impractical to collect data for excessively prolonged periods in order to accumulate a large signal to reduce the error, especially in programmes such as the current one when a large number of particles has to be analysed; the period of time over which events are observed must, of necessity, be a compromise between accuracy and practicality.

If our computer model is to be relatable to the practical situation, it must include a statistical noise to allow for the fact that the analysed chemistry of a given particle does not necessarily correspond to its true chemistry. This statistical scatter is assumed to have a normal distribution about the calculated true cementite composition, and a standard deviation of 0.5 at. % for chromium and manganese, 0.8 for molybdenum and 0.5 for silicon. These values for the standard deviation were chosen on the basis of experimental data gathered by repeated analysis of a single particle. The analysis illustrates that a scatter of this order of magnitude was inherently associated with the EDX technique, and the observed data showing statistical scatter are presented on figure 6.11. The program used to generate the data is included for reference in Appendix 2.

6.4.3 Data generated using the computer model

The new computer-generated data which included an allowance for the statistical scatter inevitable to the technique were interpreted using the regression procedures described earlier in the same way as the experimentally-obtained compositions had been. Thence, a comparison was made with the earlier computer-generated data where no such allowance for statistical scatter had been made, and with the compositions obtained experimentally.

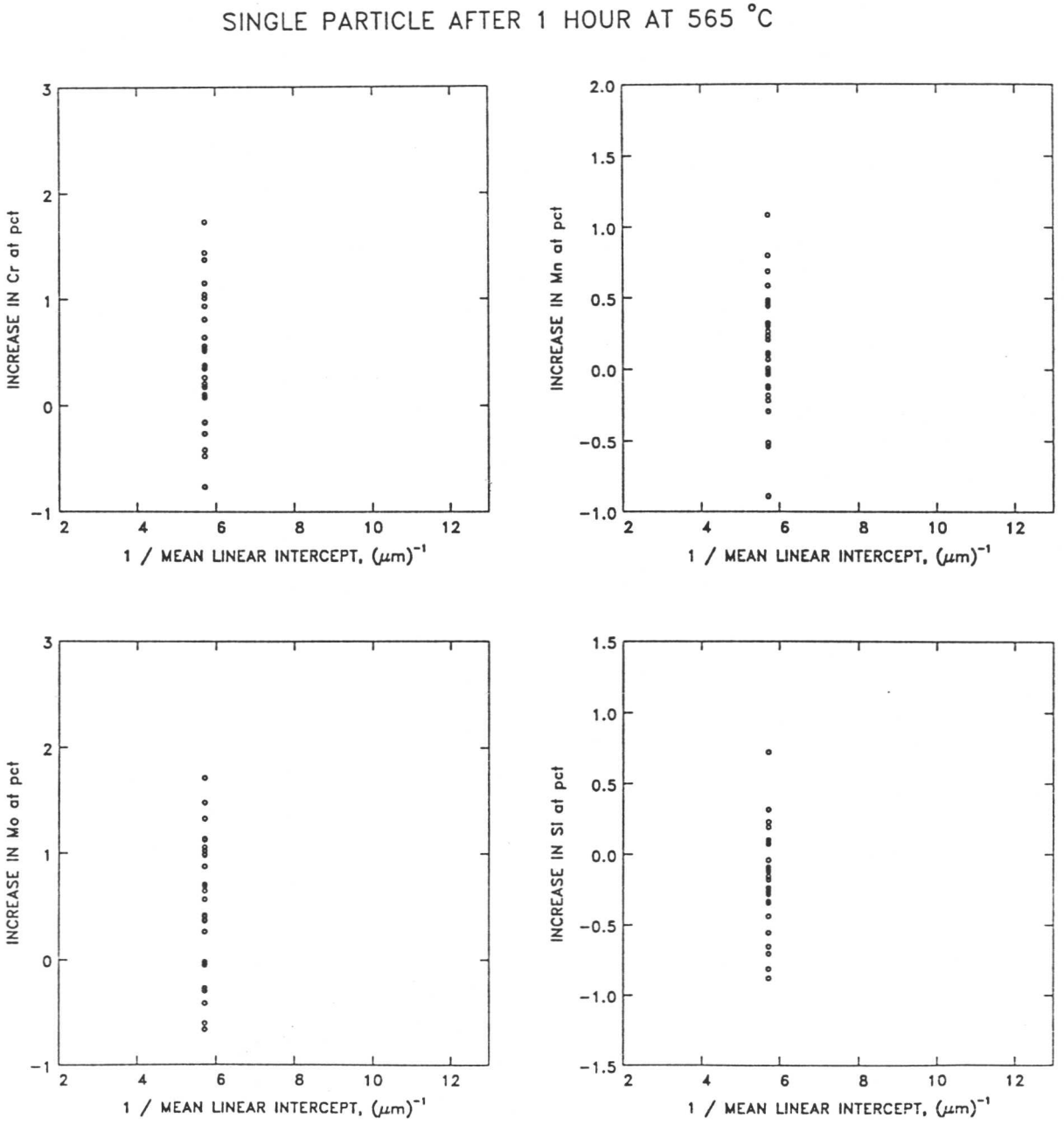

Figure 6.11: Repeated microanalysis on single particle to illustrate the statistical scatter inherent in the EDX technique

Regression analyses on the computer-generated data including scatter produced results very similar to those produced when experimental compositions were analysed, and were found to be in much better agreement with the experimental data than the computer-generated data without a statistical scatter element had been. Correlation coefficients for the $c - \bar{c}$ versus $1/x_\theta$ relationship can be obtained by carrying out the regression analysis on the compositional data obtained from both computer models. An expected value for the correlation coefficient at a particular ageing time, given the assumption that equation (6.3) holds but is masked to some degree by this statistical scatter, can be generated by repeating the regression procedure a number of times for computer-generated compositions for each ageing time, and taking the mean value of the correlation coefficients thus produced. These values, along with those obtained from experimental concentration measurements, are presented in figure 6.12–6.14.

It is of great significance that the correlation coefficients obtained from analysis of the experimental data and the computer-generated, with-scatter data are so similar, except at the longest ageing times and higher temperatures. In effect, this means that the experimental data is almost entirely explained by two factors: the size effect predicted in equation (6.2), and a statistical scatter in the EDX technique which has been both observed experimentally and modelled here.

The results demonstrate clearly that a strong particle size effect exists, whereby enrichment occurs at a faster rate when the cementite particle size is diminished. The strength of this effect is, however, masked by a statistical scatter in the microanalysis technique, especially when $(c^\theta - \bar{c})$ is relatively small.

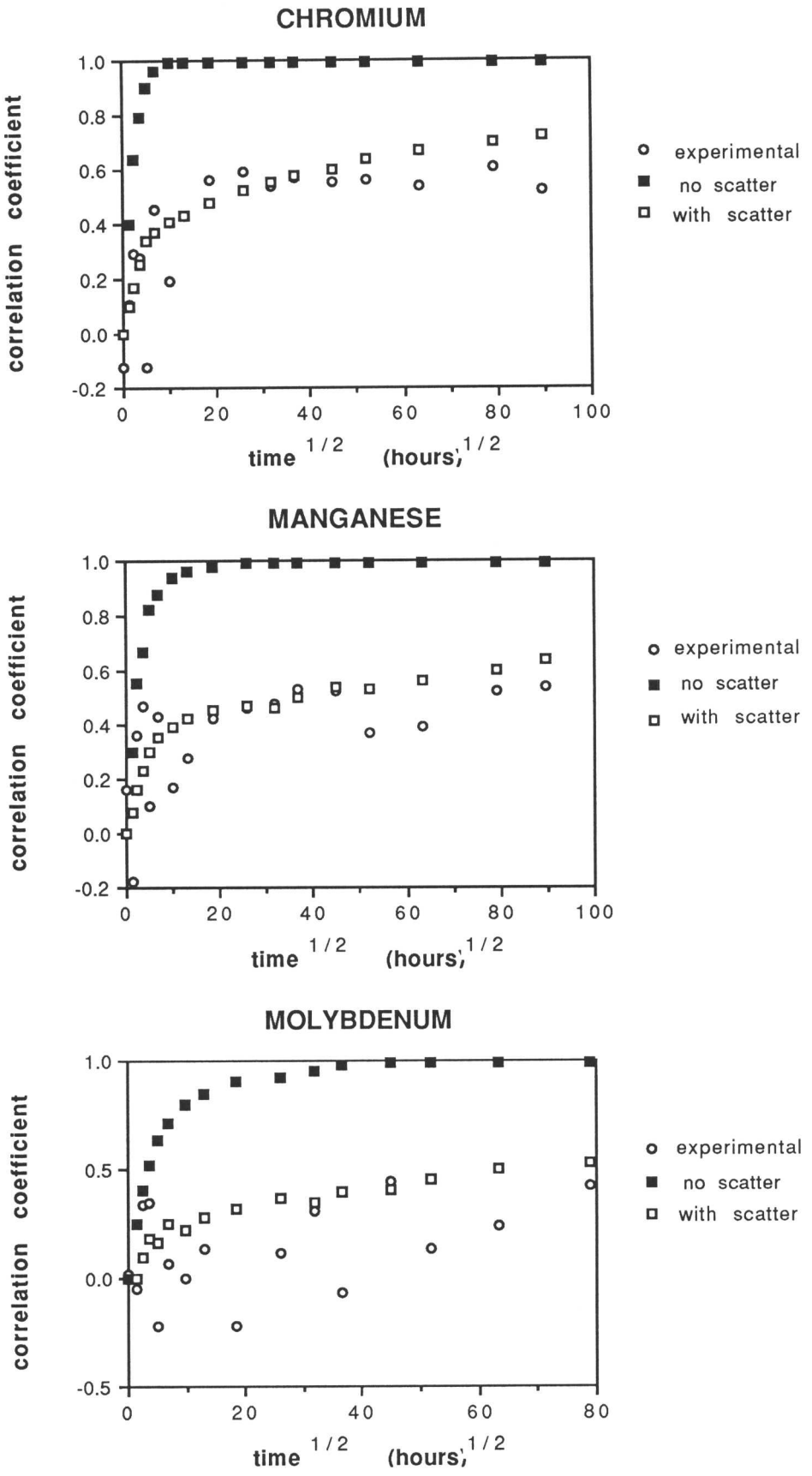

Figure 6.12: A comparison of correlation coefficients for the $(c - \bar{c}) \propto 1/x_\theta$ relationship obtained experimentally and generated by the computer model for an ageing temperature of 510°C

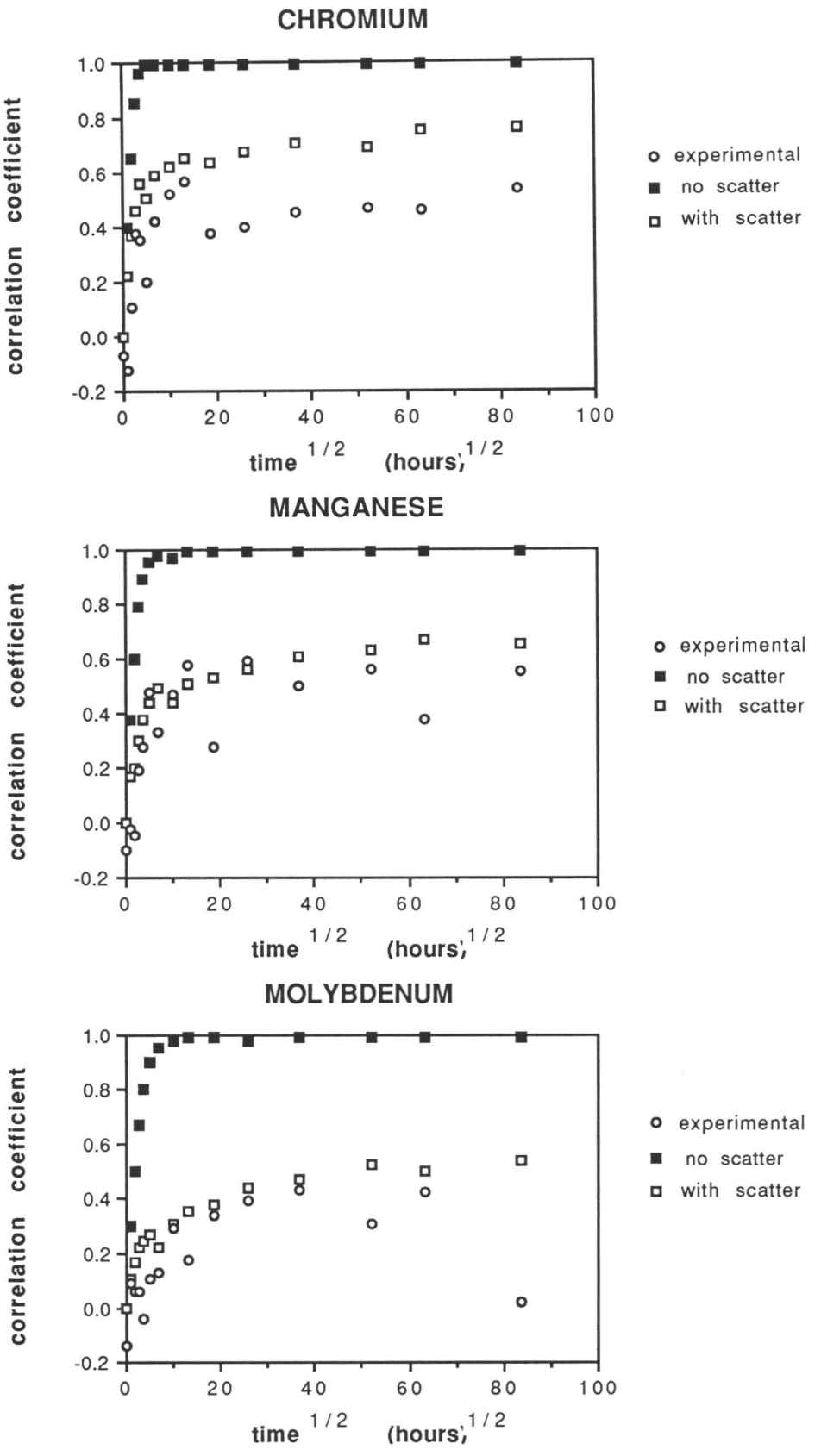

Figure 6.13: A comparison of correlation coefficients for the $(c - \bar{c}) \propto 1/x_\theta$ relationship obtained experimentally and generated by the computer model for an ageing temperature of 565°C

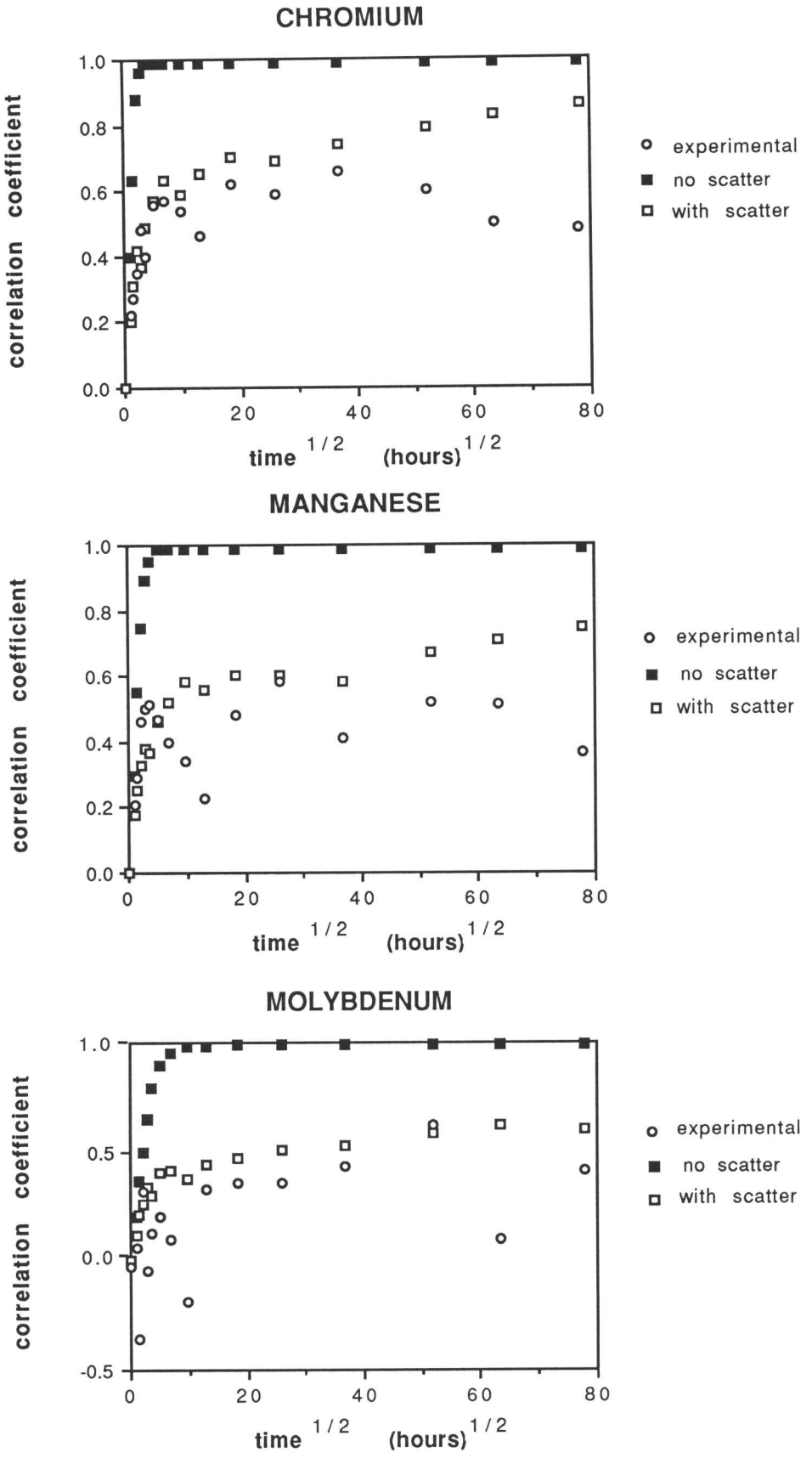

Figure 6.14: A comparison of correlation coefficients for the $(c - \bar{c}) \propto 1/x_\theta$ relationship obtained experimentally and generated by the computer model for an ageing temperature of 625°C

6.5 A Finite Element Analysis of the Ageing Process

6.5.1 Limitations of the analytical method

The current work and Bhadeshia's analysis (1989) of existing data have shown that an analytical model for the behaviour of bainitic cementite during ageing shows a reasonable agreement with experimental data, and, in particular, is an improvement on the largely empirical methods used formerly. Nevertheless, the analytical method fails to consider two important factors in a diffusion process. First, at longer ageing times the diffusion fields within ferrite associated with different cementite particles will overlap to a degree which will eventually have a significant effect on the enrichment rate, by slowing down the rate-controlling process of diffusion in ferrite. This phenomenon is referred to a soft impingement. Second, the analytical approach does not allow for a coupling of the fluxes in the two phases. As a result, a numerical method which produces a representation of the concentration profile with time and distance, and couples the fluxes across the α/θ interface is to be preferred. Bhadeshia (1989) uses a finite difference approach to achieve this, based on a procedure from Crank (1975).

6.5.2 The finite difference model

The material is treated as a complete diffusion couple between a slab of cementite of thickness x_θ, and a slab of ferrite of thickness x_α, such that:

$$\frac{x_\theta}{(2x_\alpha + x_\theta)} = V_\theta \tag{6.8}$$

Bhadeshia notes that V_θ, the volume fraction of cementite, can be calculated by application of the lever rule to $\bar{c}$ and the $\alpha/\alpha+\theta$ and $\theta/\alpha+\theta$ phase boundaries in the iron carbon system as:

$$V_\theta = \frac{(\bar{c} - c^{\alpha\theta})}{(c^{\theta\alpha} - c^{\alpha\theta})} \tag{6.9}$$

with $\bar{c}$, $c^{\theta\alpha}$, and $c^{\alpha\theta}$ representing the same values as they did in the analytical approach. However, values for V_θ have already been produced using the MTDATA package, and these are used in the subsequent analysis.

Crank (1975) notes that the use of non-dimensional variables in analytical solutions frequently leads to simplification of subsequent computation. He proposes that suitable variables for a plane sheet of thickness l would be of the form $X = x/l$, $T = Dt/l^2$, and $C = c/c_0$. In consequence, Bhadeshia proposes the following for the case of cementite in ferrite:

Distance	$X = x/x_\theta$	(6.10)
Concentration	$C = c/\bar{c}$	(6.11)
Time	$T' = Dt/(x_\theta)^2$	(6.12)

Hence, a non-dimensional version of the diffusion equation,

$$\frac{\partial c}{\partial t} = D\frac{\partial^2 c}{\partial x^2} \tag{6.13}$$

can be produced:

$$\frac{\partial C}{\partial T'} = \frac{\partial^2 C}{\partial X^2} \tag{6.14}$$

The analysis divides ferrite and cementite into a notional number of small slices, so that the X–T' space consists of a grid of rectangles of side lengths δX and $\delta T'$, as figure 6.15. Each grid point can be given the coordinates $\{i\delta X, j\delta T'\}$, at which the normalized composition is $C_{i,j}$. The Crank method uses Taylor series expansions of the normalized diffusion equation (6.14), so that:

$$C_{i,j+1} = C_{i,j} + \delta T'\left(\frac{\partial C}{\partial T'}\right)_{i,j} + 1/2(\delta T')^2\left(\frac{\partial^2 C}{\partial T'^2}\right)_{i,j} + \ldots \tag{6.15}$$

from which it follows that:

$$\left(\frac{\partial C}{\partial T'}\right)_{i,j} = \frac{C_{i,j+1} - C_{i,j}}{\delta T'} + O(\delta T') \tag{6.16}$$

where $O(\delta T')$ signifies that the leading term to have been neglected in producing the above by dividing through the previous equation is of the order of $\delta T'$.

Similarly, Taylor series expansions of equation (6.14) in the X direction for constant T' produce:

$$C_{i+1,j} = C_{i,j} + \delta X \left(\frac{\partial C}{\partial X}\right)_{i,j} + 1/2(\delta X)^2 \left(\frac{\partial^2 C}{\partial X^2}\right)_{i,j} + \ldots \tag{6.17}$$

$$C_{i-1,j} = C_{i,j} - \delta X \left(\frac{\partial C}{\partial X}\right)_{i,j} + 1/2(\delta X)^2 \left(\frac{\partial^2 C}{\partial X^2}\right)_{i,j} - \ldots \tag{6.18}$$

On adding the above:

$$\left(\frac{\partial^2 C}{\partial X^2}\right)_{i,j} = \frac{C_{i+1,j} - 2C_{i,j} + C_{i-1,j}}{(\delta X)^2} + O(\delta X)^2 \tag{6.19}$$

Bhadeshia (1989) notes that in the materials and at the temperatures under consideration, partition coefficients are large, so that the redistribution of elements is controlled by rate of diffusion in ferrite to the α/θ interface, except at very long times where c^θ approaches saturation. Equations (6.16) and (6.19) may then be substituted into the non-dimensional diffusion relationship (equation 6.14), to give an explicit finite difference formula for the rate-controlling case of diffusion in ferrite:

$$C^\alpha_{1,j+1} = C^\alpha_{i,j} + r(C^\alpha_{i-1,j} - 2C^\alpha_{i,j} + C^\alpha_{i+1,j}) \tag{6.20}$$

where $r = \delta T'/(\delta X)^2$. The value of r is determined in a semi-empirical way as a compromise between accuracy and computing time; Bhadeshia sets it to 0.4.

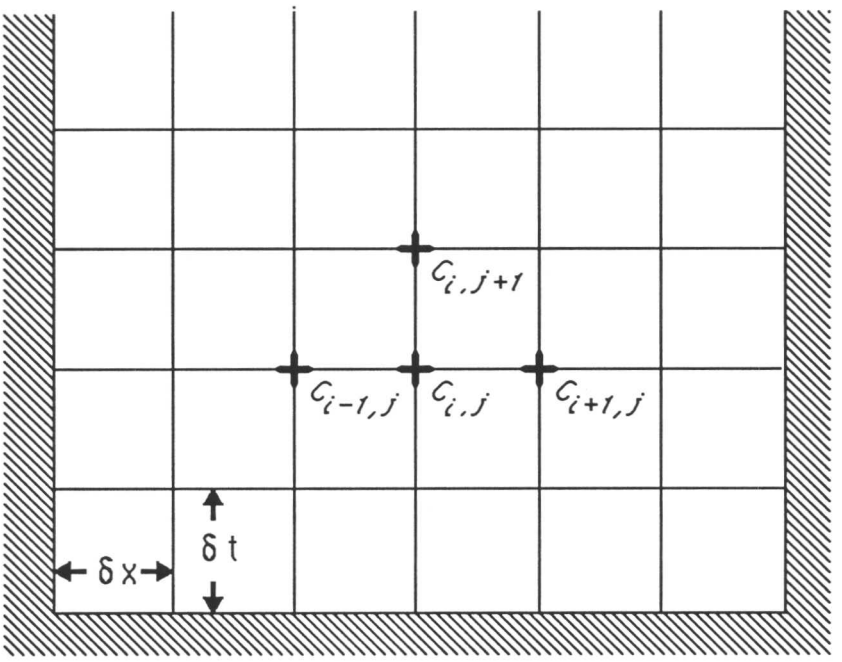

Figure 6.15: Representation of compositions in the X–T' space (Crank, 1975)

A computer program was then developed to use the above equation to determine $C_{i,j}$ for times up to the ageing time required. Initial conditions were set such that $C^{\alpha}_{i,0}$ was $c^{\alpha\theta}/\bar{c}$ for $i = 0$, and 1 for all $i > 0$. This is a satisfactory approximation when T' is small relative to ageing time, as the algorithm quickly produces a realistic composition profile; however, if the normalized time slice is large (at low temperatures), it may not be appropriate. The program couples diffusion processes in cementite and ferrite to ensure no build up of solute at the interface, *i.e.*, $C^{\theta}_{0,j}$ is determined by:

$$D_{\theta}(C^{\theta}_{0,j} - C^{\theta}_{1,j}) = D_{\alpha}(C^{\alpha}_{1,j} - C^{\alpha}_{0,j}) \tag{6.21}$$

where D_{θ} and D_{α} are the diffusion coefficients in cementite and ferrite which this analysis assumes to be equal, $C^{\theta}_{0,j}$ and $C^{\alpha}_{0,j}$ are the normalized interface compositions in cementite and ferrite, and $C^{\theta}_{1,j}$ and $C^{\alpha}_{1,j}$ are the normalized compositions in cementite and ferrite at the point one finite distance element away from the interface.

6.5.3 Change of composition profile with time

Bhadeshia's analysis divides up the cementite and the ferrite into a number (n) of finite elements of thickness x_s such that:

$$\begin{aligned} n_\theta &= x_\theta / 2x_s \\ n_\alpha &= x_\alpha / x_s \end{aligned} \tag{6.22}$$

In this way, the finite difference model can be used to produce composition profiles for the ferrite region (the area whose diffusion rate is the rate controlling step for enrichment of cementite). Typical profiles for four distinct cases are reproduced in figure 6.16 for chromium in the 1Cr–$\frac{1}{2}$Mo steel, with a 565°C ageing temperature and x_θ of 0.180μm (in keeping with the value typically found by experiment). The full 220 element plot range represents one half thickness of a hypothetical ferrite plate.

Profile 1 (after 5 hours) illustrates that in the early stages of ageing the model predicts that most of the ferrite is still at $\bar{c}$, with only the region nearest the θ/α interface denuded of chromium. Note that the composition of the first slice is greater than $c^{\alpha\theta}$ by a noticeable amount in the very early stages of this analysis. This is a consequence of the initial assumption of slice compositions, namely $C^{\alpha}_{i,0} = c^{\alpha\theta}/\bar{c}$ for $i = 0$, and 1 for all $i > 0$, rather than of fundamental significance: T' and X are large relative to the ageing time, so that the algorithm has not completely settled down to a smooth curve, but this is trivial during the long ageing times employed in practice.

Profile 2 (after 100 hours) shows a typical case during which cementite enrichment should take place as $(\text{time})^{1/2}$: diffusion through ferrite to the interface is the rate controlling step, and no soft impingement has occurred to slow it down ($C_{i,j}$ for large j remains 1, which is to say c^α in these regions is $\bar{c}$, or 0.91 atomic pct).

Profile 3 (after 1000 hours) shows the case where an observable degree of soft impingement has almost occurred, where $C_{i,j} = 1$ for only the largest j approaching n_α, so that, at the half thickness of the ferrite plate, the diffusion

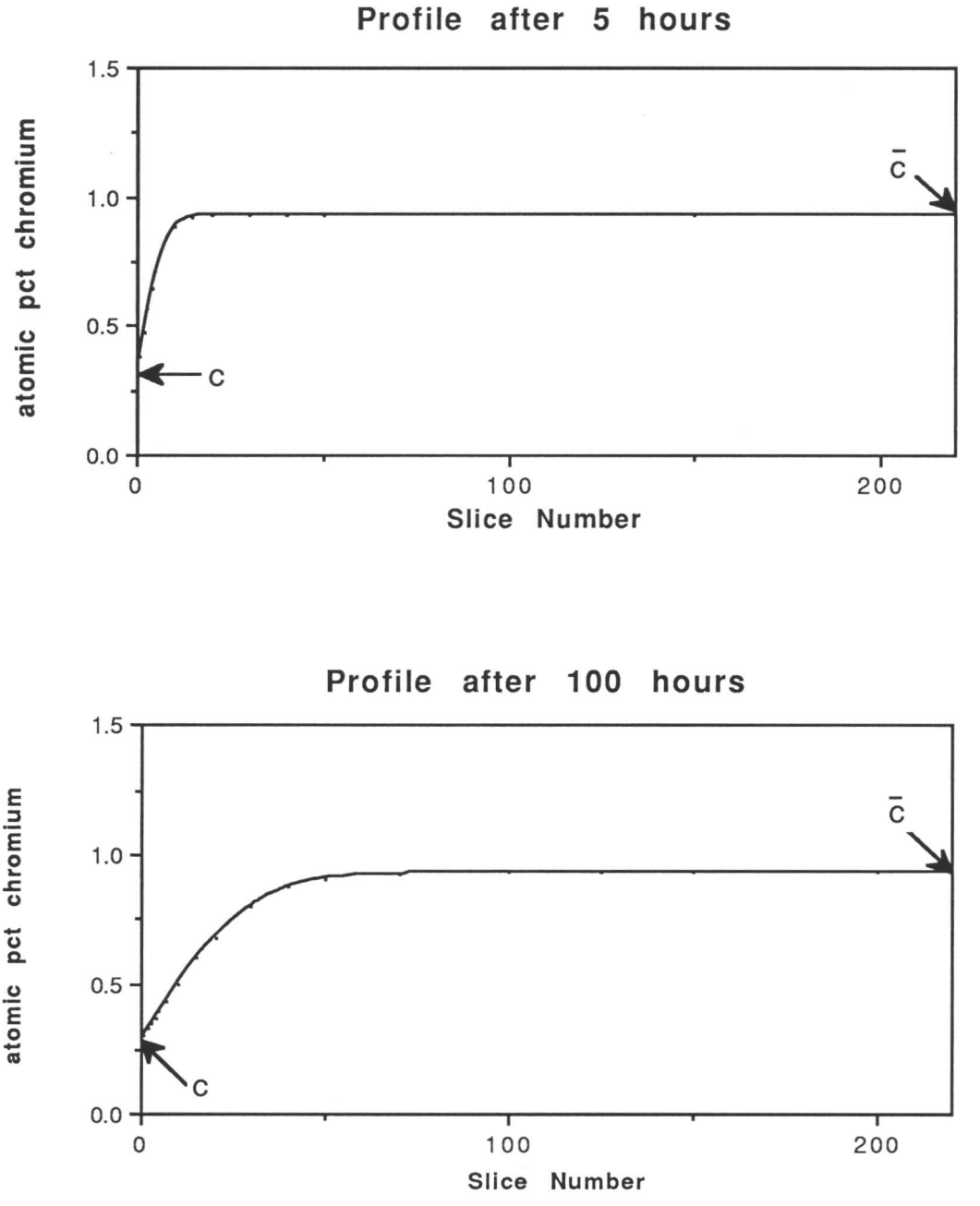

Figure 6.16: Finite element modelling of chromium composition within ferrite for the 1Cr–$\frac{1}{2}$Mo steel aged at 565°C

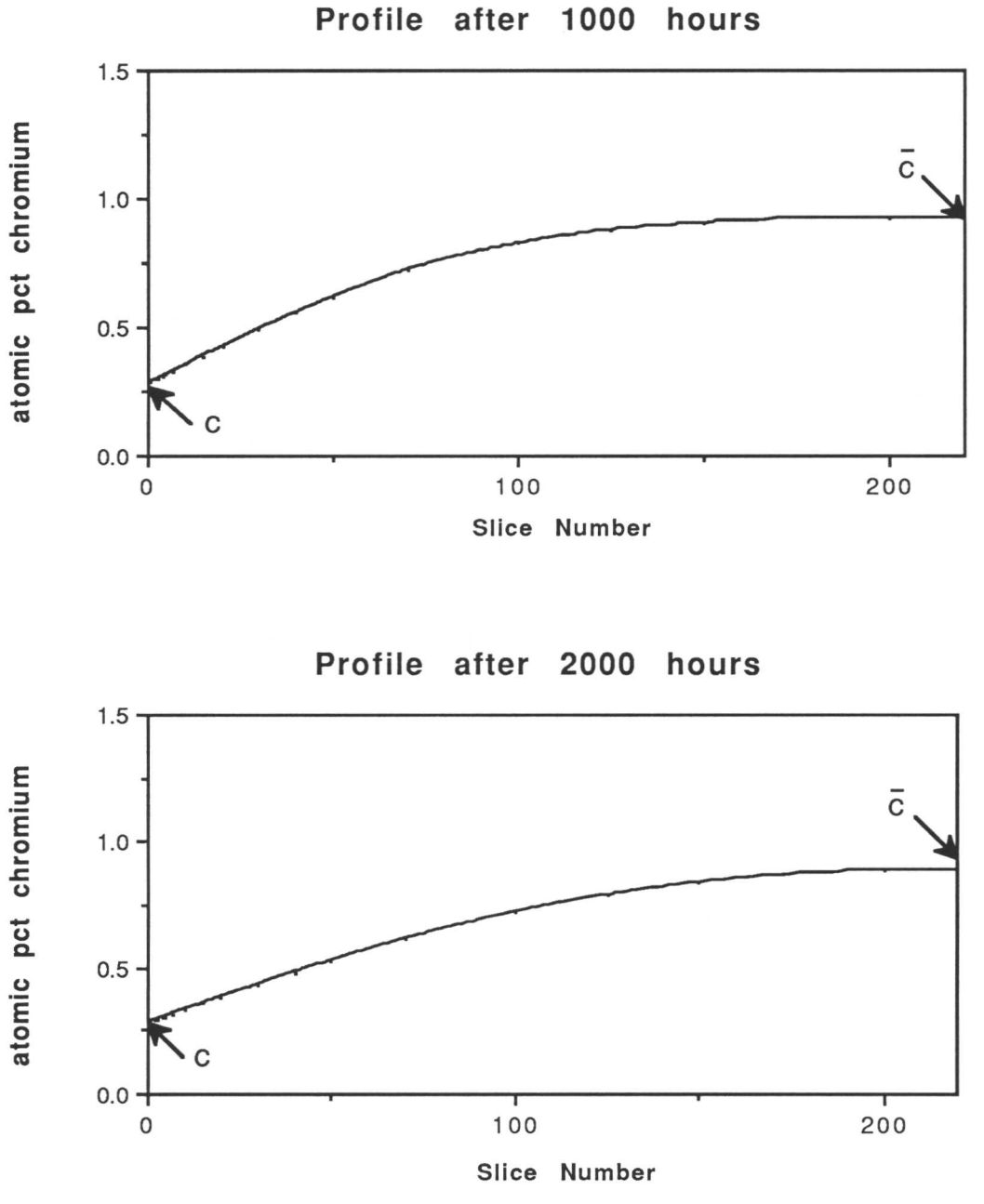

Figure 6.16: Finite element modelling of chromium composition within ferrite for the 1Cr–$\frac{1}{2}$Mo steel aged at 565°C

profile is almost interfering with the diffusion field associated with the next cementite particle. The program is set to detect soft impingement at a 1% level of overlap of diffusion fields, which is to say that $C_{n_\alpha,j} \leqslant 0.99$, but this is entirely arbitrary and the program can be used to determine the time at which soft impingement at any other level of diffusion field overlap commences.

Profile 4 shows the case after the onset of soft impingement. The fluxes of solute in the ferrite will be slowed slightly; therefore, the enrichment of cementite will occur at a concomitantly smaller rate, and enrichment will no longer be expected to fit a strictly $(\text{time})^{1/2}$ relationship.

6.6 Variation of c^θ with Time: Finite Difference Approach

6.6.1 The onset of soft impingement and its effect

The analytical approach of Section 6.3 enabled the $(\text{time})^{1/2}$ relationship to be tested against experimental data, showing good agreement in the early stages. A decreased enrichment rate was found at longer time scales, however, and it was tentatively suggested that this could be caused by either soft impingement reducing the diffusion fluxes in the rate-controlling ferrite case, or by alloy carbide precipitation. No microscopic evidence was found for the latter in this alloy; the finite difference model enables us to consider the former.

To this end, calculations were carried out using the finite difference model to determine how c^θ varied with time, and, in particular, the occurrence and effect of soft impingement. Values of x_θ for the fully-bainitic and partially-bainitic microstructures were taken as 0.180μm and 0.150μm respectively, these being typical of the particle sizes obtained experimentally, and Bhadeshia's program was modified to use interdiffusion coefficients, which were shown in section 6.3 to be more representative of what was occurring experimentally. Predicted $(c - \bar{c})$ versus $(\text{time})^{1/2}$ plots are presented for chromium, manganese and molybdenum in figure 6.17–6.19. Note that the flattening of the predicted curves for the fully-bainitic microstructure at 625°C, and for the mixed microstructure, correspond to saturation of cementite. At this point, both cementite and ferrite should be at their equilibrium compositions.

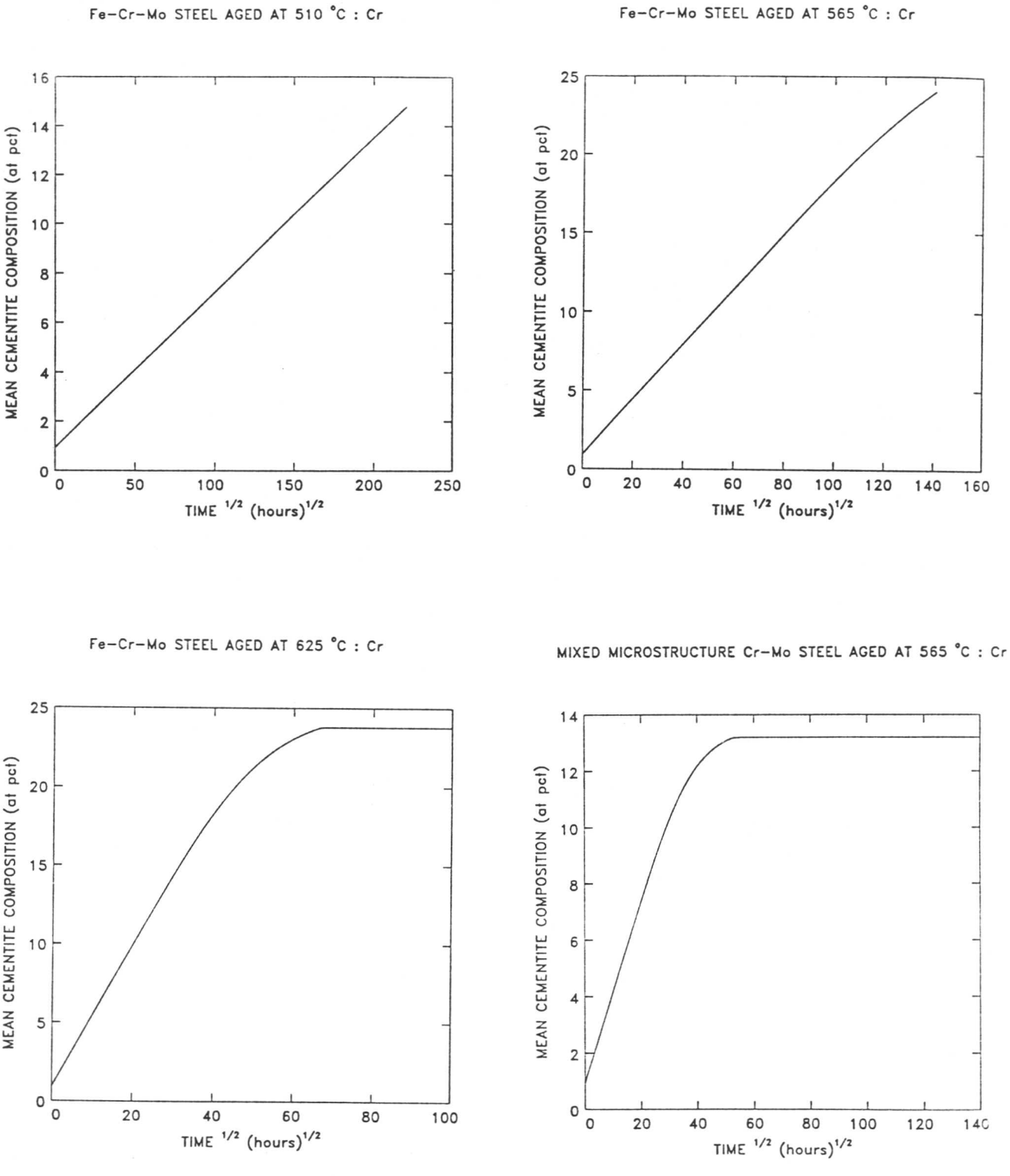

Figure 6.17: Finite difference predictions of $(c - \bar{c})$ versus (ageing time)$^{1/2}$ for chromium in the Fe–Cr–Mo power plant steel

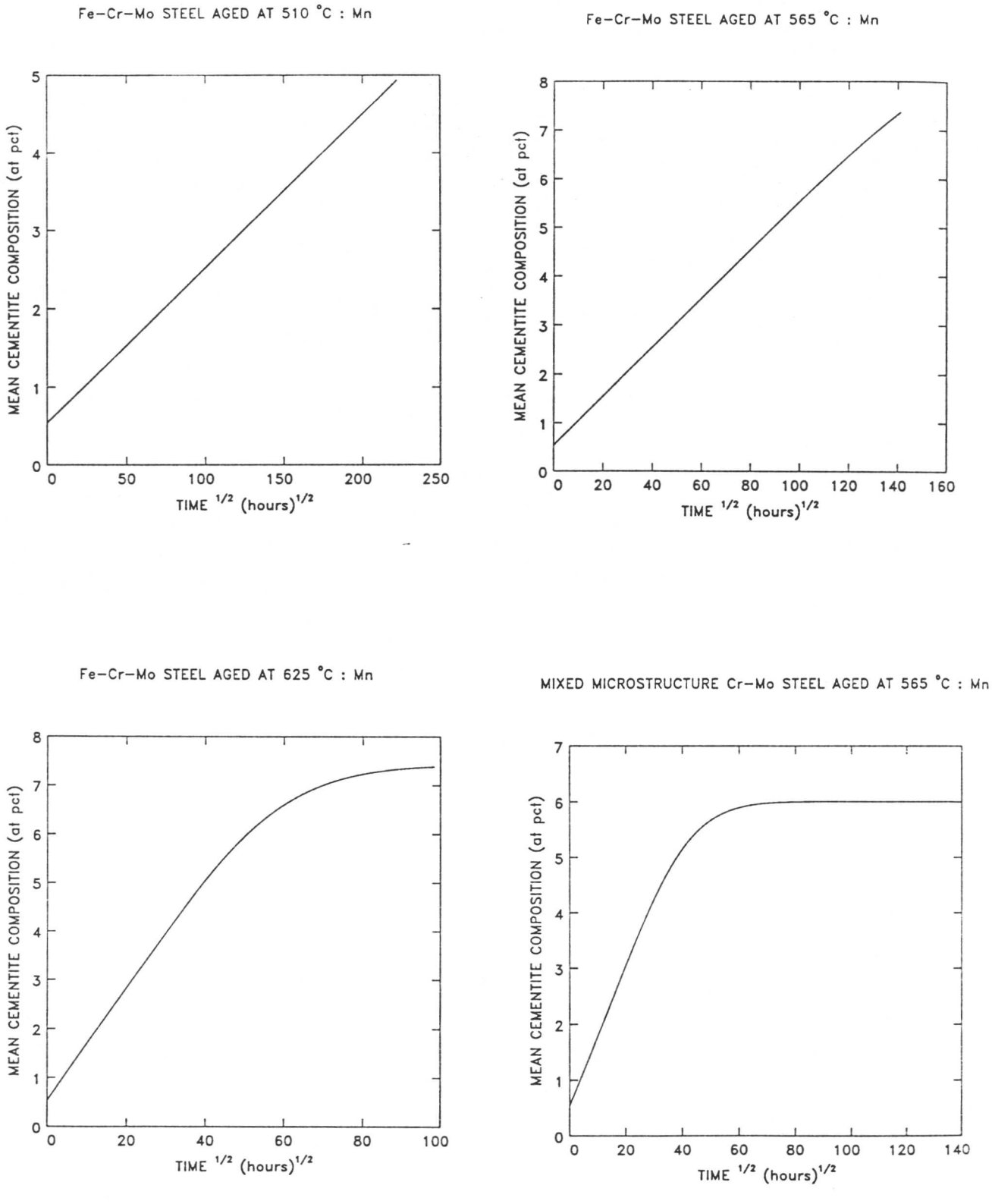

Figure 6.18: Finite difference predictions of $(c - \bar{c})$ versus (ageing time)$^{1/2}$ for manganese in the Fe–Cr–Mo power plant steel

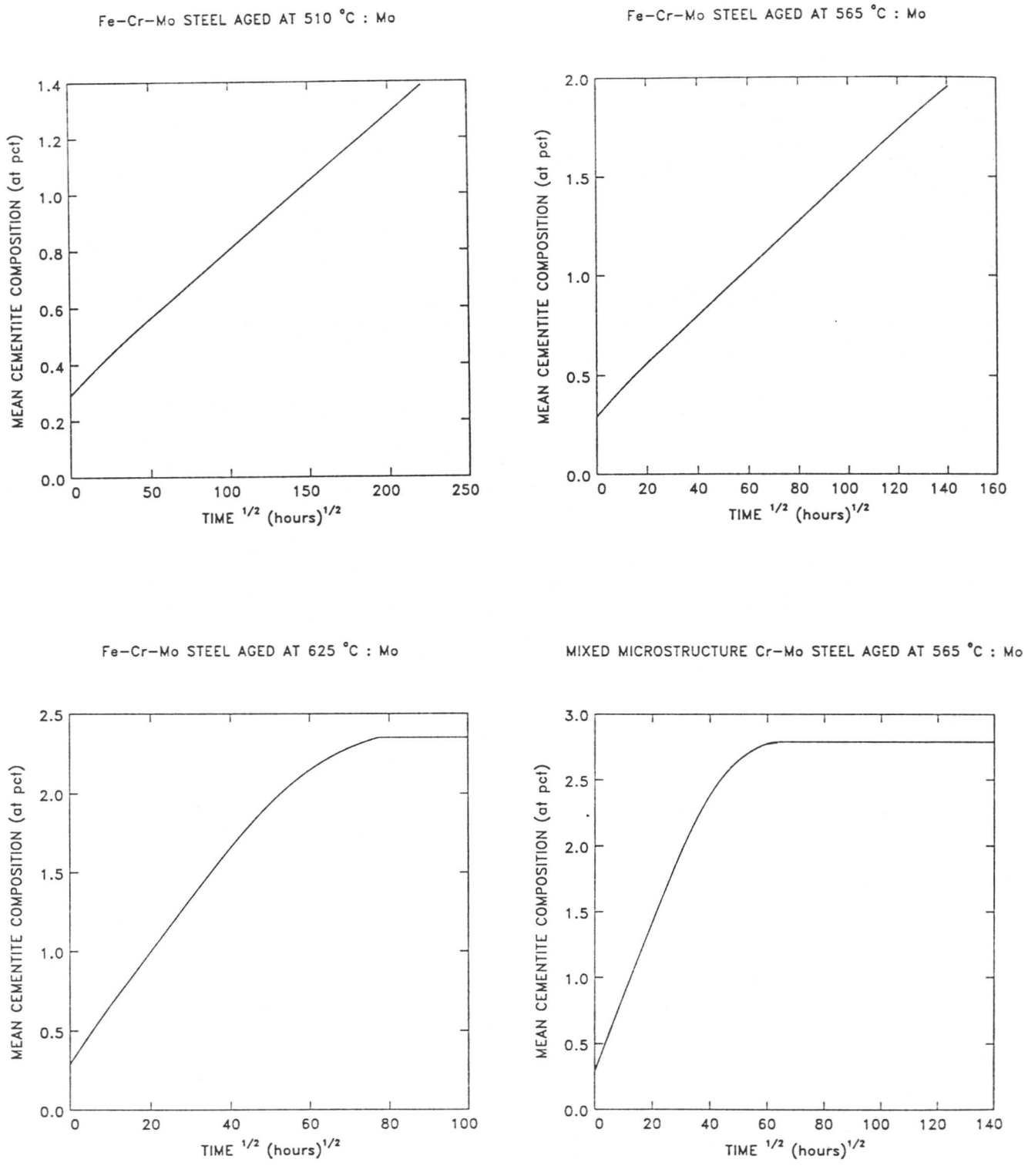

Figure 6.19: Finite difference predictions of $(c - \bar{c})$ versus (ageing time)$^{1/2}$ for molybdenum in the Fe–Cr–Mo power plant steel

The finite difference program was initially set to register soft impingement at a 1% level, which is to say that the overlap of diffusion fields is considered to be of physical significance when $C_{n_\alpha,j}$, the normalized value for composition at the mid-point of the hypothetical ferrite slab, falls below 0.99. This level is entirely arbitrary, and, in consequence, predicted soft impingement times for 1%, 2%, 5% and 10% were calculated, and are shown in table 6.13, for $x_\theta = 0.180\mu$m. A comparison of table 6.13 with the $(c-\bar{c})$ versus (ageing time)$^{1/2}$ finite element curves suggests that a marked deviation from linearity in $(c-\bar{c})$ versus (ageing time)$^{1/2}$ is not really shown until the 5–10% level. At this point, the overlap of diffusion fields becomes important in determining the diffusion rates within the ferrite, and hence the rate of enrichment of cementite.

The experimental data for chromium and manganese composition vs ageing time are compared with finite difference composition versus ageing time curves on figure 6.20 and figure 6.21 respectively. Finite difference curves were generated using two values of D_α: the reported values for interdiffusion coefficient from Fridberg *et al.* (1969), and the values of D_α which were calculated from equation (6.3) to be representative of the experimental c^θ data.

Both the graphs and the table illustrate that measured data for $(c-\bar{c})$ levels off to some degree, and ceases to fit a (time)$^{1/2}$ relationship, somewhat earlier than predicted by the soft impingement model; the model predicts negligible deviation from linearity over the time-scales and temperatures employed in this project. It is nevertheless suggested that the slowing down of enrichment rate at longer times may in part be due to such an effect. The Bhadeshia model assumes that all cementite and ferrite is notionally swept into two slabs, with the analysis obtaining x_θ from the experimentally-determined $\bar{x}_\theta$, and calculating x_α, the half thickness of the ferrite slab, from the relationship

$$\frac{x_\theta}{(2x_\alpha + x_\theta)} = V_\theta \tag{6.23}$$

with V_θ being obtained from the lever rule assuming a stoichiometric cementite composition as was explained in Chapter 2. This may be representative of a situation where cementite and bainite comprise a regular array of consistently sized

Ageing temp. °C	Predicted time for soft impingement (hours)			
	1% level	2% level	5% level	10% level
		(chromium)		
510	27051	32551	44010	59083
565	2563	3109	4252	5791
625	281	342	474	661
565 30% α_b	118	144	199	278
		(manganese)		
510	39077	47770	66691	93247
565	3825	4724	6732	9686
625	443	555	814	1222
565 30% α_b	160	201	294	441
		(molybdenum)		
510	52096	64806	93863	137 997
565	5633	7086	10525	16039
625	607	776	1194	1918
565 30% α_b	267	341	525	844

Table 6.13: Predicted time for the onset of various levels of soft impingement in ferrite using the finite difference model and experimentally-determined values of x_θ for the Fe–Cr–Mo power plant steel

plates, but, in practice, both cementite particle size and separation will vary, a factor for which the model makes no allowance. This will lead to a practical situation where the diffusion fields of those particles more closely spaced than average will interfere on a shorter time scale than that predicted by the model.

A rigorous analysis of a real system on a finite element basis, necessitating the consideration of coupling of diffusion fields from a large number of variously-sized and randomly-distributed particles, and the extension of the model from one to three dimensions will be a major undertaking; but some idea of the effect of decreased particle spacing can be obtained from figure 6.22. The figure was

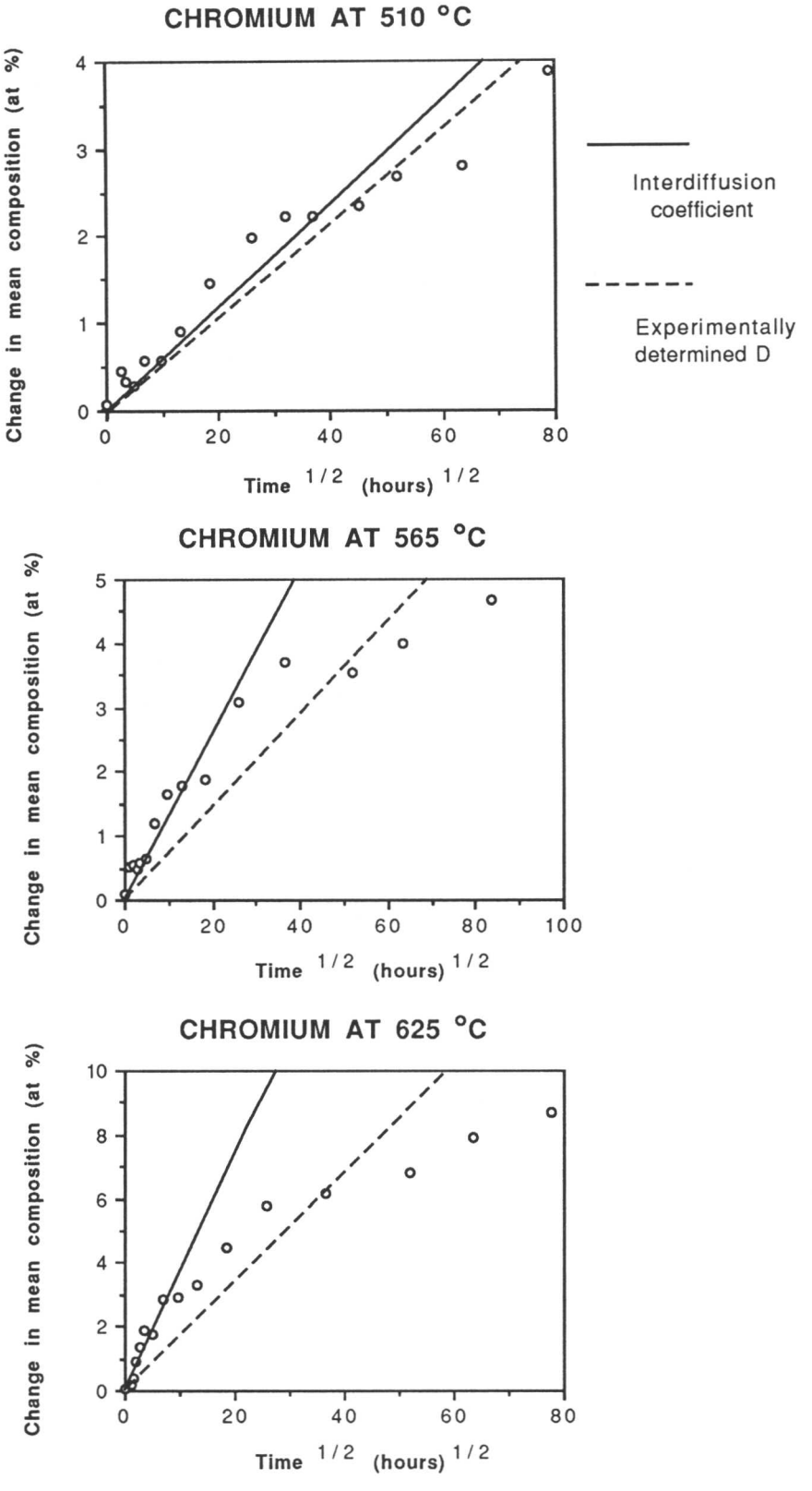

Figure 6.20: A comparison between experimental cementite enrichment results for chromium in the Fe–Cr–Mo power plant steel and the two finite difference predictions of $(c-\bar{c})$ versus (ageing time)$^{1/2}$ obtained by using the experimentally-determined and the reported values for D_α

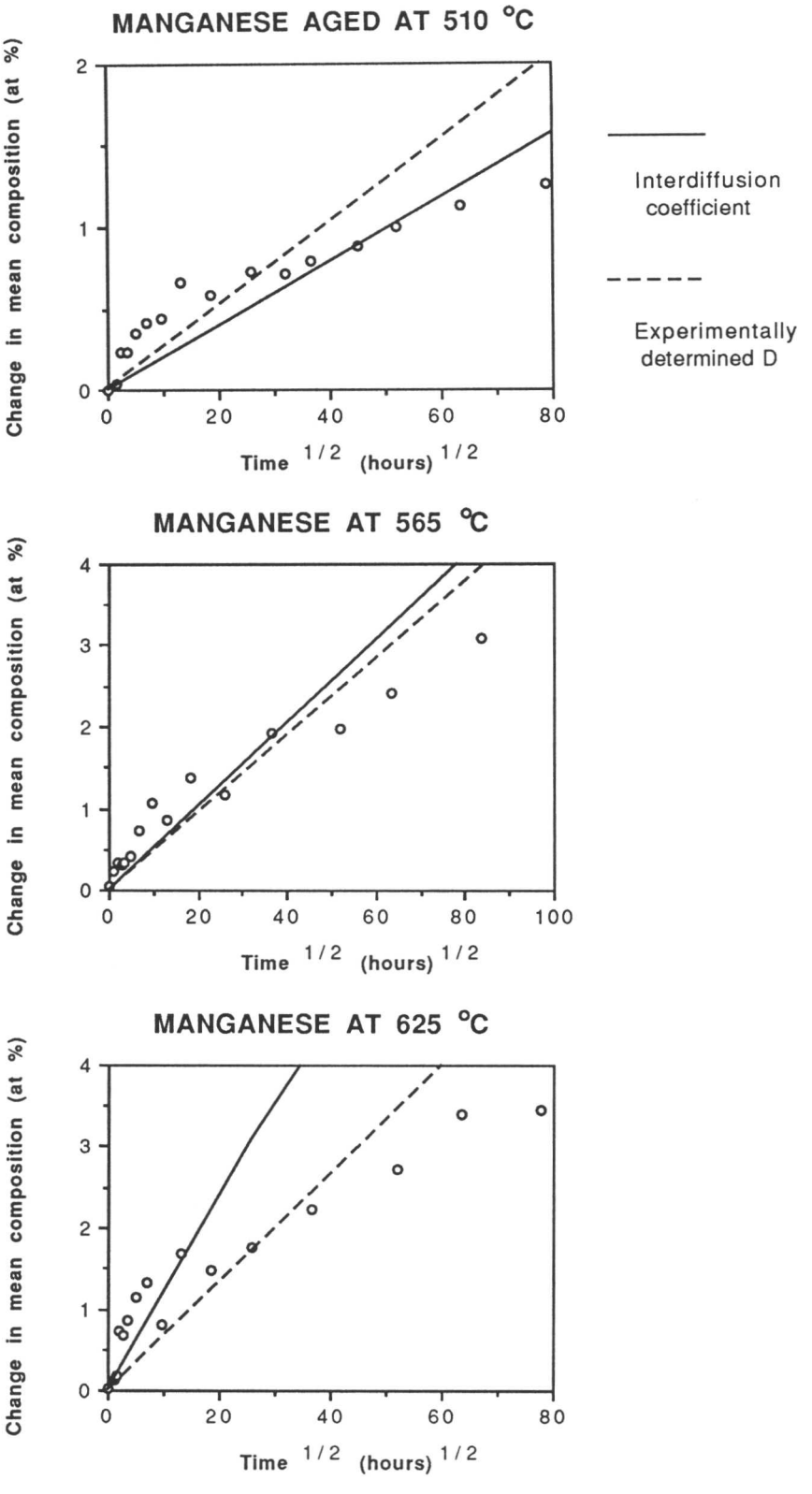

Figure 6.21: A comparison between experimental cementite enrichment results for manganese in the Fe–Cr–Mo power plant steel and the two finite difference predictions of $(c - \bar{c})$ versus (ageing time)$^{1/2}$ obtained by using the experimentally-determined and the reported values for D_α

generated by performing finite element calculations for the composition change in chromium aged at 565°C, using the typical experimental x_θ value of 0.180μm. In addition to the standard analysis, which set x_α on the basis of equation (6.23), curves were also calculated with the half-thickness of the ferrite slab set to $x_\alpha/2$, $x_\alpha/3$, and $x_\alpha/4$, in all cases keeping the other parameters constant.

It can be seen from figure 6.22 that this somewhat arbitrary adjustment to the ferrite thickness has a dramatic effect on the value of c^θ predicted by finite element analysis. This suggests strongly that it is likely that some particles will be affected by soft impingement over the time-scale and temperatures in these experiments, which would explain the observed deviation from linearity of a $(c^\theta - \bar{c})$ vs $(\text{time})^{1/2}$ plot at longer ageing times.

It is also apparent that a slowing down of enrichment rate due to soft impingement in the ferrite, by affecting small particles as well as large ones, would introduce an uncertainty into any size effect, and may be a partial explanation of the observation that the magnitude $(c - \bar{c})$ vs x_θ^{-1} size effect was not as large as predicted by equation (6.3) at higher temperatures and longer ageing times.

It should be emphasized that the flattening of the composition vs $(\text{time})^{1/2}$ curves in the $x_\alpha/3$ and $x_\alpha/4$ cases is not due to saturation of cementite, but rather to the loss of chromium from the ferritic region.

6.7 Alloy carbide precipitates

Calculations have been performed to determine the thermodynamically-stable carbide structures at the three ageing temperatures, and the relative proportions and equilibrium compositions of those phases. These were done using the MTDATA computer package which was developed by the National Physical Laboratory (NPL). The package models multicomponent systems using a database of carefully determined results from simpler systems.

The results of this calculation are presented in table 6.14, which shows that the stable carbide in this alloy at all three ageing temperatures is $M_{23}C_6$. This is the species which may be expected to precipitate out in preference to cementite for prolonged ageing, but, as noted earlier, no significant evidence of

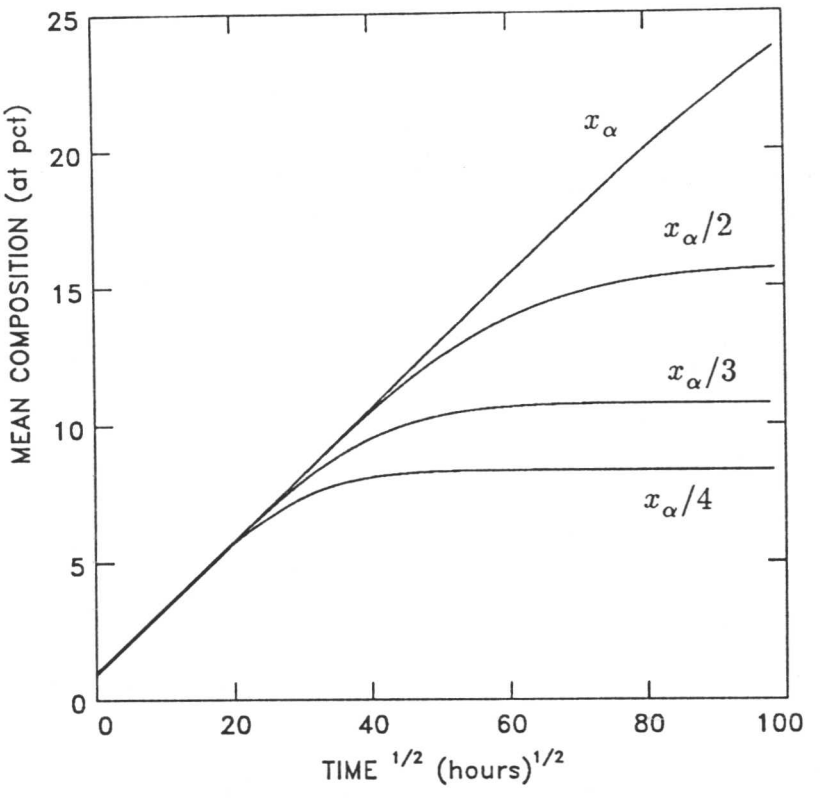

Figure 6.22: The effect of variation in ferrite thickness on a finite element analysis of the ageing of a 0.180μm cementite particle at 565°C for the 1Cr–$\frac{1}{2}$Mo type steel

this has been found in these experiments, and it appears that a longer timescale is required for the process to occur.

6.8 Summary

The measurement of cementite composition during ageing of bainitic microstructures in a 1Cr–$\frac{1}{2}$Mo type power plant steel provides evidence that the analytical model proposed by Bhadeshia (1989) (see equation (6.3)) is a good model of the real behaviour of this material before the onset of soft impingement. Cementite enrichment was found to show good agreement with the (time)$^{1/2}$ relationship that the model predicted, a prediction which is at variance with frequent industrial practice where an empirical (time)$^{1/3}$ relation has been preferred. In particular, the values for D_α which were calculated from enrichment data us-

Temp (K)	Equilibrium phases	Composition (wt %) Fe	Cr	Mn	Mo	Si	C
783	97.59% α	98.95	0.24	0.52	0.02	0.24	0.00
	2.41% $M_{23}C_6$	48.97	26.27	0.00	19.78	0.00	4.98
838	97.59% α	98.86	0.33	0.52	0.03	0.24	0.00
	2.41% $M_{23}C_6$	52.65	22.89	0.00	19.49	0.00	4.97
898	97.59% α	98.75	0.42	0.52	0.05	0.24	0.00
	2.41% $M_{23}C_6$	56.78	19.43	0.00	19.49	0.00	4.97
838	93.34% α	99.37	0.13	0.23	0.00	0.24	0.00
30% α_b	3.31% θ	77.23	8.69	7.30	0.05	0.00	6.74
	0.37% M_7C_3	36.78	39.74	13.98	0.81	0.00	8.68
	2.96% $M_{23}C_6$	67.93	10.50	0.00	16.59	0.00	4.98

Table 6.14: Calculated equilibrium phase compositions for the Fe–Cr–Mo power plant steel at the temperatures used for ageing

ing equation (6.3) can be considered strong evidence in support of the model. Furthermore, individual values of c^θ at a given time are found to vary with cementite particle size such that $(c-\bar{c}) \propto x_\theta^{-1}$, as predicted by equation (6.3). This size effect has been shown to be of particular significance once the limitations imposed on such an analysis by the unavoidable statistical scatter concomitant with the EDX technique is considered.

It can be concluded that, in this material, the mechanism effecting enrichment of cementite is predominantly diffusion of substitutional alloying elements through the ferrite to the α/θ interface. Although some evidence of cementite coarsening was found, this process does not appear to play a major rôle in the enrichment of those particles.

The finite element model analysis fits the data very well before a significant level of soft impingement occurs, and gives some quantitative prediction of the effect of soft impingement, although refinements are necessary if the variation in size and irregular distribution of cementite particles that is found in practice is to be considered properly. The experimental results suggest, in particular, that the lack of account taken by the finite element analysis of variation in

interparticle distances may be a particular problem, with some slowing down of the rate of enrichment occurring early than the model predicts in practice.

A full analysis taking account of non-uniform particle distributions, changes to cementite morphology (enlargement and shape change), and the interaction of diffusion fields in ferrite associated with many cementite particles of differing x_θ is necessary if a model which can fully quantify the later stages of ageing and the approach to saturation in real materials is to be developed. To do this rigorously would be a major undertaking, and in the mean time, the current analysis provides a good representation of the cementite enrichment processes in aged bainitic cementite in these materials.

Chapter 7

AGEING OF BAINITIC MICROSTRUCTURES:

FULLY-BAINITIC Fe–Cr MODEL ALLOY

7.1 EDX Compositional Data

The experiments described in the previous chapter were also carried out on a Fe–4.08Cr–0.3C (wt%) alloy. This steel was chosen to give a simple ternary system to contrast with the multiple alloying elements of the real power plant steel. The higher substitutional content should also encourage the formation of alloy carbides so that the effect of this on the ageing process can be studied over a more manageable timescale.

The EDX microanalytical data were collected and analysed as before, the analysis being applied only to results from cementite particles. In practice, other alloy carbides were found to precipitate after relatively short ageing times, and these precipitates are considered in a later section. It was also found that the cementite had disappeared entirely soon after this secondary precipitation commenced, presumably going back into solution to allow precipitation of the nearer-equilibrium species. This accounts for the fact that the maximum ageing time at each temperature in the c^{θ} analysis was much shorter than had been the case with the 1Cr–$\frac{1}{2}$Mo steel; the cementite was no longer present in the microstructure.

Results obtained from plotting $(c-\bar{c})$ vs $1/x_{\theta}$ are presented in table 7.1 for the series of specimens aged at 510°C, in table 7.2 for specimens aged at 565°C, and in table 7.3 for specimens aged at 625°C. The initial microstructures were fully bainitic for all three ageing temperatures. The data in the table are once again presented for convenience in units of μm for x_{θ} and at.% for $(c-\bar{c})$. Only those compositional data which were obtained from cementite are presented in these tables. It was found in this alloy that during ageing the cementite was replaced by other carbides, a process which is discussed later in the chapter.

7.2 Variation of Composition Change with Particle Size

At short ageing times, the results obtained when the regression analysis for the $(c-\bar{c}) \propto x_\theta^{-1}$ relationship (as predicted by equation (6.1)) is carried out for EDX compositional data for each ageing treatment show similar trends to those for the power plant steel: as ageing time increases, the correlation coefficient which is calculated for the predicted size effect (*i.e.*, $(c - \bar{c})$ versus $1/x_\theta$) improves; the calculated best fit gradient generally increases, indicating that the magnitude of the size effect is becoming more marked; and the statistical significance attributable to the size effect increases. Illustrations of the effect in the model alloy are provided by the plots in figure 7.1(a–c).

It is evident that these effects occur over a much more rapid time-scale than was the case for the 1Cr–$\frac{1}{2}$Mo material, a consequence of the higher substitutional content, which results in a greater imbalance between the $\bar{c}$ concentration of chromium in the two phases in the as-transformed condition and the equilibrium chromium concentrations, and a consequent increase in the driving force for the diffusion process.

As the ageing time is increased, the correlation of experimental data to the $(c - \bar{c}) \propto x_\theta^{-1}$ relationship, which was never very great, becomes poorer once more. It appears that the relationship is breaking down. This is not surprising in view of the fact that the situation is no longer a diffusion problem alone: the precipitation of alloy carbides and the disappearance of cementite are also occurring, so the analytical diffusion model cannot describe the situation in practice. Nevertheless, it can be said that during the early stages of ageing, where negligible alloy carbide precipitation is observed, the existence of the size effect predicted by equation (6.1) suggests that cementite enrichment is effected by a diffusion process, controlled by the rate of diffusion in the ferrite phase, and driven by the concentration difference between the initial ferrite composition ($\bar{c}$) and the equilibrium ferrite composition; in this respect, the process is similar to that found in the case of the power plant steel.

Ageing time (hours)	No of points	Mean c change (at %)	Mean x_θ μm	Data from best fit $(c-\bar{c})$ v x_θ^{-1}		
				correlation	gradient	significance
0	31	0.33	0.174	−0.02	−0.010	<0.90
1	29	0.25	0.173	0.02	0.021	<0.90
3	30	1.33	0.182	0.10	0.118	<0.90
6	31	0.94	0.179	0.20	0.122	<0.90
12	31	1.57	0.176	0.13	0.139	<0.90
24	27	1.09	0.177	0.24	0.233	0.90
48	29	1.90	0.169	0.33	0.262	0.95
96	29	1.62	0.162	0.22	0.156	<0.90
168	33	1.99	0.150	0.19	0.148	<0.90

Table 7.1: Fe–4.08Cr–0.3C (wt.%) model alloy, with a fully-bainitic initial microstructure, aged at 510°C.

Ageing time (hours)	No of points	Mean c change (at %)	Mean x_θ μm	Data from best fit $(c-\bar{c})$ v x_θ^{-1}		
				correlation	gradient	significance
0	36	0.32	0.173	−0.14	−0.067	<0.90
1	29	0.40	0.191	−0.17	−0.188	<0.90
2	32	1.44	0.193	0.11	0.117	<0.90
4	32	2.27	0.166	0.31	0.326	0.90
8	30	2.01	0.143	0.41	0.227	0.95
24	28	2.36	0.156	0.12	0.241	<0.90

Table 7.2: Fe–4.08Cr–0.3C (wt.%) model alloy, with a fully-bainitic initial microstructure, aged at 565°C.

Ageing time (hours)	No of points	Mean c change (at %)	Mean x_θ μm	Data from best fit $(c-\bar{c})$ v x_θ^{-1}		
				correlation	gradient	significance
0	28	0.13	0.154	−0.23	−0.151	<0.90
1	29	0.85	0.160	0.06	0.036	<0.90
2	28	1.50	0.154	0.37	0.284	0.98
4	31	2.42	0.158	0.11	0.123	<0.90
8	26	2.60	0.138	−0.06	−0.028	<0.90

Table 7.3: Fe–4.08Cr–0.3C (wt.%) model alloy, with a fully-bainitic initial microstructure, aged at 625°C.

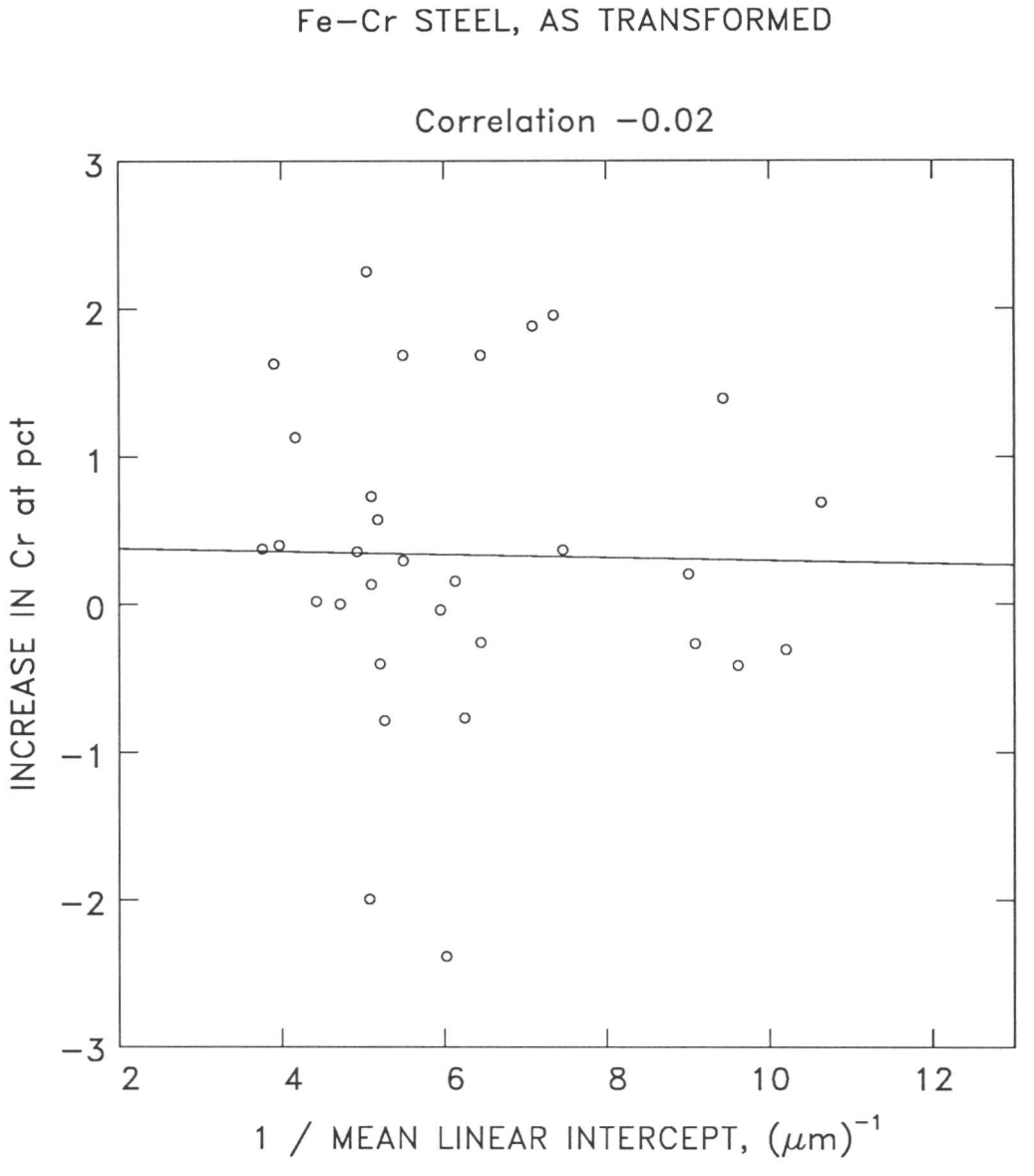

Figure 7.1(a): EDX microanalytical data for the Fe–Cr steel

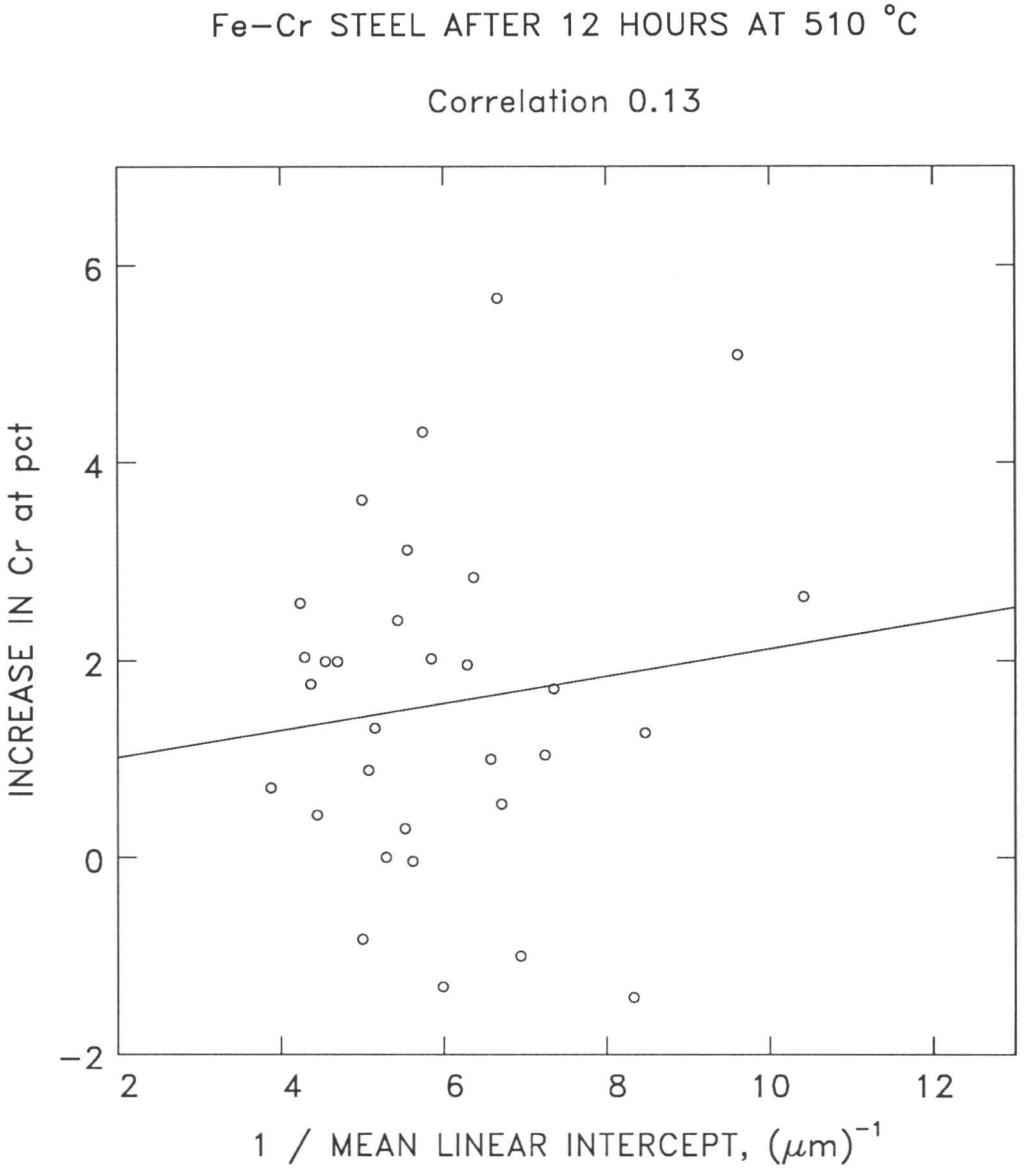

Figure 7.1(b): EDX microanalytical data for the Fe–Cr steel

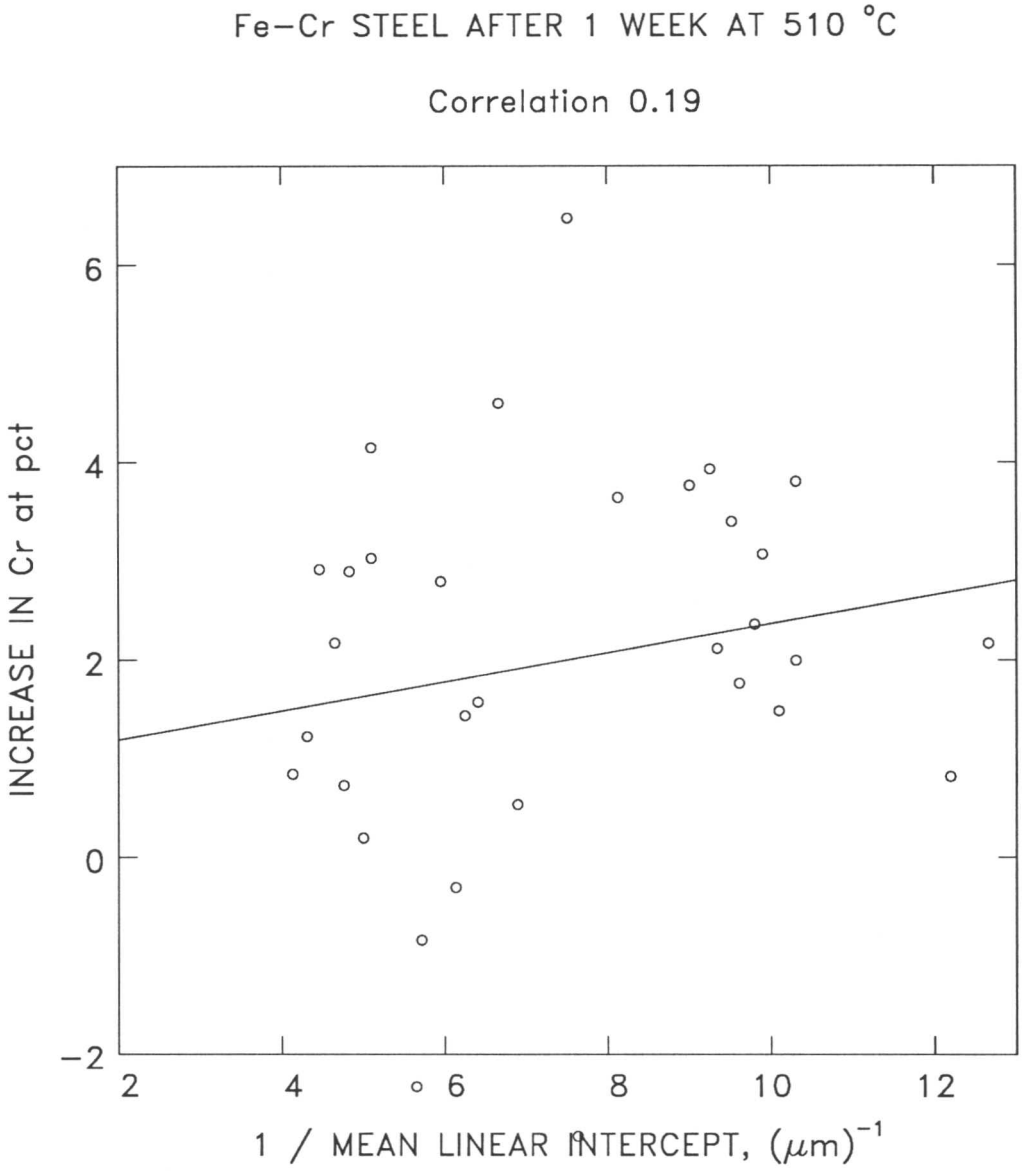

Figure 7.1(c): EDX microanalytical data for the Fe–Cr steel

7.3 Variation of c^{θ} with Time

The finite difference analysis outlined in the previous chapter was carried out for this material. A representative value for x_{θ}, the mean cementite thickness, was taken, on the basis of experimental data, to be 0.18μm. Equilibrium compositions for ferrite and cementite, and V_{θ}, were obtained from the MTDATA package as before, and are presented in table 7.4.

As was the case in the previous chapter, the equilibrium chromium concentration in the carbide is expressed both as a true atomic percent (inclusive of carbon), $c^{\theta\alpha}_{all}$, and as an atomic percent considering only substitutional elements (Cr and Fe), $c^{\theta\alpha}_{sub}$. The latter value is calculated for compatibility with measured data as EDX only detects the chromium and iron.

Temp (K)	V_{θ} (pct)	equilibrium compositions				
		weight pct		atomic pct		
		$c^{\alpha\theta}$	$c^{\theta\alpha}$	$c^{\alpha\theta}$	$c^{\theta\alpha}_{all}$	$c^{\theta\alpha}_{sub}$
783	4.18	1.05	72.3	1.13	59.2	78.9
838	4.18	1.34	65.4	1.44	53.8	71.7
898	4.17	1.68	57.7	1.80	47.8	63.7

Table 7.4: Calculated equilibrium chromium concentrations for a cementite/ferrite mixture in the Fe–Cr steel at the temperatures used for ageing

When the finite difference predictions for $(c^{\theta} - \bar{c})$ vs $(\text{time})^{1/2}$ (figure 7.2–figure 7.4) are compared with experimental data plotted to the same relationship (figure 7.5) it is apparent that the enrichment rate was substantially slower in practice than predicted by the model, even at ageing times preceding those at which significant evidence of secondary precipitation was found. The differences are especially marked at 565°C and 625°C; at 510°C the experimentally-measured enrichment rate, although lower than prediction, is of a similar order of magnitude. It seems reasonable to conclude from this observation that, even at the early stages of ageing, some secondary precipitation had occurred;

thence, the finite difference prediction for the composition profile of ferrite no longer represented the true situation, in which some solute atoms were associated with carbide particles within the ferrite, and the model could not be applied.

Nevertheless, appreciable enrichment of cementite with chromium was observed during the early stages of ageing. This observation, and the fact that a size effect (such that smaller particles had enriched more than larger at a given ageing time) was observed combine to suggest that diffusion of chromium through ferrite into cementite does take place, although at a reduced rate owing to the simultaneous precipitation of more thermodynamically-stable chromium-rich carbides. This produces some correlation of the experimental data with the diffusion model, although the agreement is relatively poor as the true situation on a microscopic level is much more complex than the simple, diffusion-only model assumes. As the newly-precipitated carbides grow at the expense of cementite, even this limited correlation ceases, and subsequently the cementite is found to disappear altogether.

It can be concluded that an analysis of bainitic cementite composition carried out in association with a diffusion-based model for enrichment of cementite will only be of value in the determination of the thermal history of an aged specimen in the absence of precipitation of a second carbide species (as was the case for the power plant steel). In this case, the presence of secondary precipitation means that the diffusion-based model alone is inadequate to describe the situation; hence, cementite compositions are not relatable to the ageing time and temperature regime on this basis.

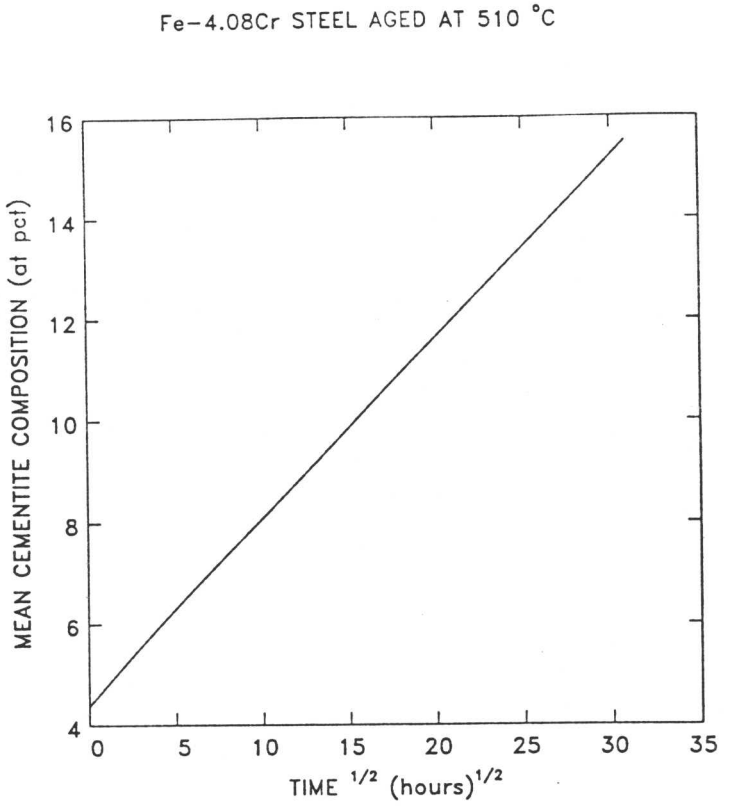

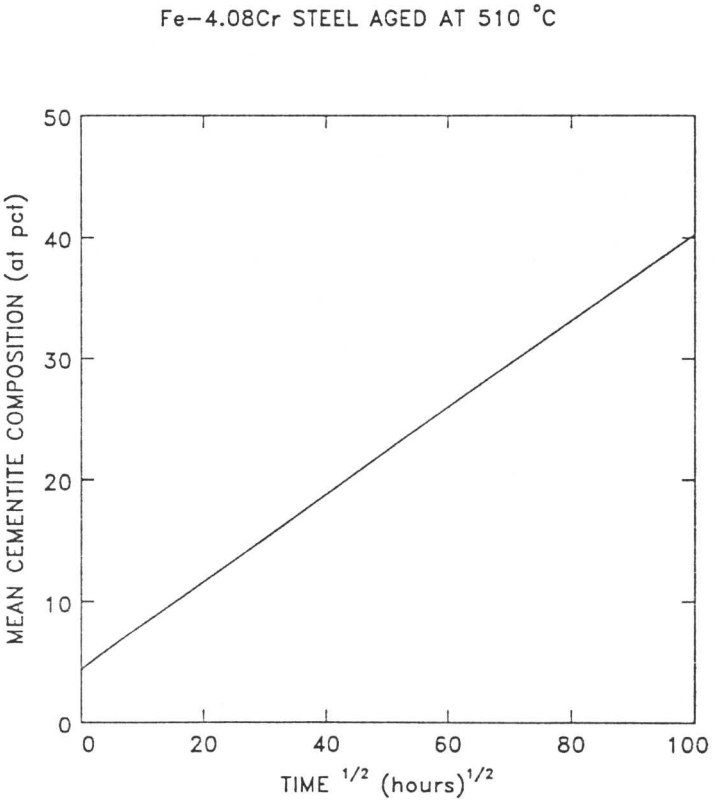

Figure 7.2: Finite difference predictions of $(c - \bar{c})$ versus (ageing time)$^{1/2}$ in the Fe–Cr steel aged at 510 °C

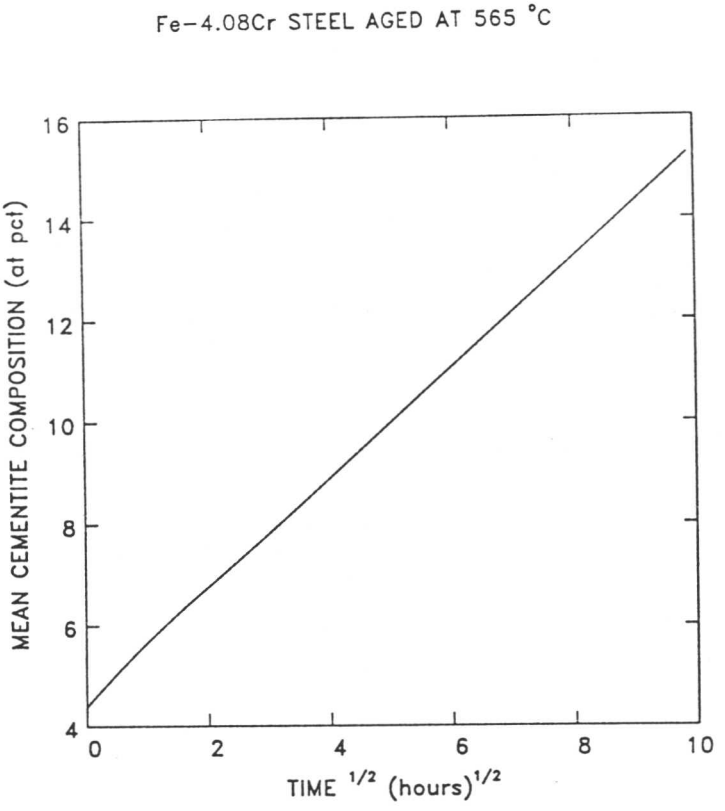

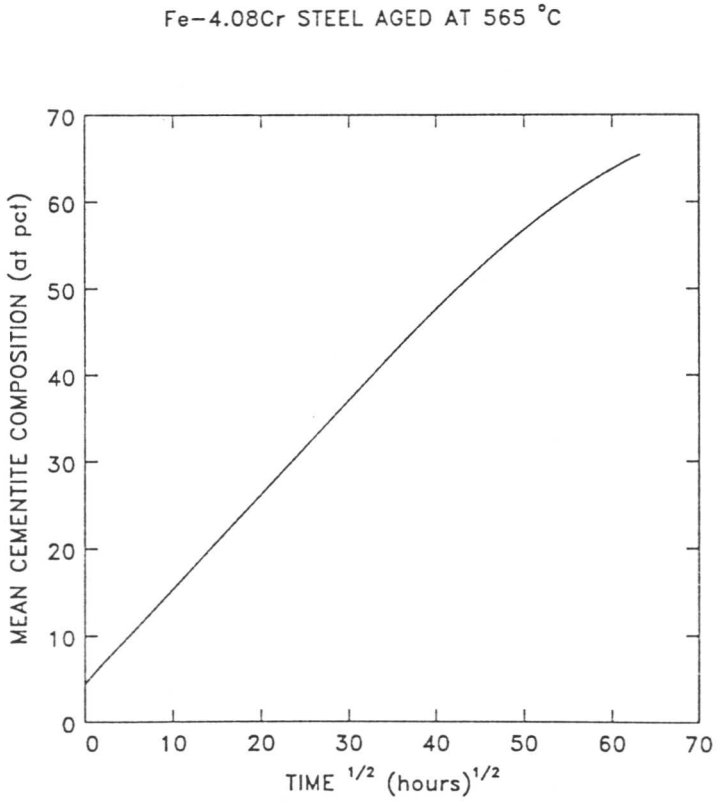

Figure 7.3: Finite difference predictions of $(c - \bar{c})$ versus (ageing time)$^{1/2}$ in the Fe–Cr steel aged at 565 °C

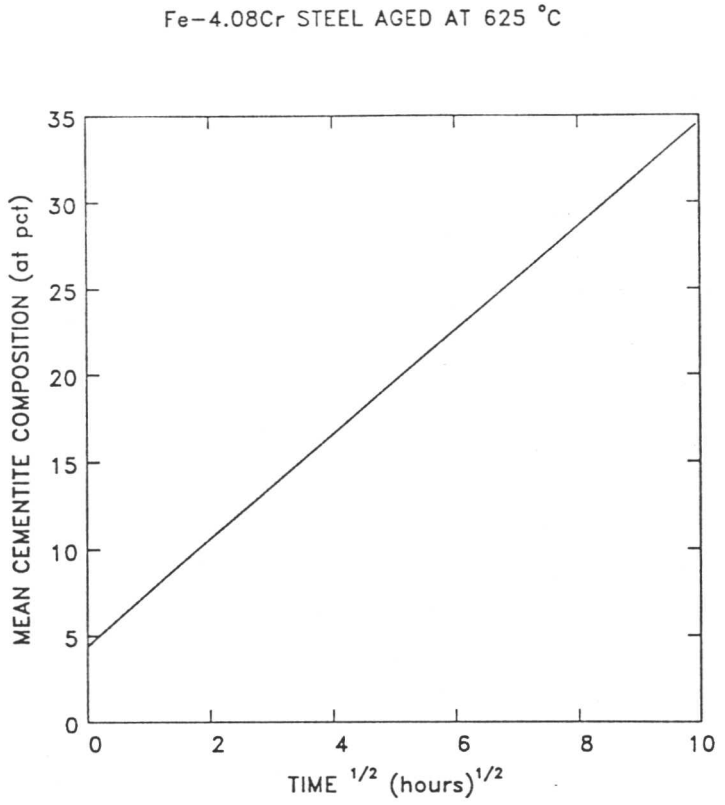

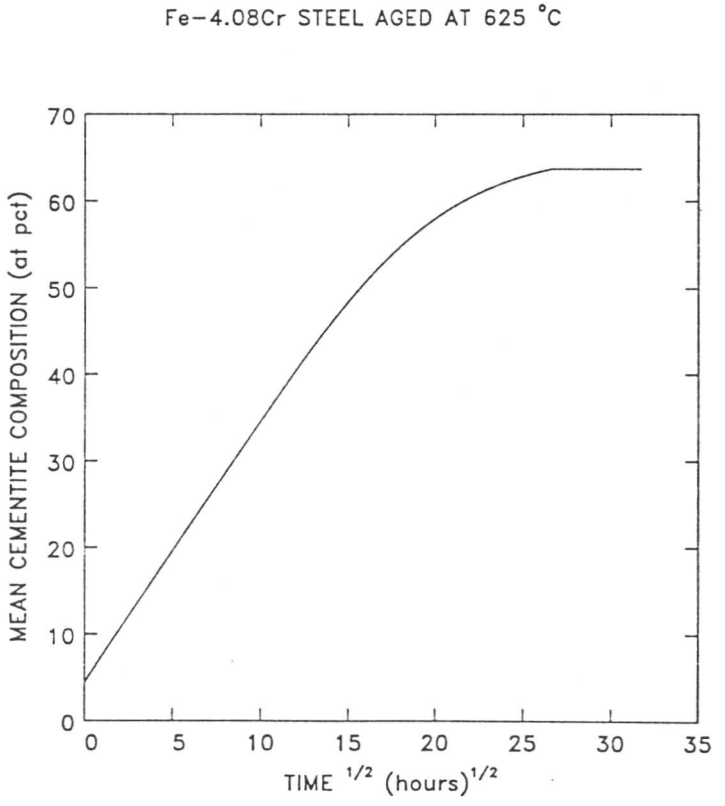

Figure 7.4: Finite difference predictions of $(c - \bar{c})$ versus (ageing time)$^{1/2}$ in the Fe–Cr steel aged at 625 °C

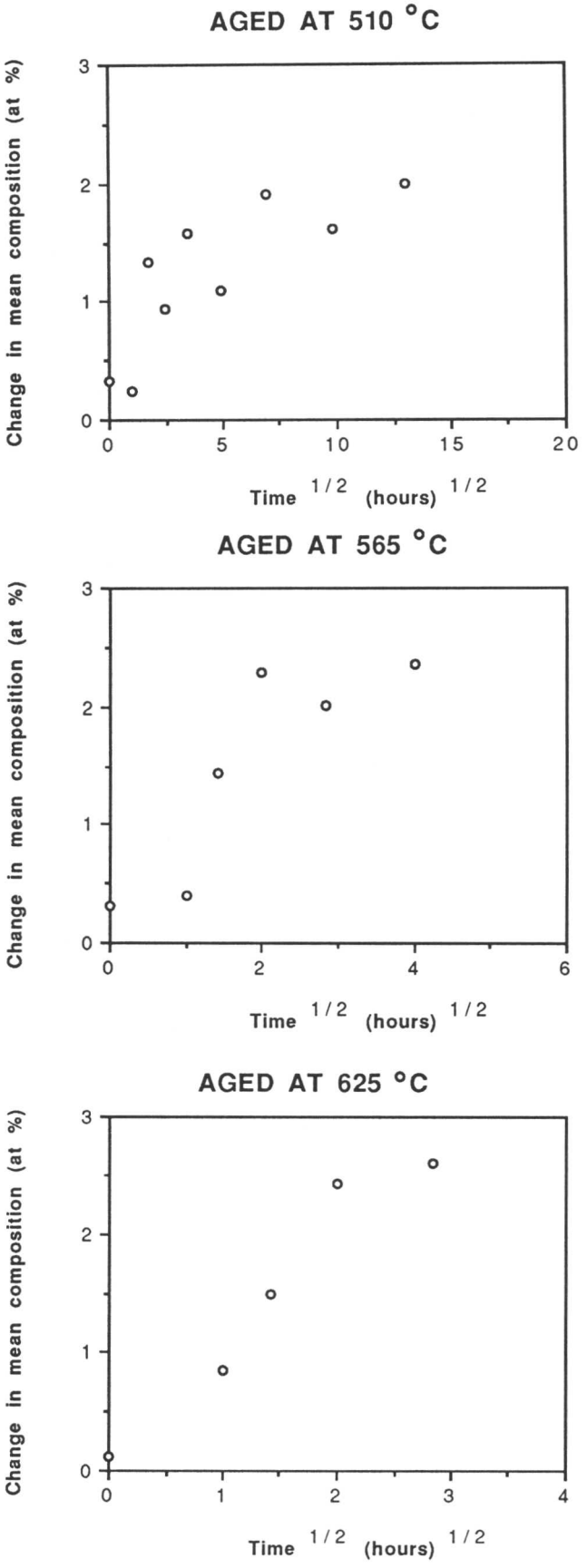

Figure 7.5: Means of measured values of $(c-\bar{c})$ at a given ageing time plotted versus (ageing time)$^{1/2}$ in the Fe–Cr steel

7.4 Alloy carbide precipitates

7.4.1 Calculated equilibrium phases and compositions

Calculations were performed to determine the thermodynamically-stable carbide structures at the three ageing temperatures, and their relative proportions and equilibrium compositions, to be compared subsequently with values measured using EDX analysis of aged specimens. These compositions and volume fractions were determined using the MTDATA computer package in the same manner as previously. The results of these calculations are presented in table 7.5, which shows that the stable carbide in this alloy at all three ageing temperatures is M_7C_3. As the equilibrium phase, this is the carbide which may be expected to form eventually, but not necessarily as the first non-cementite precipitate to form, which may be some sort of intermediate species, and not necessarily of equilibrium composition.

Temp (K)	Equilibrium phases	Composition (wt %) Fe	Cr	C	At% ratio Fe/Fe+Cr	Cr/Fe+Cr
783	96.76% α	98.74	1.26	0.00	98.65	1.35
	3.34% M_7C_3	5.58	85.45	8.96	5.74	94.26
838	96.75% α	98.64	1.36	0.00	98.54	1.46
	3.35% M_7C_3	8.45	82.59	8.97	8.69	91.31
898	96.73% α	98.75	1.42	0.00	98.48	1.52
	3.37% M_7C_3	11.20	79.82	8.98	11.56	88.44

Table 7.5: MTDATA calculations showing the equilibrium phases, and the compositions of those phases, in the Fe–Cr steel at the three ageing temperatures used

7.4.2 EDX compositional measurements

The non-cementite precipitates were analysed for composition as the cementite had been. Two ageing times were used at each temperature, the first corresponding to the time at which significant levels of precipitate other than cementite

were first observed, and the second after a much greater degree of ageing, to test whether the secondary precipitation took place at around equilibrium, or at a non-equilibrium concentration followed by enrichment. Around 60 particles were analysed in all six cases.

The mean values of chromium concentration (expressed as a percentage of substitutionals only, *i.e.,* chromium and iron) and particle size were calculated from the data, and are presented in table 7.6. It is evident that compositions are very close to those predicted for the equilibrium M_7C_3 phase by the MTDATA package at both the shorter and the longer ageing times. It appears that M_7C_3 precipitates and grows at a sufficiently slow rate to allow sufficient diffusion of substitutional atoms for the maintenance of an approximately equilibrium composition. Consequently, an analysis of particles precipitated in this fashion will not give any indication of the thermal history or degree of ageing to which the material has been subjected.

	short ageing			long ageing		
Temp (K)	time (hours)	particle size, μm	Cr/Fe+Cr at% ratio	time (hours)	particle size, μm	Cr/Fe+Cr at% ratio
783	24	0.061	91.75	672	0.079	91.70
838	16	0.064	88.72	672	0.061	87.71
898	8	0.059	83.11	336	0.074	87.50

Table 7.6: Mean measured chromium concentrations for the non-cementite particles in the Fe–Cr steel

Individual particle compositions were also plotted against particle size for each temperature (see figures 7.6–7.8). No relationship between composition and particle size was observed in the data, which is in accordance with the supposition that the nucleation and growth of the M_7C_3 particles occurred at roughly equilibrium compositions. It can be seen on the figures that the scatter of individual compositions about the mean is generally greater than it was for cementite, which may be a real effect, suggesting that M_7C_3 will tolerate a greater deviation from equilibrium than M_3C.

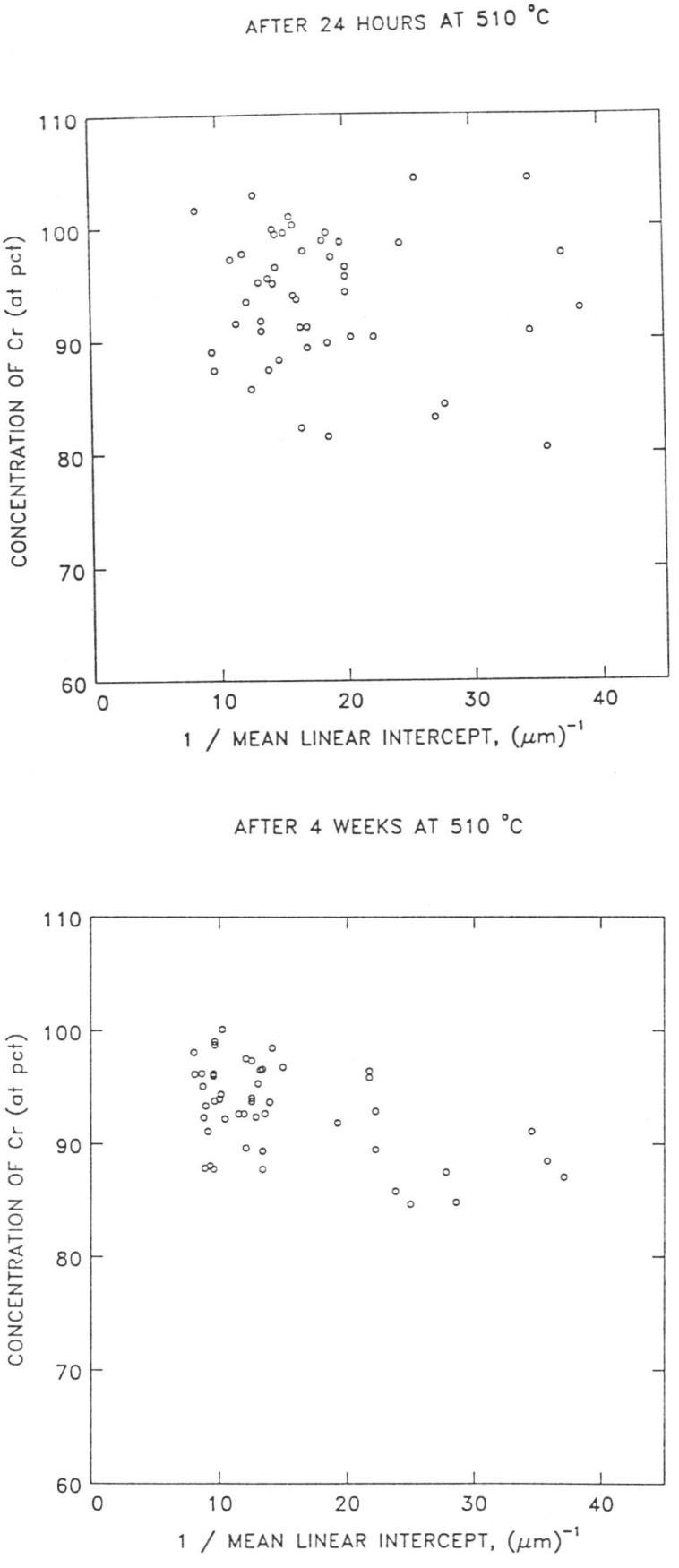

Figure 7.6: Measured compositions of M_7C_3 particles in the Fe–Cr steel aged at 510°C

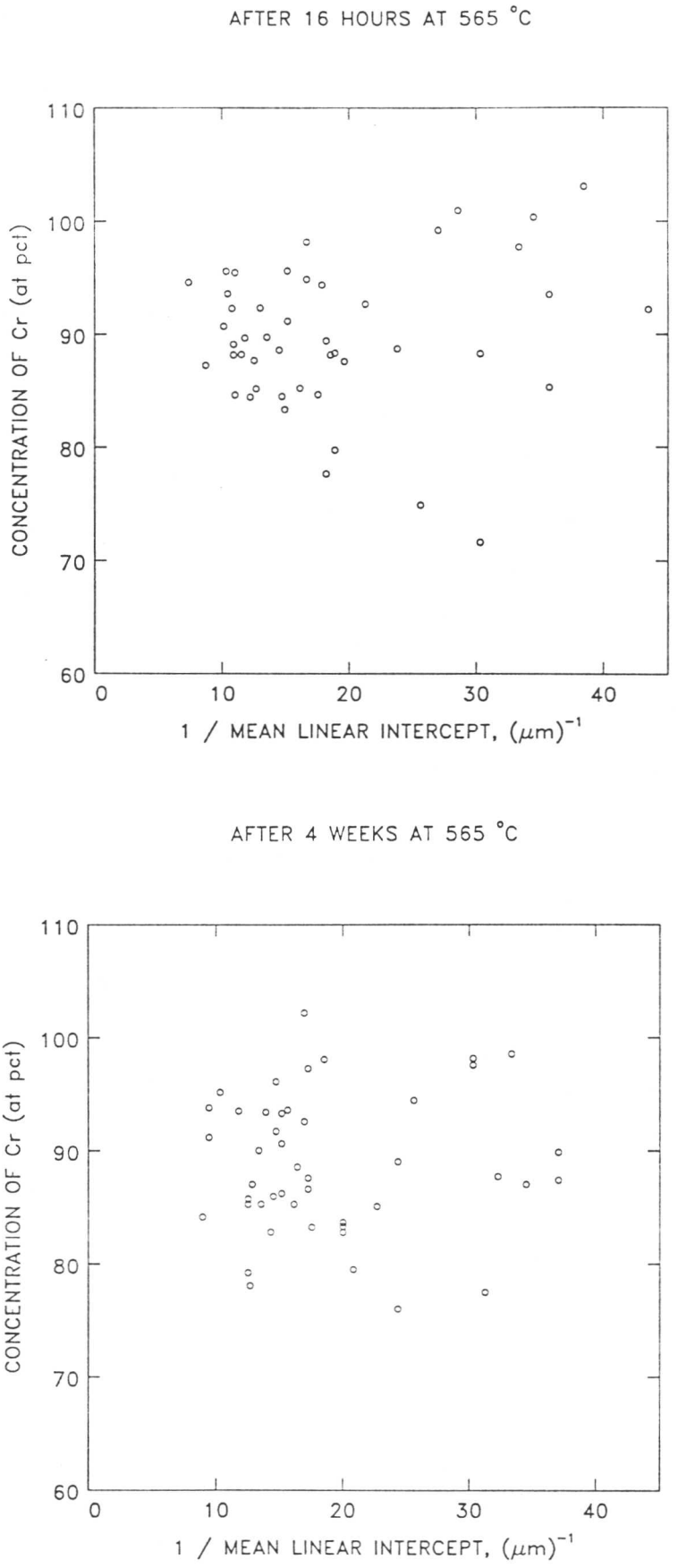

Figure 7.7: Measured compositions of M_7C_3 particles in the Fe–Cr steel aged at 565°C

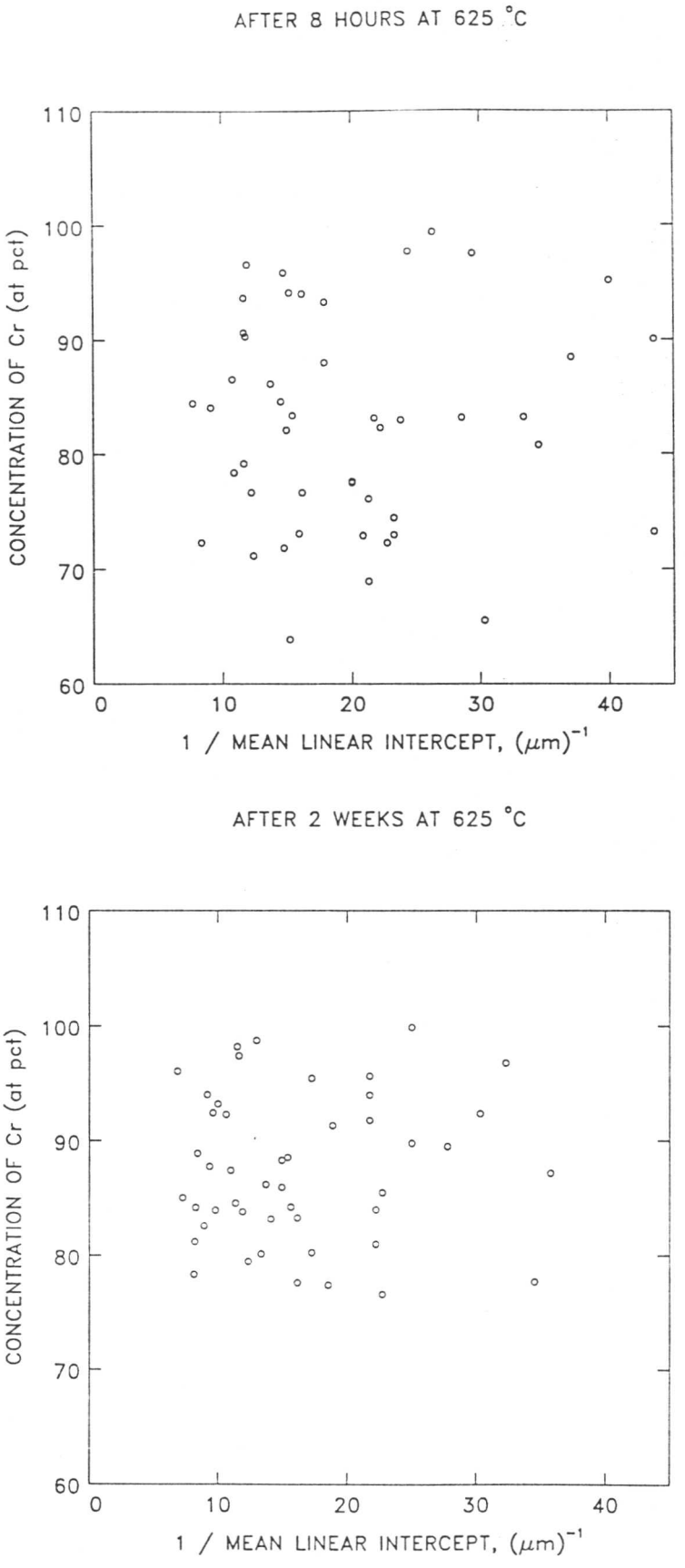

Figure 7.8: Measured compositions of M_7C_3 particles in the Fe–Cr steel aged at 625°C

Note that the occasional EDX result producing an apparent chromium : chromium+iron ratio of greater than 100% has to be included as it is a consequence of stochastic scatter in the X-ray process (iron content is so small that the associated signal is of the same order of magnitude as background noise, giving rise to the possibility of a negative value for iron content, hence a value for the normalized chromium content which exceeds 100%; see section 5.4.4 for a more detailed discussion of this problem).

7.5 Summary

The bainitic microstructures generated from this material were found during ageing to undergo simultaneous enrichment of cementite with chromium and precipitation of chromium rich carbides. The secondary precipitation appeared to occur in the ferrite matrix independent of cementite, which continued to enrich to some degree during the early stages of ageing. This process will denude the surrounding ferrite region of chromium, which would be expected to suppress chromium carbide precipitation and may explain the fact that this secondary precipitation appeared to occur away from the cementite.

Although enrichment of cementite was observed, the cementite enrichment rate was found to be significantly slower than predictions from the finite difference model, which can be explained by the effect of the secondary precipitation on the enrichment-rate-controlling process of diffusion of substitutional alloying elements within ferrite. Furthermore, at later stages of ageing, the metastable cementite phase was found redissolve at the expense of the more thermodynamically-stable M_7C_3. Consequently, the model cannot be used to relate ageing time and temperature to degree of enrichment of cementite in this material; nor can the cementite composition be used as an indicator of thermal history on which to base a remanent life estimate in components manufactured from materials in which significant secondary precipitation occurs.

EDX analysis of the secondary precipitate indicated that it formed with a composition which was close to the equilibrium, in accordance with predictions

made from the MTDATA database. As a result, the composition of M_7C_3 cannot relate to ageing time, and any model which was intended to relate microstructure to thermal history in this material would need to be based on subsequent coarsening of the secondary precipitate, rather than enrichment.

It is evident that the diffusion-based model for enrichment of cementite is relatable to the thermal history of the material only for those alloys where no significant secondary precipitation is observed in the bainitic region, but the metastable cementite phase is retained for the full ageing period. Where secondary precipitation is occurring, it will interfere with the diffusion process, making the enrichment model inapplicable to the physical situation.

Chapter 8

SUMMARY

8.1 Composition Changes During Ageing of Bainitic Cementite

8.1.1 The simple analytical model

A model was tested for the enrichment of bainitic cementite during ageing, which was derived by considering a single cementite slab in a semi-infinite ferrite matrix, and considering diffusion within ferrite to be the enrichment-rate-controlling process. This model relies on the absence of any soft impingement within ferrite, or coarsening of cementite.

Experimental measurement of changes in cementite composition during ageing of bainitic microstructures in a 1Cr–$\frac{1}{2}$Mo type power plant steel provides evidence that the model successfully describes the enrichment behaviour of this material providing the ageing time is not so large that soft impingement in the ferrite becomes significant. In particular, the experimental data agreed with the model in that:

(i) The degree of cementite enrichment was found to be in accordance with a $(\text{time})^{1/2}$ relationship as expected from the model, which differs from frequent industrial practice where an empirical $(\text{time})^{1/3}$ relation has been preferred.

(ii) Individual values of c^{θ} at a given ageing time are found to be dependent on cementite particle size, such that $(c - \bar{c}) \propto x_{\theta}^{-1}$, in accordance with the analytical model. Furthermore, the limited correlation shown between experimental data and prediction for this size effect has been explained as arising from stochastic scatter concomitant with the EDX technique. If the limitations thus imposed on such an analysis are considered, then the correlation between experimental data and the $(c - \bar{c}) \propto x_{\theta}^{-1}$ relationship is strong.

(iii) The enrichment rate, obtained from the gradient of a graph of $(c - \bar{c})$ vs $(\text{time})^{1/2}$, can be used to produce a diffusion coefficient corresponding to the experimental data. The calculated values of D_α were very close to previously reported values of interdiffusion coefficient for chromium and manganese.

At longer ageing times, this linearity with $(\text{time})^{1/2}$ tended to break down, and the enrichment rate slowed, which is strongly suggestive of soft impingement within ferrite causing a reduction in the rate of diffusion of substitutional alloying elements to the cementite particles. This effect was noted after a timescale of months at 565°C, rather than the years these materials experience in service in power plant, so an analysis which allows for soft impingement is necessary to model the remanent life problem. Nevertheless, the analytical model provides an excellent description of cementite ageing prior to the onset of significant levels of soft impingement, and it can be concluded that cementite enrichment is primarily effected by diffusion of substitutional alloying elements through the ferrite to the α/γ interface, driven by the excess of substitutionals in the ferrite phase.

8.1.2 The finite difference model

The finite difference model was developed to include an analysis of the effect of soft impingement in ferrite on the enrichment rate. The model was found to be in excellent agreement with experimental results before a significant level of soft impingement occurred, and to give a reasonable estimate of the time after which soft impingement had a substantive effect on the enrichment rate. However, the slowing down of cementite enrichment at longer stages of ageing was somewhat greater than expected, and it is suspected that this arises from the failure of the model to account for the variation in size and irregular distribution of cementite particles that is found in practice.

If the finite element model is to be improved so that more accurate predictions can be made for the real situation, the following refinements can be proposed:

(i) Account should be taken of non-uniform particle distributions and sizes, especially to allow for the fact that soft impingement will become significant at an earlier stage for more closely spaced particles. Adapting the model to consider a large number of different particles would lead to a huge increase in the computing time required, and would also necessitate a proper analysis of the interaction between diffusion fields in ferrite associated with many cementite particles, as the procedure used by the present form of the model of reflection at the last finite element in the ferrite could not be applied.

(ii) An allowance should be made of changes to cementite morphology (enlargement and shape change) during ageing. Although the degree of coarsening observed in these experiments was small, and diffusion in ferrite shown to be the dominant process, over the timescales used, some change in cementite morphology can be expected to occur during the long ageing times which these materials are subjected to in industrial use. It is desirable that the effect of these changes on the enrichment process can be modelled.

If these limitations are borne in mind, the current analysis can provide an adequate model for the cementite enrichment processes during ageing of bainitic cementite in these materials.

8.2 Remanent Life Prediction

8.2.1 The engineering problem of remanent life prediction

It is suspected that a significant proportion of the high-temperature, high-pressure steam plant in contemporary power generation may be replaced unnecessarily, owing to the lack of an accurate method of determining the amount of potential life remaining in a component, and the resultant need for large safety factors. It has been suggested that this uncertainty arises from three principal sources:

(i) The absence of a rigorous mechanistic model for microstructural degradation and creep damage accumulation in these materials during service.

(ii) Large fluctuations which occur in practice in the pressure and temperature conditions to which the component is subjected.

(iii) Problems in accurately measuring those pressure and temperature conditions.

8.2.2 Applicability of current work to remanent life prediction

It has been proposed that problems (ii) and (iii) could largely be eliminated if a model predicting to a high enough degree of accuracy the ageing behaviour of the material could be developed: analysis would then provide an indication of the thermal history of the component without the difficulties of constant on-plant monitoring of conditions.

It is evident that the limitations in the current model at the later stages of ageing which were uncovered in this work make it impossible to relate a cementite composition to an ageing regime with the required degree of accuracy at present. Nevertheless, significant groundwork for research into this problem has been made by advancing a procedure which models the early stages of ageing very successfully, and by illustrating the problems which must be addressed before the later stages of ageing can be similarly modelled.

REFERENCES

Aaronson, H.I., 1962, "Decomposition of Austenite by Diffusional Processes", Interscience, New York, pp. 387-546

Aaronson, H.I., Laird, C. and Kinsman, K.R., 1970, "Phase Transformations", ASM, Metals Park, Ohio, pp. 313-396

Afrouz, A.M., Collins, M.J. and Pilkington, R., 1983, *Metals Tech.,* **10,** 461

Ashby, M.F. and Ebeling, R., 1966, *Trans. Met. Sci. AIME,* **236,** 1396

Atkinson, C., Aaron, H.B., Kinsman, K.R. and Aaronson, H.I. [Atkinson *et al.*], 1973, *Met. Trans.,* **4,** 783

Ballinger, N.K. and Honeycombe, R.W.K., 1980, *Met. Sci.,* **14,** 121

Balluffi, R.W. and Siegle, L.L., 1957, *Acta Metall.,* **5,** 449

Batte, A.D. and Honeycombe, R.W.K., 1973, *J. Iron and Steel Inst.,* **211,** 284

Berry, F.G. and Honeycombe, R.W.K., 1970, *Metall. Trans.,* **1,** 3279

Bhadeshia, H.K.D.H. and Edmonds, D.V., 1979, *Metall. Trans.,* **10A,** 895

Bhadeshia, H.K.D.H. and Edmonds, D.V., 1980, *Acta Metall.,* **28,** 1265

Bhadeshia, H.K.D.H. and Waugh, A.R., 1982, *Acta Metall.,* **30,** 775

Bhadeshia, H.K.D.H., 1980, *Acta Metall.,* **28,** 1103

Bhadeshia, H.K.D.H., 1981a, *Acta Metall.,* **29,** 1117

Bhadeshia, H.K.D.H., 1981b, *Met. Sci.,* **15,** 175

Bhadeshia, H.K.D.H., 1982, *Met. Sci.,* **16,** 159

Bhadeshia, H.K.D.H., 1985, *Progress in Materials Sci.,* **29,** 321

Bhadeshia, H.K.D.H., 1988, Phase Transformations '87, *(Conf. Proc.),* Inst. of Metals, London, p. 309

Bhadeshia, H.K.D.H., 1989, *Mat. Sci. Tech.,* **5,** 131

Borggren, K. and Huntley, P., 1984, 2nd Int. Conf. on Creep & Frac. of Eng. Mats., *(Conf. Proc.),* Swansea, **2,** 1251

Buckle, H., 1973, "The Science of Hardness Testing and its Research Applications", ASM, Metals Park, Ohio, pp. 453–485

Campbell, K. and Honeycombe, R.W.K., 1974, *Met. Sci.,* **8,** 197

Cane, B.J. and Browne, R.J., 1982, *Int. J. Pressure Vessels and Piping,* **10,** 11

Cane, B.J. and Needham, N.G., 1983, Advances in Life Prediction, *(Conf. Proc.),* ASME, Albany, N.Y.

Cane, B.J. and Townsend, R.D., 1984, CEGB Report No. TPRD/L/2674/N84

Cane, B.J. and Williams, J.A., 1987, *Int. Mat. Review,* **32,** 241

Cane, B.J. and Williams, K.R., 1979, Int. Conf. of Mechanical Behaviour of Mats., *(Conf. Proc.),* Cambridge, **2**, 255

Cane, B.J., 1978, *Matl. Sci. and Eng.,* **35,** 229

Cane, B.J., 1979, 3rd Int. Conf. Mech. Behaviour of Matls, *(Conf. Proc.),* **2**, 173

Cane, B.J., 1983, *High Temperature Tech.,* **1,** 4

Cane, B.J., 1986, *Materials Forum,* **9,** 5

Carruthers, R.B. and Collins, M.J., 1981,, "Quantitative Microanalysis With High Spatial Resolution", *(Conf. Proc.),* Institute of Metals, London

Carruthers, R.B. and Collins, M.J., 1983, *Metal Science,* **17,** 107

CEGB, 1982, Procedure for boiler header creep life assessment, GOM101A

Chance, J. and Ridley, N., 1981, *Metall. Trans.,* **12A,** 1205

Christian, J.W. and Edmonds D.V., 1984, "Phase Transformations in Ferrous Alloys", Met. Soc. AIME, New York, pp. 293–325

Cliff, G. and Lorimer, G.W., 1972, 5th European Congress on Electron Micrscopy, *(Conf. Proc.),* Bristol I. O. P., 140

Cliff, G. and Lorimer, G.W., 1975, *J. Microscopy,* **103,** 203

Coleman, M.C. and Rowley, T., 1973, CEGB Note No. RD/M/N 710

Coleman, M.C., Parker, J.D., Walters, D.J. and Williams, J.A., [Coleman *et al.*] 1979,, 3rd Int. Conf. Mech. Behaviour of Matls, *(Conf. Proc.),* **2**, 193

Collins, M.J., 1978, *Metals Technology,* **5,** 325

Crevecoeur, G., 1985, Remanent Life: Assessment & Extension, *(Conf. Proc.),* Brussels, Sec. III, Paper 1,

Darbyshire, J.M. and Knight, S.D., 1977 CEGB Report No RD/L/N 29/77

Darken, L.S. and Gurry, R.W., 1953, "Physical Chemistry of Metals", McGraw-Hill, New York, p.146

Davenport, A.T., Berry, F.G. and Honeycombe, R.W.K., 1968, *Met. Sci.,* **2,** 104

Day, R.V., Rowley, T. and Williams, J.A., 1979, CEGB Internal Report No. RD/M/R.227

Dyson, B.F. and McLean, M., 1983, *Acta Metall.,* **31,** 17

Dyson, B.F., 1976, *Metal Science,* **10,** 349

Edmonds, D.V. and Honeycombe, R.W.K., 1978, *Met. Sci.,* **12,** 399

Evans, W.J., 1976, *Met. Sci.,* **10,** 170

Felix, W. and Geiger, T., 1961, *Sulzer Tech.,* **3/1961,** p. 37

Fridberg, J., Tŕndahl, L-E. and Hillert, M., 1969, *Jerkont. Ann.,* **153,** 263

Gladman, T. and Woodhead, J.H., 1960, *J. Iron and Steel Inst.,* **194,** 189

Goldstein, J.A. and Yakowitz, H. (Eds.), 1975, "Practical Scanning Electron Microscopy, Electron and Ion Microprobe Analysis", Plenum Press

Goldstein, J.A., Costley, J.L., Lorimer, G.W. and Reed, S.J.B., [Goldstein *et al.*] 1977 *S. E. M.,* **1,** 315

Goldstein, J.A., Lorimer, G.W. and Cliff, G., 1976, 6th European Congress on Elecron Microscopy, *(Conf. Proc.),* Jerusalem, p. 56

Goldstein, J.A. and Williams, D.B., 1978, *Scanning Electron Microscopy,* **1,** 427

Gooch, D.J. and Townsend, R.D., 1986,

Hart, R.V., 1976, *Metals Technology,* **3,** 1

Hart, R.V., 1977a, *Metals Technology,* **4,** 442

Hart, R.V., 1977b, *Metals Technology,* **4,** 447

Hart, R.V., 1980, Engineering Aspects of Creep, *(Conf. Proc.),* Sheffield, **2**, 207

Hehemann, R.F., Kinsman, K.R. and Aaronson, H.I., 1972 *Metall. Trans.,* **3,** 1077

Hehemann, R.F., 1970, "Phase Transformations", ASM, Metals Park, Ohio, pp. 397–432 J

Hillert, M., 1952, *Jern. Ann.,* **136,** 25

Hillert, M., 1962, "The Decomposition of Austenite by Diffusional Process", Interscience, New York, p. 197

Honeycombe, R.W.K. and Pickering, F.B., 1972, *Metall. Trans.,* **3,** 1099

Honeycombe, R.W.K., 1984, "Phase Transformations in Ferrous Alloys", Met. Soc. AIME, New York, pp. 259–280

Hultgren, A., 1947, *Trans. ASM,* **39,** 415

Jenkins, C.H.H. and Mellor, C.A., 1942, *J. Iron and Steel Inst.,* **143,** 31

Kachanov, L.M., 1958, *Izv. Akad Nauk. USSR Otd. Tekd. Nank,* **8,** 26

Kinsman, K.R. and Aaronson, H.I., 1967, "Transformation and Hardenability in Steels", Climax Mo Co., Ann Arbor, Mich., pp. 39–53

Kinsman, K.R., Eichen, E. and Aaronson, H.I., 1975, *Metall. Trans.,* **6A,** 303

Ko, T. and Cottrell, S.A., 1952, *J. Iron and Steel Inst.,* **174,** 307

Laird, C. and Aaronson, H.I., 1970, *Acta Metall.,* **18,** 845

Liu, Y.C. and Aaronson, H.I., 1969, *Acta Metall.,* **17,** 505

Lorimer, G.W., Al-Salman, S.A. and Cliff, G., 1977, EMAG '77, *(Conf. Proc.),* Inst. of Phys. Conf. Series, p. 369

Ludwigsen, P.B., 1985, Remanent Life: Assessment & Extension, *(Conf. Proc.),* Brussels, Sec III, Paper 3

Manier, G.N. and Szirmae, A. (coordinators), 1973, ASTM STP 547, pp. 20–23

Mehl, R.F., 1939, "Hardenability of Alloy Steels", ASM, pp. 1–54,

Morris, P.L., Davies, N.C. and Treverton, J.A., 1977, EMAG '77, *(Conf. Proc.),* Inst. of Phys. Conf. Series, p. 377

Murphy, M.C. and Branch, G.D., 1969, *J. Iron and Steel Inst.,* **207,** 1347

Needham, N.G., and Gladman,T., 1980, *Met. Sci.,* **14,** 64

Ohmori, Y., 1971, *Trans. I.S.I. Japan,* **11,** 95

Parker, J.D. and Sidey, D., 1986, *Materials Forum,* **9,** 78

Pickering, F.B., 1967, "Transformation and Hardenability in Steels", Climax Mo Co., Ann Arbor, Mich., pp. 102–129

Prado, J.M., 1986, *J. Mat. Sci. Letters,* **5,** 1075

Price, A.T. and Williams, J.A., 1982, "Recent advances in Creep & fracture of Engineering Materials", Pineridge Press, Swansea, U.K.

Puls, M.P. and Kirkaldy, J.S., 1972, *Metall. Trans.,* **3,** 2777

Purdey, G.R. and Hillert, M., 1984, *Acta Metall.,* **32,** 823

Rabotnov, Y.M., 1969, XIIth Int. Union Theoretical and App. Mech. Cong., *(Conf. Proc.),* Berlin, p. 342,

Ricks, R.A., Howell, P.R. and Honeycombe, R.W.K., 1980, *Met. Sci.,* **14,** 121

Robinson, E.L., 1952, *Trans. ASME,* **74,** 777

Rostoker, W. and Dvorak, J.R., 1977, "Interpretation of Metallographic Structures", 2nd Ed., Academic Press, New York

Russ, J.C., 1984, "Fundamentals of Energy-Dispersive X-Ray analysis", Butterworths

Russell, K.C., 1969, *Acta Metall.,* **17,** 1123

Sargent, P.M., 1979a, "Factors Affecting the Microhardness of Solids", PhD Thesis, Cambridge Univ., pp. 88–98

Sargent, P.M., 1979b, *ibid.,* pp. 66–87

Senior, B., 1988, EUREM '88, *(Conf. Proc.),* York, *in press*

Shahinian, P. and Achter, M.R., 1963, Joint Int. Conf. on Creep, *(Conf. Proc.),* Inst. Mech. Eng/ASME, paper 28

Shahinian, P. and Achter, M.R., 1965, "High Temperature Materials", J. Willey, London

Smith, C.S., 1953, *Trans. A. S. M.,* **45,** 433

Smith, G.M. and Honeycombe, R.W.K., 1982, 6th Int. Conf. on Strength of Metals and Alloys, *(Conf. Proc.),* Melbourne, p. 407

Stark, I., Smith, G.W.D. and Bhadeshia, H.K.D.H., 1987, Phase Transformations '87, *(Conf. Proc.),* Inst. of Metals, London,

Steen, M., 1983, *Int. J. Pressure Vessels and Piping,* **14,** 201

Steen, M., 1984, 2nd Int. Conf. on Creep & Frac. of Eng. Mats., *(Conf. Proc.),* Swansea, **2**, 1195

Stevens, R. and Flewitt, P.E.J., 1984, *Metall. Trans.,* **15A,** 707

Townsend, R.D., 1986, *Materials Forum,* **9,** 90

Umetoto, M., Furuhara, T. and Tamura, I., 1986, *Acta Metall.,* **34,** 2235

Umetoto, M., Horiuchi, K. and Tamura, I., 1982, *Trans. I.S.I. Japan,* **22,** 854

Vierros, P., 1985, Remanent Life: Assessment & Extension, *(Conf. Proc.),* Brussels, Sec. III, Paper 4

Watson, J.D. and McDougall, P.G., 1973, *Acta Metall.,* **21,** 961

Widgery, D.J. and Knott, J.F., 1978, *Met. Sci.,* **12,** 8

Williams, K.R., 1976, *Met. Sci.,* **10,** 332

Williams, K.R., 1981, Int. Conf. on Creep & Frac. of Eng. Mats., *(Conf. Proc.),* Swansea, 489

Wilson, M., 1986, *Materials Forum,* **9,** 53

Zener, C., 1946, *Trans. AIME,* **167,** 50

APPENDIX ONE

STEELS USED IN THE PROGRAMME

We are grateful to the CEGB for provision of materials for the experimental programme outlined in this dissertation. This material comprised a large segment of power station steam pipe in the as-fabricted condition and two plugs of service exposed material from superheater steam header. The former sample was used extensively as a base material for a large programme of experimental work; the latter used principally in theoretical studies as a typical composition source. Details of the compositions and thermal histories of these specimens are given below.

The Large Pipe Segment

The chemical composition (wt %) of this material was as follows:

C	Si	Mn	P	S	Al	Cr	Mo
0.12	0.23	0.51	0.011	0.009	0.009	0.87	0.50

It had been subjected to the following heat treatments:

30 minutes at 930°C; air cooled
60 minutes at 700°C; air cooled

The pipe was then given an additional stress relief at 650°C in 1.5 hours, and supplied for use in several CEGB remanent creep life programmes

The Service Exposed Material

The CEGB also supplied two plugs of material from superheater steam headers. These were taken from non-critical areas which had partially exhausted their anticipated service life. Both plugs were taken from headers made from material originating in the same cast, which was manufactured by an electric

arc steel making process. The steam headers were fabricated by the Chesterfield Tube Company.

The chemical analysis of the original cast (wt %) was:

C	Si	Mn	S	P	Ni	Cr	Mo
0.13	0.25	0.55	0.027	0.015	0.14	1.01	0.54

Design operating conditions for the header are given below.[1]

Pressure:	2450 psi (16.9 MPa) [drum 2680 psi (18.5 MPa), final superheater outlet 2400 psi (16.5 MPa)]
Temperature:	548°C (final outlet 565°C)
Dimensions:	17 7/8 in. (454 mm) outer diameter, 11 1/8 in. (283 mm) inner diameter, 3/8 in. (86 mm) thick, 43 ft. 9 in. (13.34 m) in length.
Design stress:	36.3 N/mm^2 plain cylinder stress, 44.8 N/mm^2 inter-alignment stress.

Actual service conditions were such that an effective average pressure of 1900 psi (13.1 MPa) was experienced, corresponding to a 27.5 N/mm^2 plain cylinder stress and a 34.0 N/mm^2 interligament stress.

Two of the plugs trepanned from this service exposed steam header material were supplied, both from non-critical areas (*i.e.*, , predicted life fraction consumed significantly less than unity).

PLUG U3B1: Sampled after 73 000 hours in service with a measured local temperature of 519°C. Present theory leads to an estimate of life fraction consumed for this material of 0.017 – 0.040 (mean estimate 0.025).

[1] The figures given are quoted directly in the same units as CEGB information. Approximate S.I. equivalents to these parameters are given in parentheses.

PLUG U4A1: Sampled after 61 000 hours in service with a measured local temperature of 560°C. This corresponds to an estimated life fraction consumed in this material of 0.125 – 0.330 (mean estimate 0.19).

These plugs had measured chemical compositions (in wt %) of:

	C	Si	Mn	S	P	Ni	Cr	Mo
U3B1	0.11	0.19	0.43	0.031	0.018	0.12	0.89	0.54
U4A1	0.13	0.22	0.52	0.026	0.017	0.13	1.02	0.53

APPENDIX TWO

PROGRAM TO SIMULATE STOCHASTIC SCATTER IN EDX COMPOSITION ANALYSIS

```
C
C
C calculates c - cbar from x as time increases.
C for consistency with the way experimental data was recorded,
C X is in micrometres, c in at %, in the input dataset,
C and data is converted in the prog.
C typical dataset:
C   time (hours) ,temp (C), sample size
C   diff coefficient, c alphatheta, c bar     (for Cr)
C   diff coefficient, c alphatheta, c bar     (for Mn)
C   diff coefficient, c alphatheta, c bar     (for Mo)
C
      DOUBLE PRECISION X(500), C0(3,500), C1(3,500),
     +RESULT(20), CC(3,500), CALTH(3), CBAR(3), DIFF(3),
     +SCAT(3), X2(100), CC2(100)
      INTEGER I, II, J, IFAIL, RAN(100), SAMPLE
      CHARACTER*10 NAME
C reads in ageing time (hours), temp (C), and size of sample
      READ (5,*) TIME, TEMP, SAMPLE
      TIME=TIME*3600.0
      TEMPA=TEMP+273.15
C reads in diff coeff, c alphatheta, c bar, standard deviation
C of stochastic scatter in measured c; the last three are all
C in ** atomic fraction **
      READ (5,*) (DIFF(II),CALTH(II),CBAR(II),SCAT(II), II=1,3)
      CALL G05CCF (0)
      DO 20 II=1,3
        DO 10 I=1,500
        C0(II,I) = G05DDF (CBAR(II), SCAT(II))
        IF (II .EQ. 1) THEN
   13     X(I) = G05DDF (0.16, 0.05)
          IF (X(I) .LT. 0.05) GOTO 13
          X(I) = X(I) * 1.0D-06
        ENDIF
   10   CONTINUE
   20 CONTINUE
C
      CALL CHANGE(X,C0,C1,CC,TIME,DIFF,CALTH,CBAR)
      CALL SCATTER(CC,SCAT)
      CALL RANDOM(RAN,SAMPLE)
C
C making random selection and converting to microns and atomic
C percent for compatibility with experimental data
```

```
      DO 40 II=1,3
        DO 30 I=1,SAMPLE
          IF (II .EQ. 1) X2(I) = 1.0 / (X(RAN(I)) * 1.0D06)
          CC2(I) = CC(II,RAN(I))*100.0
   30   CONTINUE
        IF (II .EQ. 1) NAME='CHROMIUM'
        IF (II .EQ. 2) NAME='MANGANESE'
        IF (II .EQ. 3) NAME='MOLYBDENUM'
        CALL REG(X2,CC2,SAMPLE,RESULT,NAME)
   40 CONTINUE
C
      END
C
      SUBROUTINE CHANGE(X,C0,C1,CC,TIME,DIFF,CALTH,CBAR)
C calculates new mli and composition after given time
      DOUBLE PRECISION X(500), C0(3,500), C1(3,500), CC(3,500),
     +CALTH(3), CBAR(3), DIFF(3), TIME
      INTEGER I, II
      DO 20 II=1,3
        DO 10 I=1,500
        C1(II,I) = C0(II,I) +
     &  ((CBAR(II)-CALTH(II))/X(I))*((TIME*DIFF(II))**0.5)*2.25676
        CC(II,I) = C1(II,I) - CBAR(II)
   10   CONTINUE
   20 CONTINUE
      RETURN
      END
C
      END
C
      SUBROUTINE SCATTER (CC,SCAT)
C introduces random, normally distributed scatter into each
C value of c calculted in CHANGES.
      DOUBLE PRECISION CC(3,500), XX, SCAT(3)
      INTEGER I,II
      CALL G05CCF (0)
      DO 20 II=1,3
        DO 10 I=1,500
        XX = G05DDF (0.0, SCAT(II))
        CC(II,I) = CC(II,I)+XX
   10   CONTINUE
   20 CONTINUE
      RETURN
      END
C
      SUBROUTINE RANDOM (RAN, SAMPLE)
C selects random readings from CHANGE output
      DOUBLE PRECISION X
      INTEGER SAMPLE
      INTEGER RAN(SAMPLE)
      CALL G05CCF (0)
```

```
      DO 5, I=1,SAMPLE
      X = G05CAF (X)
      RAN(I)=(SAMPLE*X+1)
    5 CONTINUE
      RETURN
      END
C
C
      SUBROUTINE REG(X,Y,N,RESULT,NAME)
      IMPLICIT REAL*8 (A-H,O-Z)
      DOUBLE PRECISION X(200), Y(200), RESULT(20)
      INTEGER I, IFAIL, N
      CHARACTER*10 NAME
      WRITE(6,99998) NAME
      WRITE(6,99996)(I,X(I),Y(I),I=1,N)
      IFAIL = 1
      CALL G02CAF(N, X, Y, RESULT, IFAIL)
C
C     TEST IFAIL
C
      IF (IFAIL) 20, 40, 20
   20 WRITE (6,99995) IFAIL
      GO TO 60
   40 WRITE (6,99994) (RESULT(I),I=1,5)
      WRITE (6,99993) RESULT(6), RESULT(8), RESULT(10)
      WRITE (6,99992) RESULT(7), RESULT(9), RESULT(11)
      WRITE (6,99991) (RESULT(I),I=12,20)
   60 CONTINUE
99998 FORMAT (/,14H0   ELEMENT : ,A10)
99997 FORMAT (2F10.5)
99996 FORMAT (/,36H0 CASE     INDEPENDENT     DEPENDENT/10H NUMBER   ,
     * 25H  VARIABLE       VARIABLE//(1H , I4, 2F15.4))
99995 FORMAT (22H0ROUTINE FAILS, IFAIL=, I2/)
99994 FORMAT (46H0MEAN OF INDEPENDENT VARIABLE               = ,
     * F8.4/46H MEAN OF   DEPENDENT VARIABLE               = ,
     * F8.4/46H STANDARD DEVIATION OF INDEPENDENT VARIABLE = ,
     * F8.4/46H STANDARD DEVIATION OF   DEPENDENT VARIABLE = ,
     * F8.4/46H CORRELATION COEFFICIENT                    = , F8.4)
99993 FORMAT (46H0REGRESSION COEFFICIENT                    = ,
     * D12.4/46H STANDARD ERROR OF COEFFICIENT              = ,
     * F8.4/46H T-VALUE FOR COEFFICIENT                    = , F8.4)
99992 FORMAT (46H0REGRESSION CONSTANT                       = ,
     * D12.4/46H STANDARD ERROR OF CONSTANT                 = ,
     * F8.4/46H T-VALUE FOR CONSTANT                       = , F8.4)
99991 FORMAT (32H0ANALYSIS OF REGRESSION TABLE :-//13H       SOURCE,
     * 55H        SUM OF SQUARES  D.F.    MEAN SQUARE     F-VALUE//
     * 18H DUE TO REGRESSION, F14.4, F8.0, 2F14.4/14H ABOUT  REGRES,
     * 4HSION, F14.4, F8.0, F14.4/18H TOTAL            , F14.4,
     * F8.0)
      RETURN
      END
```

APPENDIX THREE

FINITE DIFFERENCE PROGRAM TO ANALYSE AGEING OF BAINITIC CEMENTITE

```
Copyright Dr. H. K. D. H. Bhadeshia, Department of Materials Science
C and Metallurgy, University of Cambridge, Pembroke Street, Cambridge
C CB2 3QZ, U. K.  Telephone Cambridge 334301
C
C Last update of this version: P. Wilson, 3rd November 1989
C
C Program using finite difference method for the solution of the
C problem of enrichment of cementite with substitutional alloying
C elements during the ageing of bainitic steels
C
C
C EQFER=Equilibrium wt.% of X in ferrite at ageing temperature
C EQCEM=Equilibrium wt.% of X in cementite at ageing temperature
C EBAR=Average X wt.% in alloy
C FERS normalised concentration of X at ferrite surface
C CEMS normalised concentration of X at cementite surface
C TIMH time in hours
C TIM = Time, in seconds
C KTEMP=Absolute temperature
C TCEM=Thickness of cementite in metres
C TFER= Half thickness of ferrite in metres
C DFER=Diffusivity of X in ferrite
C DCEM=Diffusivity of X in cementite
C Concentrations normalized relative to average alloy concentration
C Dimension normalize relative to carbide particle thickness
C ICEM, IFER, J1 are the number of finite slices
C                for dimension and time respectively
C                IFER and J1 are calculated by the program
C A3 controls the amount of information that is printed out
C SETIME controls the time in hours that the experiment runs.
C JTEST modifies the mass balance condition when the CEMS reaches
C        the equilibrium concentration. Hence mass conserved.
C        Value set to true when CEMS reaches equilibrium.
C SOFTFER tests for soft impingement in ferrite (value true
C         after onset of soft impingement
C SOFTCEM likewise for cementite
C
C Typical data
C 838.15 0.5D-03 39.0D+00 2.5D+00 1.0D-07 2.0D-06 1000 5
C 0.0003D+00 2.0D+00 1.0 1.0
C 1.11D-19    (Interdiffusion)
C End of data
C
```

```
C
      IMPLICIT REAL*8(A-H,K-Z), INTEGER(I,J)
      DOUBLE PRECISION CFER(1500,2),CCEM(20,2),INTER,DFER,DCEM
      LOGICAL SOFTFER, SOFTCEM, JTEST
      SOFTFER=.FALSE.
      SOFTCEM=.FALSE.
      JTEST=.FALSE.
        READ(5,*)KTEMP,EQFER,EQCEM,EBAR,TCEM,TFER,ICEM
        READ(5,*)CFER(1,1),CCEM(1,1),A3,SETIME
        READ(5,*)INTER
        RFER=0.40D+00
        RCEM=RFER
        DFER=INTER
        DCEM=INTER
        STCEM=0.5D+00*TCEM/ICEM
        IFER=DINT(TFER/STCEM)
        STFER=TFER/IFER
        TIME=RFER*STFER*STFER/DFER
        J1=DINT(3.6D3*SETIME/TIME)
      WRITE(6,28)DFER,DCEM,TFER,TCEM,EQFER,EQCEM,KTEMP,ICEM,IFER
     &,STCEM,STFER
C
C all except the first slices set to a normalised C of 1.0
       DO 6 I=2,ICEM
       CCEM(I,1)=1.0D+00
6      CONTINUE
       DO 26 I=2,IFER
       CFER(I,1)=1.0D+00
26     CONTINUE
C
      FERS=EQFER/EBAR
      DR=DFER/DCEM
      WRITE(6,12)CCEM(1,1),CFER(1,1)
C
C Finite difference analysis
C
      TIM=0.0D+00
      WRITE(6,34)
      DO 1 J=2,J1
       TIM=TIM+TIME
       TIMH=TIM/3600.0D+00
       IF(TIMH .GT. SETIME)GOTO 101
       CEMM=0.0D+00
C
C                    ****    Ferrite    ******
C
C  First slice
C
      IF(JTEST) FERS=((CCEM(1,1)-CEMS)/DR) + CFER(1,1)
C Note: surface concentration in ferrite is  at equilibrium
C       until CEMS reaches the equilibrium concentration
```

```
C
      CFER(1,2)=CFER(1,1) + RFER*(FERS - 2.0D+00*CFER(1,1)
     &+ CFER(2,1))
      FER=CFER(1,2)*EBAR
      XTFER=STFER
      FERR=FER
      CFER(1,1)=CFER(1,2)
C
C
      DO 20 II=2,IFER-1
      CFER(II,2)=CFER(II,1)+RFER*(CFER(II-1,1)
     &-2.0D+00*CFER(II,1)+CFER(II+1,1))
      FER=CFER(II,2)*EBAR
      XTFER=STFER*II
      FERR=FER+FERR
      CFER(II,1)=CFER(II,2)
20    CONTINUE
C
C Ensure reflection at last slice
      CFER(IFER,2)=CFER(IFER,1)+RFER*(CFER(IFER-1,1)
     &-2.0D+00*CFER(IFER,1)+CFER(IFER-1,1))
      IF (.NOT.SOFTFER) CALL SOFT(CFER(IFER,2),1,SOFTFER,TIMH)
      FER=CFER(IFER,2)*EBAR
      XTFER=STFER*IFER
      FERR=FER+FERR
      CFER(IFER,1)=CFER(IFER,2)
C
C
C                    ******   Cementite  ********
      DO 2 I=1,ICEM
C
      IF(I .EQ. 1) THEN
         CEMS=DR*(CFER(1,1)-FERS)+CCEM(1,1)
         IF(CEMS .GT. (EQCEM/EBAR)) THEN
           CEMS=EQCEM/EBAR
           IF(.NOT.JTEST) THEN
             WRITE(6,35)TIMH
             JTEST=.TRUE.
           ENDIF
         ENDIF
         CCEM(1,2)=CCEM(1,1) + RCEM*(CEMS-2.0D+00*CCEM(1,1)
     &   + CCEM(2,1))
C
C Reflect at position of symmetry
      ELSEIF(I .EQ. ICEM) THEN
         CCEM(ICEM,2)=CCEM(ICEM,1)+RCEM*(CCEM(ICEM-1,1)
     &   -2.0D+00*CCEM(ICEM,1)+CCEM(ICEM-1,1))
         IF (.NOT.SOFTCEM) CALL SOFT(CCEM(ICEM,2),2,SOFTCEM,TIMH)
      ELSE
         CCEM(I,2)=CCEM(I,1)+RCEM*(CCEM(I-1,1)
     &   -2.0D+00*CCEM(I,1)+CCEM(I+1,1))
```

```
      ENDIF
C Calculate surface concentration in cementite appropriate for mass
C balance
      CEM=CCEM(I,2)*EBAR
      XTCEM=I*STCEM
      CEMM=CEM+CEMM
      CCEM(I,1)=CCEM(I,2)
2     CONTINUE
C
C
C
      CEMM=CEMM/ICEM
      FERR=FERR/IFER
      DUMMY=J/A3
      DUMMY=DINT(DUMMY)-DUMMY
      IF(DUMMY .NE. 0.0)GOTO 1
      AVER=(FERR*TFER + CEMM*0.5D+00*TCEM)/(TFER+0.5D+00*TCEM)
      WRITE(6,27)TIMH,CEMM,FERR,AVER,FERS*EBAR,CEMS*EBAR
1     CONTINUE
101   WRITE(6,25)
      DO 44 I=1,ICEM
      IF(CCEM(I,2) .LT. 1.0001)GOTO 46
      WRITE(6,7) I,CCEM(I,2),CCEM(I,2)*EBAR
44    CONTINUE
46    WRITE(6,24)
      DO 45 J=1,IFER
      IF(CFER(J,2) .GT. 0.999) GOTO 47
      WRITE(6,7) J,CFER(J,2),CFER(J,2)*EBAR
45    CONTINUE
47    CONTINUE
29    FORMAT(' TIME, s =',D12.4,'  TIME, hrs. =',F12.3)
28    FORMAT(' Diffusion coefficient in ferrite, m**2/s = ',
     &D12.4/' Diffusion coefficient in cementite, m**2/s, = ',D12.4/
     & ' Half thickness of ferrite, m =',D12.4/
     & ' Thickness of cementite, m =',D12.4/
     & ' Eq. conc. of X at interface, in ferrite, wt.% = ',D12.4/
     & ' Eq. conc. of X at interface, in cementite, wt.% = ',D12.4/
     & ' Absolute Temperature = ', F8.2, ' ICEM, IFER = ',2I9/
     & ' STCEM (m) = ',D12.4, '  STFER (m) = ',D12.4//)
34    FORMAT('      HOURS    CEM   FERRITE  AVERAGE X  FERS    CEMS')
27    FORMAT(D12.4,F9.4, F9.4,F9.4,F9.4,2F9.4)
24    FORMAT('      No   Norm. Conc.  wt.%X in Ferrite')
25    FORMAT(' No   Norm. Conc.    wt.%X in Cementite')
7     FORMAT(I8,D12.4,2F10.4)
11    FORMAT('-----------------------------------------------------')
12    FORMAT(' Time 0, slice 1, cementite and ferrite norm conc ',
     &2F12.4/)
35    FORMAT(' CEMENTITE SURFACE COMPOSITION AT EQUILIBRIUM'
     &,F10.2,' hours')
      STOP
      END
```

```
C
C
      SUBROUTINE SOFT(A,I,TEST,TIMH)
      DOUBLE PRECISION A,TIMH
      LOGICAL TEST
      GOTO (1,2) I
1     IF(A .LT. 0.99) THEN
         WRITE(6,10)TIMH
         TEST=.TRUE.
      ENDIF
      GOTO 3
2     IF(A .GT. 1.01D+00) THEN
         WRITE(6,11)TIMH
         TEST=.TRUE.
      ENDIF
3     RETURN
10    FORMAT(' SOFT IMPINGEMENT IN FERRITE', F10.2,' hours')
11    FORMAT(' SOFT IMPINGEMENT IN CEMENTITE',F10.2,' hours')
      END
```